EFFECTS OF SOLIDIFICATION VARIABLES
ON THE STRUCTURE OF
ALUMINUM BASE INGOTS

by

G. E. Nereo
M. C. Flemings

Casting and Solidification Section
Department of Metallurgy
Massachusetts Institute of Technology
Cambridge, Massachusetts

EFFECTS OF SOLIDIFICATION VARIABLES ON THE STRUCTURE OF ALUMINUM BASE INGOTS

by

G. E. Nereo

M. C. Flemings

Casting and Solidification Section

Department of Metallurgy

Massachusetts Institute of Technology

Cambridge, Massachusetts

ABSTRACT

This work comprises a theoretical and experimental study of macrosegregation in solidification of ingots and castings. A general expression is given for macrosegregation, which is viewed as resulting from mass flow into, or out of, local regions of the ingot during solidification. The mass flow considered in detail results from flow of solute rich liquid to feed solidification and thermal contraction.

Detailed solutions are given for unidirectional heat flow (but where fluid flow is not necessarily unidirectional). It is shown that "inverse segregation" and at least some types of macroscopic "banding" can be quantitatively understood in terms of the analysis. Mold-metal interface resistance is shown to strongly influence macrosegregation, and variations in heat transfer rate during solidification are shown to result in high or low solute bands. Changes in solidification cross-section also result in macrosegregation.

Solutions of the macrosegregation equations are next examined for cases where heat flow is multidirectional. It is shown that center-line segregation can result from the same basic mechanism examined above; i.e., flow of liquid to feed solidification contractions. Other types of segregation considered include (1) the "negative cone" of segregation often found at the base of ingots and (2) high solute regions found under some risers (hot tops). These types of segregation also result in whole or in part from the same mechanism.

A subsequent section considers briefly some types of segregation which may result primarily from thermal contraction or other types of mass flow of solid within the solidifying ingot. This mass flow of solid can accentuate centerline segregation, cause "hot tearing" types of segregation, and result in segregation from settling or floating of solid in early stages of solidification

Numerical examples of macrosegregation are given for selected limiting cases; calculations are based on simplified forms of the general macrosegregation equation to permit analytical solution. Results of laboratory experiments which qualitatively and quantitatively confirm the analysis are presented. Results are compared with simple analytical solutions, and with more precise results of numerical analysis solutions based on actual thermal data.

The experiments reported are on aluminum-4.5 per cent copper alloy, and include experiments on the following mold designs: (1) simple unidirectional, (2) unidirectional with restricted fluid flow, (3) unidirectional with variable heat extraction rate to illustrate banding, (4) unidirectional with reduced cross sections, (5) edge-risered unidirectional to illustrate centerline segregation, (6) ingot with bi-directional heat flow to illustrate centerline segregation.

TABLE OF CONTENTS

LIST OF FIGURES

PREFACE

This report summarizes the fourth year of research on study of effects of solidification variables on casting and ingot structure. All experimental work has been on aluminum and magnesium base alloys, but portions of the work are equally applicable to ferrous and other alloys.

Work during the first two years of the research concentrated primarily on microsegregation. Analyses were developed for prediction of effects of alloy and solidification variables on microsegregation; these have shown excellent agreement with experiment[1-4]. Work during the second year also considered theoretically and experimentally the problem of pore formation in solidification[2,5]. Finally, in the second year, consideration was also given to dendrite structure, and effects of solidification variables on this structure[2,4,6].

In the third year of the research, detailed study was made of elimination of microsegregation by solution treatment[7]. This work was undertaken because previous studies had shown that mechanical properties of both cast and wrought aluminum alloys are strongly dependent on degree of homogeneity obtained in the solution treatment[8-10]. The previous studies also showed it is extremely difficult to obtain a high degree of homogeneity in most such alloys. A detailed understanding of the kinetics of solutionizing aluminum alloys was therefore felt to be of considerable engineering importance.

Note: References for this Preface will be found on the following page. References for the rest of the report will be found at the end of the report.

In the third year of the research, work was also conducted on the outer "chill zone" found in ingot solidification, and it was shown that the classical theory of "copious nucleation" in the region is inadequate to explain experimental results. Dendrite structure at the chill surface was shown to be different from that in the bulk metal in some rather surprising ways[7].

Finally, a series of experiments were conducted from which it was concluded that dendrite arm spacing in usual casting and ingot solidification was determined by coarsening ("ripening"). A simple analysis, based on coarsening kinetics, was found to be of engineering applicability to predict effects of alloy analysis and other solidification variables on dendrite arm spacing[7].

During the period for which this report is written, research has been continued on effects of coarsening kinetics on dendrite structure, and on structure in rapidly solidified alloys. In addition, limited work has been conducted on solidification in composites, and on effects of melt agitation on structure. Finally, a significant effort has been initiated to study mechanical properties of ultra-high strength wrought aluminum-base alloys, produced using solidification techniques to assure complete homogeneity of the original ingot. These studies are to be summarized in a later report; this report will deal with work that has comprised the major effort during this contract year - i.e., macrosegregation in casting and ingot solidification.

This work has provided, for the first time, a basis for understanding a wide variety of apparently different types of macrosegregation. The basic analysis presented provides quantitative as well as qualitative understanding of effects such as inverse segregation, centerline segregation, and banding. The results should be of considerable engineering usefulness in understanding and controlling macrosegregation in ferrous, as well as non-ferrous alloys.

Theoretical portions of this work employ a model for solute redistribution in dendritic solidification discussed in detail by Brody and Flemings[1,3], and Bower, Brody, and Flemings[2,4]. Concepts employed in considering the interdendritic fluid flow are those described by Piwonka and Flemings[5]. Theoretical work of Scheil[11] and Kirkaldy and Youdelis[12] on inverse segregation has served as an important foundation for thus study. Finally, special acknowledgement is made of stimulating discussions with Professor John Cahn of Massachusetts Institute of Technology.

REFERENCES TO PREFACE

1. Brody, H. D., and Flemings, M. C., "Investigation of Parameters
    Influencing Solidification Behavior of Aluminum Alloys", Annual
    Report, Contract No. DA-19-020-ORD-5706(A), (June 1962 - June
    1963) to Army Materiel Command, Frankford Arsenal.

2. Bower, T. F., Brody, H. D., and Flemings, M. C., "Effects of
    Solidification Variables on the Structures of Aluminum Base
    Ingots", Annual Report Contract No. DA-19-020-ORD-5706(A), (June
    1963 - June 1964) to Army Materiel Command, Frankford Arsenal.

3. Brody, H. D., and Flemings, M. C., "Solute Redistribution in
    Dendritic Solidification", Trans. Met. Soc. AIME, 1966, Vol. 236, p. 3.

4. Bower, T. F., Brody, H. D., and Flemings, M. C., "Measurements of
    Solute Redistribution in Dendritic Solidification", Trans. Met.
    Soc. AIME, 1966, pp. 624-634.

5. Piwonka, T. S., and Flemings, M. C., "Pore Formation in
    Solidification", to be published, Trans. Met. Soc. AIME.

6. Bardes, B., Flemings, M. C., "Dendrite Arm Spacing and
    Solidification Time", to be published, Trans. AFS, 1966.

7. Flemings, M. C., Bower, T. F., Kattamis, T. Z., and Brody, H. D.,
    "Effects of Solidification Variables on Ingot Structures",
    Annual Report, Contract No. DA-19-020-ORD-5706(A), (June 1964 -
    June 1965) to Army Materiel Command, Frankford Arsenal.

8. Passmore, E. M., Flemings, M. C., and Taylor, H. F., "Fundamental
    Studies on Effects of Solution Treatment, Iron Content, and
    Chilling of Sand Cast Aluminum-Copper Alloy", Trans. AFS, 1958,
    Vol. 66, pp. 96-104.

9. Flemings, M. C., "Controlled Solidification", Proceedings Twelfth
    Sagamore Army Materials Research Conference, August 1963.

10. Lipson, S., Antes, H., and Rosenthal, H., unpublished work,
    Frankford Arsenal.

11. Scheil, E, Metallforschung, Vol. 2, 1947, p. 69.

12. Kirkaldy, J. S., and Youdelis, W. V., "Contribution to the Theory
    of Inverse Segregation", Trans. AIME, Vol. 212, 1958, p. 833.

BLANK PAGE

I. INTRODUCTION

In the works of Vannoccio Biringuccio[1] published in 1540, one
of the first references to macrosegregation is noted. He refers to
the problem of exudation and inverse segregation encountered in the
manufacture of bronze gun barrels. From that day to this, the pro-
blem of macrosegregation has been studied by many researchers. The
usual approach has been to isolate one type of macrosegregation
(i.e. centerline segregation, negative cone of segregation, exudation,
inverse segregation, banding, etc.) with the exclusion of all other
types. The result has been a multiplicity of theories, each one
designed to explain a specific type of macrosegregation. This section
will consider many of these macrosegregation effects, present some of
the pertinent literature and discuss theories pertaining to each
effect. In a subsequent section it will be shown that many of the
different types of macrosegregation are not due to unrelated phenomena
but can be understood simply in terms of the direction and velocity of
solute rich liquid which flows to feed solidification and thermal
contractions.

A. Inverse Segregation

One of the most thoroughly investigated macrosegregation effects
is inverse segregation. In the late 1920's and early 1930's many
theories were proposed to explain the mechanism of inverse segregation.
Brick and Phillip[2] have reviewed these proposals and rejected most of
the suggested mechanisms as being either speculative or unconfirmed by

experimental observations. They did accept, as most observers do today, that inverse segregation is due to solidification and thermal volume contraction with resulting flowback of solute enriched liquid, increasing local average composition above C_o (average melt composition).

Most of the definitive work which substantiates the volume contraction and interdendritic flow theory for explaining inverse segregation was published in the 1940's. Adams[3] studied inverse segregation in aluminum-copper alloys (3 per cent and 7 per cent copper) and reported extensive experimental results. However, he, along with Sauerwald[4] and Masing[5], while attempting quantitative predictions, derived no analytical expressions. The first analytical work to predict inverse segregation which could be checked experiment-ally was proposed by Scheil[6]. His expression predicted maximum segregation at the chill face as a function of alloy content. Good order agreement was obtained with experiment. Kirkaldy and Youdelis[7] recognized that the basic mechanism that explains inverse segregation accounts for the details of the segregation distribution in a uni-directionally solidified ingot. They correlated previously available data on inverse segregation in aluminum-copper alloys, and developed expressions in differential form to predict macrosegregation throughout the length of a unidirectionally solidified ingot; these were solved by numerical analysis. Later Youdelis and Colton[8] extended the work to a study of inverse segregation in aluminum-zinc ingots. A limiting case of the macrosegregation expression, given later, is exactly that

of Kirkaldy and Youdelis[7]; in addition, it is shown that by making

certain approximations, a simple analytical solution is possible.

The literature abounds with investigations on inverse

segregation. Some of the data are of very early origin and experiment-

al procedures and results are questionable. Extensive reviews of the

literature are also available, notably by Vaughn[9] reviewing work to

1937, by Pell-Walpole[10] covering work to 1949 and most recently by

Vosskuhler[11] where 65 references are cited, many recent, on inverse

segregation. In the theoretical section it will be shown how not

only inverse segregation but also the "negative cone" of segregation,

banding, centerline segregation, and localized high or low solute

regions can be related to the same mechanism which causes inverse

segregation; namely flow of solute enriched liquid to feed solidifica-

tion and thermal contraction. For this section, however, existing

theories on these effects will be considered.

B. Negative Cone of Segregation

Probably no macrosegregation phenomena is less understood than

the cone of negative segregation which often appears at the bottom

of large ingots. The usual explanation for this macrosegregation

effect is related to initial crystals which form being of lower

composition than the average composition of the melt. As the crystals

form they are said to settle to the bottom of the ingot (since they

are more dense than the liquid) and pile up in a cone of high purity,

low solute composition[12]. Several difficulties exist with the theory:

1. In an ingot, the liquidus temperature is reached by most of the bulk liquid before solidification starts[13,14].

2. It can be shown from Stokes' law that the rate of descent of crystals, in liquid metals, compared to solidification times, is too slow to descend the required distance in the available time[15].

One of the new ideas on this phenomena is reported by Marburg[16]. He associates the "negative cone" with accelerated vertical and transverse solidification after the initiation of solidification. In a subsequent section this will be discussed and related to the flow of solute rich liquid to feed solidification contraction.

C. <u>Centerline Segregation</u>

Another macrosegregation effect little understood is centerline segregation. While data are available on the magnitude of the segregation encountered[17], theories usually are limited or speculative. Until recently, the generally accepted theory related centerline segregation to a buildup of solute ahead of the interface of the columnar grains growing away from the vertical wall[18,19]. As the grains grow toward the center, the rejected solute was visualized as being pushed ahead resulting in a solute rich centerline where the growth fronts converge. Recently, however, it has been shown that there can be no significant solute buildup in front of growing tips of dendrites at the growth rates and gradients encountered in usual casting processes[20,37,38]. In a following section the mechanism for

centerline segregation will also be considered as being related to
solute rich fluid flow to feed solidification contraction.

D. Banding

Probably no problem gives the ingot maker or foundryman more
problem than banding type macrosegregation. Banding refers to regions
where an impurity of solute in the base alloy is localized in a narrow
band or strip. In ferrous alloys these bands may be high in inclusion
content, but in all alloys are of somewhat different composition than
the base alloy (typically .05 to 1.00 per cent, depending on base
solute). Banding occurs in large ingots, centrifugal castings and
continuously cast billets, and often seems to occur in a random
manner. In large steel ingots, Marburg[16] has associated inverted V
and V-type banding segregation with changes in the rate of solidifica-
tion. Takenaka[21] shows that banding type defects in centrifugally
cast steel pipe are influenced by vibration in the centrifugal
casting system and solidification rate in the melt. This appears to
be as close as anyone comes to relating banding to a mechanism similar
to that of inverse segregation. Northcott[22] suggests that vibration
might cause banding by affecting the boundary layer in front of the
growing dendrites. In view of the very small thickness of this
layer[20,37,38], however, it seems unlikely that this theory is correct.

Cumberland[23] proposes a theory based on the bands being incipient
laps resulting from irregularities in the manner of liquid metal
flow within the rotating mold. This theory, however, again requires
extensive buildup of solute at the tips of the solidifying interface.

An older theory by Howson[24] relates banding to a mechanical
separation of elements due to centrifugal forces. The theory,
however, does not take into account solidification time which can
be quite rapid.

Finally, while it is not strictly a banding effect, consideration
will be given to the segregation in continuously cast billets and
slabs. Wolf[25] discusses this problem in Al-Zn-Mg-Cu alloys and
reports on similar investigations by other researchers. While much
data are reported and conclusions drawn as to what affects the
segregation in continuous castings, little seems to be available
concerning possible mechanisms. Compositions toward the center of
continuously cast ingots were found to decrease[25] which can again be
related to solute flow to feed shrinkage.

E. Solute Enriched Regions

A type of macrosegregation related to banding is the phenomenon
of localized high solute regions usually found in castings and ingots.
By localized enrichment is meant any region where solute content can
be significantly higher than average base alloy composition. The
types of macrosegregation effects usually associated with this
phenomena are exudation, hot tearing type defects and solute enrich-
ment under risers. These three phenomena will be considered
separately even though they are associated effects, related by the
mechanism involved.

1. Exudation.

Exudation is usually found in conjunction with inverse segregation, and the two effects are often confused. Exudation occurs at the mold-metal or chill-metal interface, apparently as a result of metal-mold gap formation. After solidification is started at a wall or chill, contraction of the metal causes an air gap to form. When solute enriched liquid is forced from between dendrites to fill the gap, a layer of enriched solid which can approach eutectic composition is formed. Exudation has been studied and the variables discussed which affect thickness of the layer[26,27] and its formation[28,29]. All data indicate, that exudation is related, as are many macrosegregation effects, to the flow of solute enriched interdendritic liquid.

2. Solute Enrichment Under Risers.

One of the effects readily related to solute enriched fluid flow is macrosegregation beneath casting risers and ingot "hot tops". At the later stages of solidification (i.e., when casting or ingot is almost completely solid) some solidification has already occurred in the riser or hot top. Because of the partial solidification in the riser or hot top the liquid has become enriched in solute. When further contraction occurs in the casting or ingot the solute enriched liquid feeds from the riser to the casting. The result is the greatest enrichment in the casting or ingot at the last location to solidify (directly under the hot top or riser). Bishop et al[30]

have reported extensively on this effect in steel castings. It is presently being studied at the MIT casting and solidification section[31] using aluminum-4.5 per cent copper alloy. It will be seen later in this report that this under-riser segregation is expected to be most severe when the riser is of inadequate size, or inadequately insulated.

3. Hot Tearing.

The final type of macrosegregation to be considered is "filled hot tears". "Hot tearing" is associated with the solid contraction which occurs when a casting or ingot cools. When the contraction is hindered by the mold, cores, or differences in casting section size, complete rupture of a segment of the casting or ingot may occur. When these fractures occur within the liquid-solid zone, they are termed "hot tears" and when an incipient tear is fed from a surrounding region, the result is a "filled hot tear", generally rich in solute. Rosenberg et al[32] have studied hot tearing in aluminum-copper alloys and report data which can be accounted for by solute rich flow feeding the "hot tear". While much work has been done on the fundamental mechanism of "hot tearing" in steel[33,34] and non-ferrous alloys[35,36] little attention has been given to the resulting solute enriched flow necessary when the "hot tear" is fed.

In summary, five different types of macrosegregation with variations have been discussed, primarily on the basis of generally accepted exsiting theories. In the next section it will be shown that all these

effects are related to solute enriched fluid flow feeding

solidification and thermal contraction, and that they can be

quantitatively, as well as qualitatively, understood on this basis.

II. THEORETICAL DEVELOPMENT

In two recent papers[37,38], the problem of microsegregation in dendritic solidification was considered. It was concluded that for usual casting and ingot solidification, microsegregation in binary alloys can accurately be predicted by the "non-equilibrium freezing equation" provided there is no diffusion in the solid and no macro-segregation. Up to the limit of solubility of the primary solid phase this is written:

$$(1 - k)C_L df_L = -f_L dC_L \tag{1}$$

where: C_L = liquid composition within the "volume element" (a small volume the order of size of the dendrite arm spacing)

f_L = weight fraction liquid in the volume element

k = equilibrium partition ratio

For the special case of constant partition ratio, equation (1) is:

$$f_L = \left(\frac{C_L}{C_0}\right)^{-\frac{1}{1-k}} \tag{2}$$

or, since $C_S^* = kC_0$ and $f_S = (1 - f_L)$

$$C_S^* = kC_0(1 - f_S)^{k-1} \tag{3}$$

where: C_S^* = solid composition at the liquid-solid interface

f_S = weight fraction solid

Equation (3), for the case of no solid diffusion, describes solid composition as a function of weight fraction solid after, as well as during, solidification. It therefore completely describes "severity of microsegregation", although not its geometry[37,38].

Here consideration is first given to how the foregoing, and particularly equation (1), is modified by mass flow in or out of the volume element during solidification. The net change in composition of the element at the end of solidification is then calculated (i.e., "macrosegregation").

PART I: GENERAL MACROSEGREGATION EXPRESSIONS

A. Local Solute Redistribution

Consider a small volume element at coordinates, x, y, z within a solidifying ingot. These coordinates are to be such that no solid material enters or leaves the volume element during solidification. Hence the location x, y, z may move with respect to the mold wall as a result of thermal contraction or other solid movement, but refers to the same local region of a given dendrite. Solute enters or leaves the element only by liquid flow to feed shrinkage. Mass flow by diffusion is neglected; such mass flow has been shown to be negligible in the absence of convection sufficiently vigorous to penetrate interdendritic regions. Local perturbations of the macro-scopic composition gradient are assumed negligible so C_L is uniform

within the volume element. This model is identical to that described earlier[37,38], except that solidification contraction and thermal contraction are considered. The change in total solute in the element per unit time during solidification is then:

$$\frac{d}{dt}(\bar{\rho}\bar{C}) = -\nabla \cdot \rho_L g_L C_L \vec{v} \tag{4}$$

$$\text{(a)} \qquad\qquad \text{(b)}$$

where:
$\bar{\rho}$ = local average density (of liquid and solid), gm/cm^3

$\bar{C}$ = local average composition of liquid and solid, gm/gm

ρ_L = liquid density, gm/cm^3

$\vec{v}$ = local velocity of liquid relative to solid (resulting from solidification contraction), cm/sec

g_L = volume fraction liquid

The two terms are:

(a) Total local rate of change of solute during solidification

(b) Local rate of change of solute resulting from liquid flow relative to the solid.

The change in total mass in the element per unit time is:

$$\frac{d\bar{\rho}}{dt} = -\nabla \cdot \rho_L g_L \vec{v} \tag{5}$$

and this change is the sum of volume changes in the liquid and solid during solidification:

$$\frac{d\bar{\rho}}{dt} = \frac{d}{dt} (\rho_S g_S + \rho_L g_L) \tag{6}$$

where: ρ_S = solid density, gms/cm^3

g_S = volume fraction solid

In the absence of pore formation:

$$g_S + g_L = 1 \tag{7}$$

The term on the right of equation (4) may be rewritten:

$$-\nabla \cdot \rho_L g_L C_L \vec{v} = -C_L \nabla \cdot \rho_L g_L \vec{v} - \rho_L g_L \vec{v} \nabla C_L \tag{8}$$

Substituting equations (3) - (8) in (4):

$$\frac{d}{dt} (\bar{C}_S \rho_S g_S + C_L \rho_L g_L) = C_L \frac{d}{dt} (\rho_S g_S + \rho_L g_L) - \rho_L g_L \vec{v} \nabla C_L \tag{9}$$

Assuming the partition ratio applies at the interface, no diffusion in the solid, and constant solid density, ρ_S:

$$d(\bar{C}_S \rho_S g_S) = k C_L \rho_S dg_S \tag{10}$$

Combining (9) and (10):

$$\rho_S C_L (1 - k) \frac{dg_L}{dt} = -\rho_L g_L \left(\frac{dC_L}{dt} \right) - \rho_L g_L \vec{v} \nabla C_L \tag{11}$$

or:

$$\frac{dC_L}{dt} = -\left(\frac{1-k}{1-\beta}\right)\frac{C_L dg_L}{g_L dt} - \vec{v}\nabla C_L \tag{12}$$

where β is the "solidification shrinkage":

$$\beta = \frac{\rho_S - \rho_L}{\rho_S}$$

Equation (12) is the basic local solute redistribution equation used hereafter to calculate macrosegregation. It is written for the general case of three dimensional heat and fluid flow, for (a) constant solid (but not liquid) density during solidification, and (b) negligible net solute change from diffusion.

B. Local Solute Redistribution, Planar Isotherms

Assume isotherms are planar and perpendicular to x axis where x is the distance from the mold wall. Liquid composition at the liquid-solid interface is a function only of temperature provided undercooling from solute, radius of curvature, and kinetics effects is negligible. Hence, planar isotherms require planar isoconcentrates and:

$$\nabla C_L = i\left(\frac{\partial C_L}{\partial x}\right) \tag{13}$$

also:

$$\vec{v} = iv_x + jv_y + kv_z \tag{14}$$

Combining (13) and (14) with (12):

$$dC_L = -\left(\frac{1-k}{1-\beta}\right)\frac{C_L dg_L}{g_L} - \left(\frac{\partial C_L}{\partial x}\right) v_x dt \tag{15}$$

Now C_L is a function only of temperature. Isotherms and isoconcentrates move with velocity $\frac{dx}{dt}$ at x. Hence,

$$\left(\frac{\partial C_L}{\partial x}\right)\frac{dx}{dt} = -\frac{dC_L}{dt} \tag{16}$$

and:

$$\frac{\partial C_L}{\partial x} = -\frac{dC_L}{dx} \tag{17}$$

Similarly:

$$\frac{\partial T}{\partial x} = -\frac{dT}{dx} \tag{18}$$

where: T = temperature

Now, let $G = \frac{\partial T}{\partial x} = -\frac{dT}{dx}$ (temperature gradient), and $\epsilon = \frac{dT}{dt}$ (rate of temperature change), then:

$$\frac{\epsilon}{G} = -\frac{dx}{dt} \tag{19}$$

Combining (17), (18), and (15):

$$\frac{dg_L}{g_L} = -\left(\frac{1-\beta}{1-k}\right)\left(1 + \frac{v_x G}{\epsilon}\right)\frac{dC_L}{C_L} \tag{20}$$

Equation (20) is the solute redistribution expression (equation 12) for the case of unidirectional heat flow, but where fluid flow is not necessarily unidirectional, k and β are, in general, functions of C_L.

G and ε (at x, y, z) are also functions only of temperature, and hence of C_L; these quantities are readily measured experimentally, or in principle, calculated from heat flow considerations. Equation (20) becomes identical to that of Kirkaldy and Youdelis[7] when $v_y = v_z = 0$. Evaluation of v_x is discussed below.

C. Evaluation of Flow Velocity Vector, Planar Isotherms

1. Flow Perpendicular to Isotherms.

Consider first the case of flow only perpendicular to planar isotherms. Equation (5) and (6) then become, for locations x':

$$\frac{d\bar{\rho}}{dt} = -\frac{\partial}{\partial x'} (\rho_L' g_L' v_x') = \frac{d}{dt} (\rho_S' g_S' + \rho_L' g_L') \qquad (21)$$

where: x' is distance from the chill face to the location
considered.

When the chill face is above the non-equilibrium solidus, T_E, $0 < x' < x$, and when the chill face is below T_E, $x_E < x' < x$. The primes on other quantities denote that these are at x'. Now assuming constant ρ_S and considering the case where the chill face (x' = 0) is above T_E:

$$- \int\limits_{0}^{\rho_L g_L v_x} \partial(\rho_L g_L v_x) = \int\limits_{x'=0}^{x'=x} (\rho_L' - \rho_S') \frac{dg_L'}{dt} \partial x' + \int\limits_{x'=0}^{x'=x} g_L' \left(\frac{d\rho_L'}{dt}\right) \partial x'$$

or

$$\rho_L g_L v_x = \int\limits_{x'=0}^{x'=x} (\rho_S' - \rho_L')\left(\frac{dg_L'}{dt}\right)(\partial x') - \int\limits_{x'=0}^{x'=x} g_L'\left(\frac{d\rho_L'}{dt}\right) \partial x' \qquad (22a)$$

when the chill face is below the non-equilibrium solidus, in the
case of an alloy containing some eutectic, eutectic of volume
fraction g_E precipitates at the non-equilibrium solidus, T_E. Then:

$$\rho_L g_L v_x = \int\limits_{x'=x_E}^{x'=x} (\rho_S' - \rho_L')(\frac{dg_L'}{dt}) \, \partial x' - \int\limits_{x'=x_E}^{x'=x} g_L' (\frac{d\rho_L'}{dt}) \, \partial x' -$$

$$(\rho_{SE} - \rho_{LE}) \, g_E u_E \qquad (22b)$$

where: ρ_{SE}, ρ_{LE} = densities of solid and liquid eutectic
respectively

U_E = velocity of eutectic isotherm, T_E

dg_L' is a function of x' as well as macrosegregation at x'.
Hence, to rigorously determine local solute redistribution at x,
equation (22) and equation (30) must be solved by a tedious iterative
procedure. To permit simpler, analytical, solutions for the segrega-
tion, an alternate procedure is employed in much of the following.
ρ_S, ρ_L and k are assumed constant, and for velocity calculation, g_L
is assumed to vary linearly with temperature within the liquid-solid
zone.

1. Flow Not Perpendicular to Isotherms.

Calculation of the general case of macrosegregation when fluid
flow is not perpendicular to isotherms requires detailed knowledge
of $v_x' = f(x', y', z')$. In the special case where fluid flow is not

unidirectional but where v'_x and g'_L are independent of y' and z', an expression similar to equation (22b) is written (for the chill face below T_E):

$$A\rho_L g_L v_x = \int_{x'=x_E}^{x'=x} (\rho'_S - \rho'_L)(\frac{dg'_L}{dt})A'\partial x' - \int_{x'=x_E}^{x'=x} g'_L (\frac{d\rho'_L}{dt})A'\partial x' -$$

$$A_E(\rho_{SE} - \rho_{LE})g_E U_E \quad (23)$$

where A, A' and A_E are cross sectional areas at x, x' and x_E, respectively

U_E = velocity of eutectic isotherm

D. Calculation of Macrosegregation

Macrosegregation at x, y, z, is defined as

$$\Delta C = \bar{C}_S - C_0 \quad (24)$$

where: $\bar{C}_S$ = average composition at x, y, z after solidification

C_0 = bulk composition

"Positive segregation" refers to $\bar{C}_S > C_0$, and "negative segregation" for $\bar{C}_S < C_0$. For a binary alloy containing a primary phase α and some eutectic, the segregation after solidification is given by:

$$\Delta C = \frac{\rho_\alpha g_\alpha \bar{C}_\alpha + (1 - g_\alpha)(\rho_{SE} C_E)}{\rho_\alpha g_\alpha + (1 - g_\alpha)\rho_{SE}} - C_0 \qquad (25)$$

where: ρ_α, ρ_{SE} are densities of α and eutectic, respectively
($\rho_\alpha = \rho_S$ = constant)

$\bar{C}_\alpha$ = average composition of the entire amount of primary α phase in the final solid ingot

C_E = composition of eutectic

The average composition, $\bar{C}_S$, of any portion of the α phase, g_S, is given by:

$$\rho_S \bar{C}_S \Delta g_S = \rho_S \int_{g_S}^{g_S + \Delta g_S} C_S dg_S \qquad (26)$$

and the mass of solute in the entire primary phase, $\rho_S g_\alpha \bar{C}_\alpha$ determined by summing equation (26) for all portions of the phase Δg_S, which total to g_α. C_S as a function of g_S is determined from equation (20) recalling that $C_S = kC_L$, and $g_S = 1 - g_L$.

E. Incomplete Feeding

In the foregoing and in most of the following, it is assumed that feeding is complete. However, under many, if not most, solidification conditions, pores are expected to develop in the late stages of solidification as a result of resistance to fluid flow, precipitation of dissolved gas or a combination of both[39]. The preceeding analyses are readily adaptable to treatment of macrosegregation under these conditions.

In the simplest case, feeding is assumed to stop completely at a critical fraction, liquid, g_L^v, at time t_v, location x_v and liquid composition becomes C_L^v. Hence flow velocity to feed shrinkage will be less in the case of pore formation, since the lower integration limit on, for example, equation (22b) becomes x_v instead of x_E.

Further, in evaluation of the solute redistribution expression, equation (20), one set of limits now becomes g_L^v and C_L^v; for $g_L < g_L^v$ no further feeding occurs. Final macrosegregation is then simply calculated from summing the solute in the solid and liquid phases at t_v (since after t_v no further solute enters or leaves the volume element, although solidification progresses).

PART II: UNIDIRECTIONAL SOLIDIFICATION

As examples of application of the foregoing to calculations of macrosegregation, the case of "unidirectional" solidification is first considered; i.e., solidification with planar isotherms, unidirectional heat flow. Some limiting cases are first considered, and then segregation versus distance from the chill wall is examined for various conditions of heat and fluid flow.

A. Limiting Cases

As examples of the foregoing, solutions to equation (20) for three limiting cases are considered first here: (a) $v_x G/\varepsilon = 0$, (b) "steady state solidification", and (c) non "steady state", but finite $v_x G/\varepsilon \neq f(g_L)$. β and β_e are assumed constant and equal.

1. $\dfrac{v_x G}{\epsilon} = 0.$

At a chill face, $v_x = 0$, and provided G/ϵ is finite, $v_x G/\epsilon = 0$. For constant, k, β and no solid movement during solidification, equation (20) becomes:

$$\int_{1}^{g_L} \frac{dg_L}{g_L} = -\left(\frac{1-\beta}{1-k}\right) \int_{C_0}^{C_L} \frac{dC_L}{C_L} \tag{27}$$

and

$$g_L = \left(\frac{C_L}{C_0}\right)^{-\frac{1-\beta}{1-k}} \tag{28}$$

Here, increasing β results in increasing C_L at a given g_L and hence in greater positive macrosegregation.

2. Steady State Solidification.

Consider now unidirectional "steady state" solidification of a long ingot; i.e., planar isotherms move at a constant velocity $U = -\epsilon/G$, along the x' direction in an ingot of constant cross section, and chill face is below the non-equilibrium solidus. For $\beta = \beta_e = $ constant, equation (22b) reduces to:

$$v_x = \left(\frac{\beta}{1-\beta}\right) \frac{\epsilon}{G} \tag{29}$$

Substitution of equations (29) in (20) and integrating from the limit $g_L = 1$ at $C_L = C_0$ to g_L, C_0 yields:

$$g_L = \left(\frac{C_L}{C_0}\right)^{-\frac{1}{1-k}} \tag{30}$$

Equation (30), for the special case of $\beta = \beta_e$ = constant yields, at the end of solidification, precisely the same solute distribution as equation (2). The final composition (weight fraction or volume fraction solute) is exactly that of the original liquid and no macro-segregation results.

3. Finite $\frac{v_x G}{\epsilon}$, Non "Steady State", $\frac{v_x G}{\epsilon} \neq f(g_L)$.

As will be shown later $\frac{v_x G}{\epsilon}$ can vary substantially from that value at the chill face (0 for finite G/ϵ), or that value at steady state $\left(\frac{\beta}{1-\beta}\right)\left(\frac{\epsilon}{G}\right)$. Positive values of $\frac{v_x G}{\epsilon}$, different than the steady state value result from (a) cross sectional area change of the ingot, (b) change in solidification rate at locations between the non-equilibrium solidus and x, (c) change in G or ϵ (at x). Negative values of $\frac{v_x G}{\epsilon}$ result when liquid feed metal flows in the same direction as the direction of movement of isotherms at x, as by reheating (remelting) at locations between the non-equilibrium solidus and x. Examples other than those mentioned above will be considered later.

For the special cases where $\frac{v_x G}{\epsilon} \neq f(g_L)$, and where the chill face is below the solidus temperature, equation (20) can be directly integrated:

$$g_L = \left(\frac{C_L}{C_0}\right)^{-\left(\frac{1-\beta}{1-k}\right)\left(1+\frac{v_x G}{\epsilon}\right)} \tag{31}$$

P. Limiting Cases, Numerical Examples

Consider for numerical example of the foregoing, aluminum-4.5 per cent copper alloy, solidifying unidirectionally from a chill face. The appropriate portion of the phase diagram is shown in Figure 1a; Figure 1b shows schematically the liquid-solid "mushy" zone during solidification. Dendrite tips are at the liquidus temperature, T_L, and liquid exists within the dendrite arms to the eutectic temperature T_E (Figure 1c). It should be noted that while dendrites are shown schematically, the following analysis is independent of dendrite morphology.

From the phase diagram, $k = 0.172$, maximum solid solubility at the eutectic is 5.65 per cent copper, and eutectic composition is 33 per cent copper, and assume $\beta = \beta_e = .055$, a constant. (β is not, in fact, a constant for this alloy; however, the assumed value of .055 results in calculated segregation in good agreement with that observed experimentally, as will be shown later.)

Using the foregoing data, the solute redistribution equations for each of the foregoing limiting cases are plotted in Figure 2; that for the third case is plotted for $\dfrac{v_x G}{\epsilon} = \dfrac{10\beta}{1 - \beta}$. In each case the final average composition at the location in question is given by the area under the curve drawn; this average composition decreases with increasing $\dfrac{v_x G}{\epsilon}$.

This final average composition is readily determined graphically or by solution of equation (26). Figure 3 shows the general result
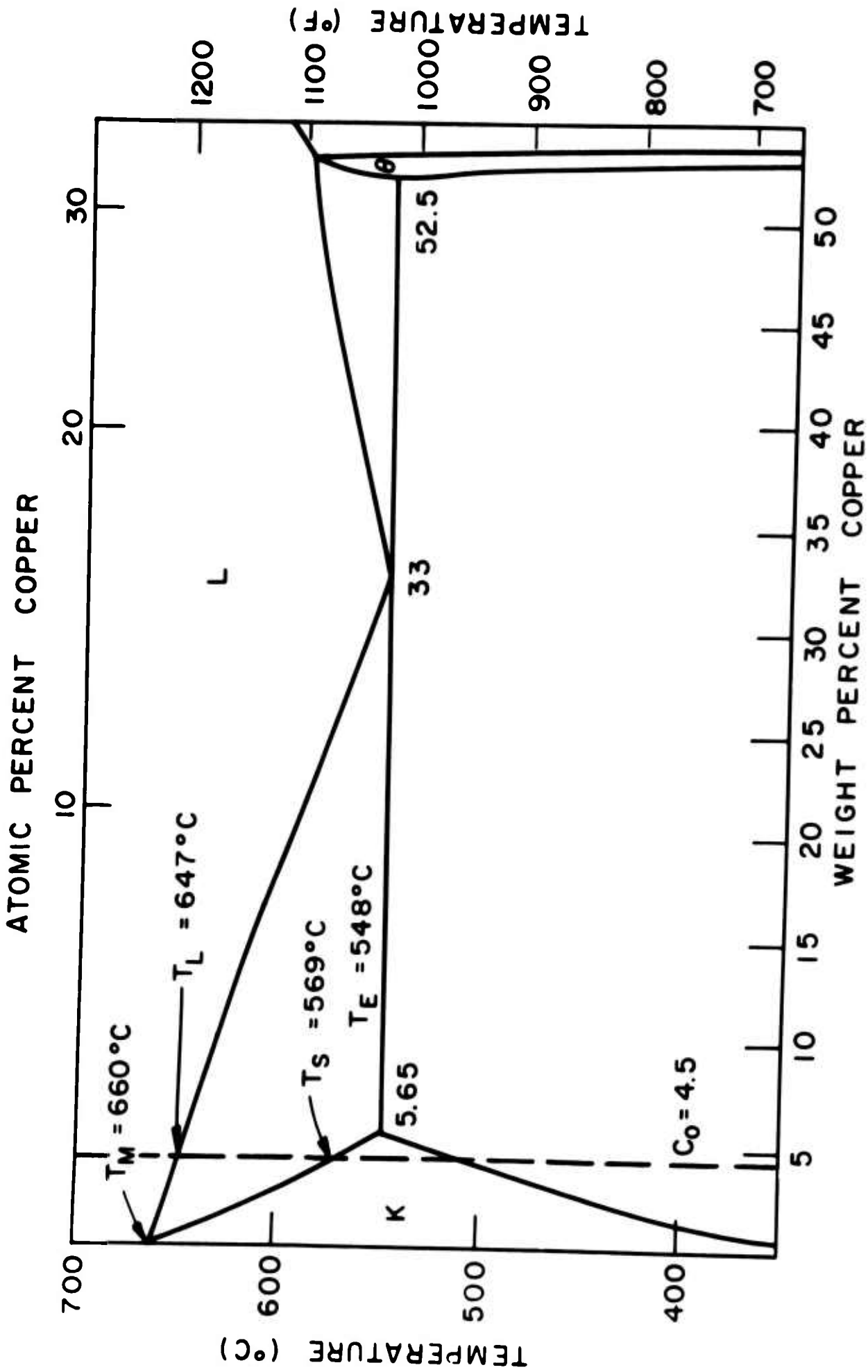
Figure 1a: Aluminum rich portion of aluminum-copper phase diagram.
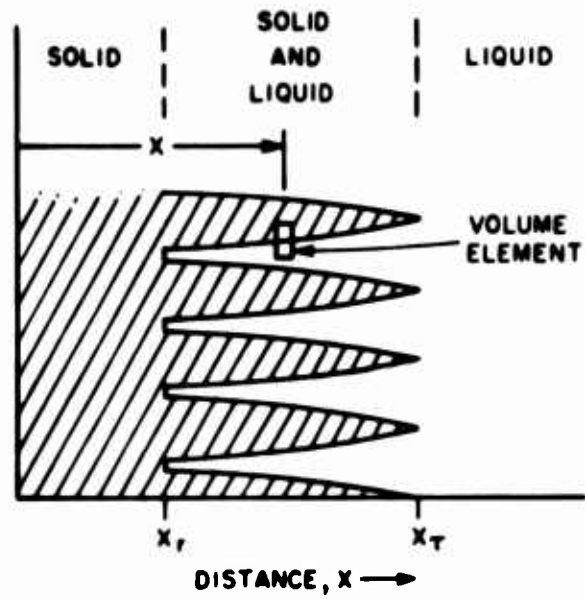
(b)
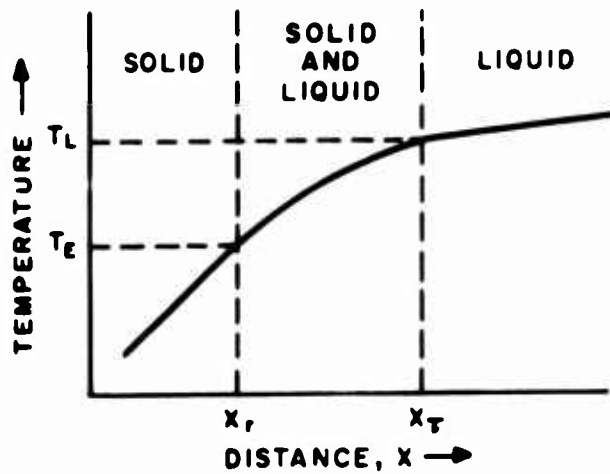
(c)

Figure 1b: Schematic diagram of dendrites in liquid-solid mushy zone during solidification.

Figure 1c: Temperature distribution in unidirectional solidification.
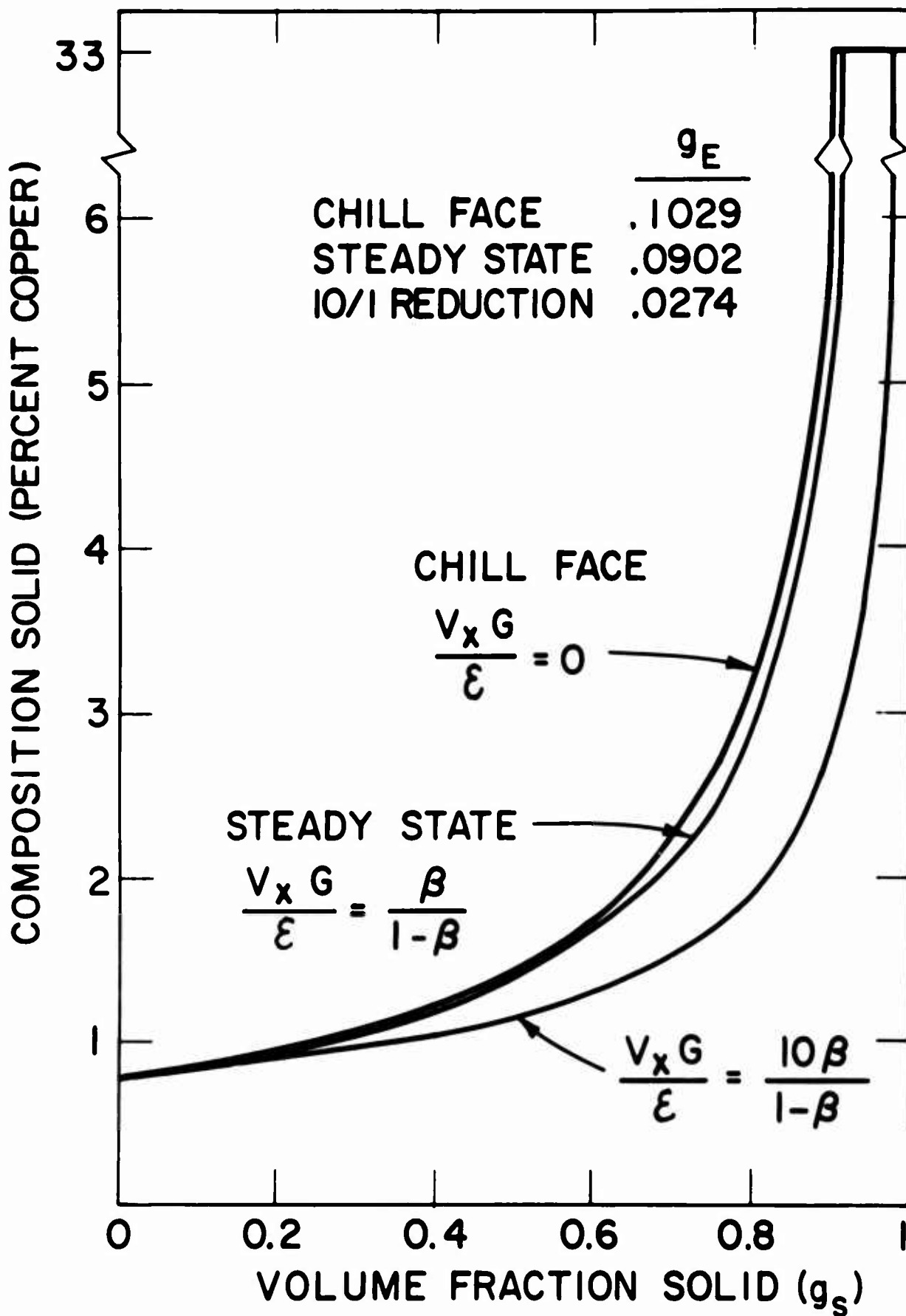
Figure 2: Solute redistribution for three solidification cases
(a) $v_x G/\epsilon = 0$, i.e., chill face solidification,
(b) $v_x G/\epsilon = \beta/(1 - \beta)$, i.e., steady state solidification,
(c) $v_x G/\epsilon = 10\beta/(1 - \beta)$, i.e., 10/1 change in solidification cross section.
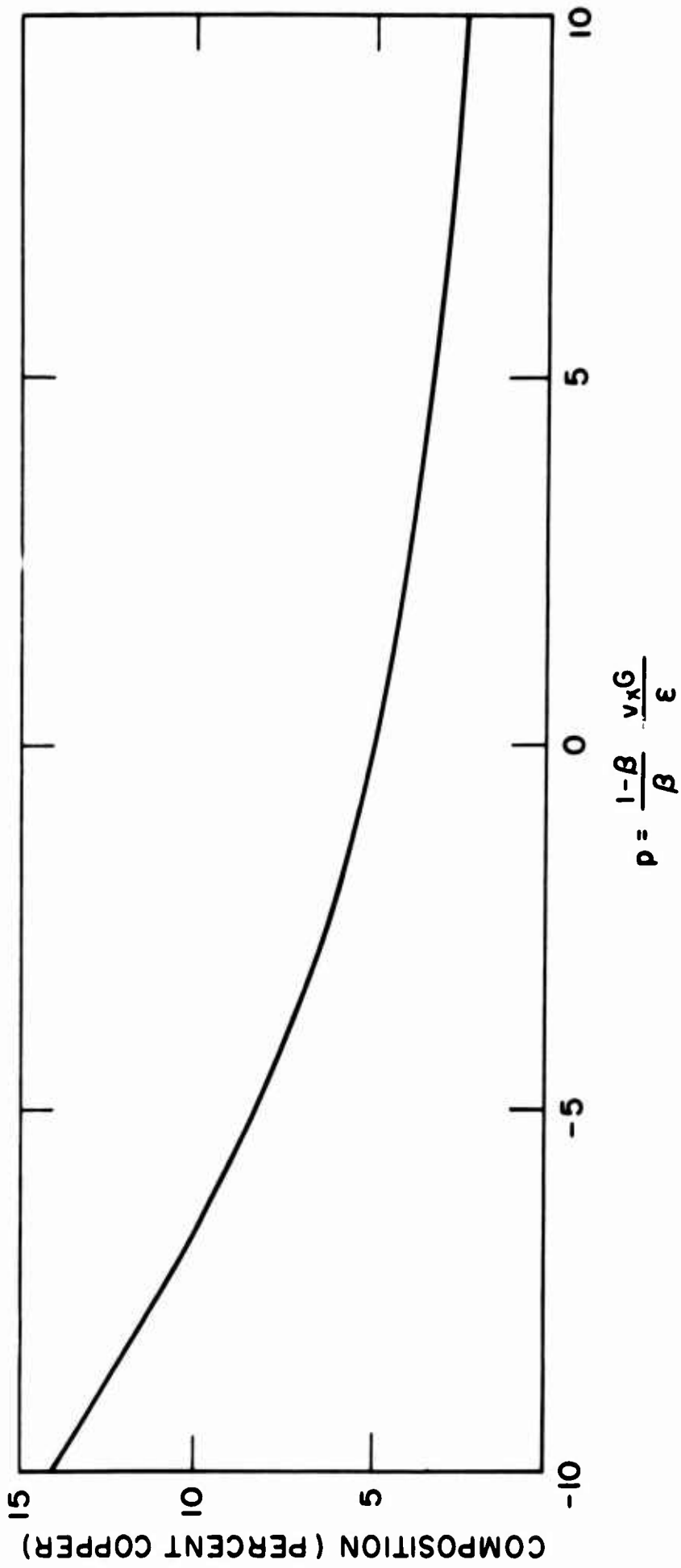
Figure 3: Average composition versus $\frac{v_x G}{\varepsilon}\left(\frac{1-\beta}{\beta}\right)$ for aluminum-4.5 per cent copper alloy.

of average composition $\bar{C}_S$ (and segregation, ΔC) plotted against the dimensionless group of variables, $p = \frac{v_x G}{\epsilon} \frac{1 - \beta}{\beta}$. For the case of the chill face, $p = 0$, for steady state, $p = 1$. In the general case, however, p can have a wide range of positive or negative values with the marked segregation illustrated.

C. Macrosegregation Versus Distance from Chill

1. Description of Model, Constant k, β.

We consider first the case of macrosegregation versus distance from the chill, assuming constant k and β. Assume, as in Figure 4a, liquidus and non-equilibrium solidus (eutectic) isotherms move according to the general relations:

$$x_L = n_L t^b + a_L \tag{32a}$$

$$x_E = n_E t^b + a_E \tag{32b}$$

where x_L and x_E are the distance from the chill to the liquidus and eutectic isotherm respectively, t is time and constants are as defined by Figure 4a. By proper choice of a_L and a_E we can readily use relations derived above for a variety of unidirectional solidification cases including (1) solidification, at constant rate and gradient (Figure 4b), (2) x_L and x_E proportional to $t^{1/2}$ as expected for unidirectional solidification against a chill wall with no mold-metal interface resistance (4c) and (3) x_L and x_E proportional to $t^{1/2}$ plus a constant; expected for unidirectional solidification against a chill wall with mold-metal interface resistance[38].
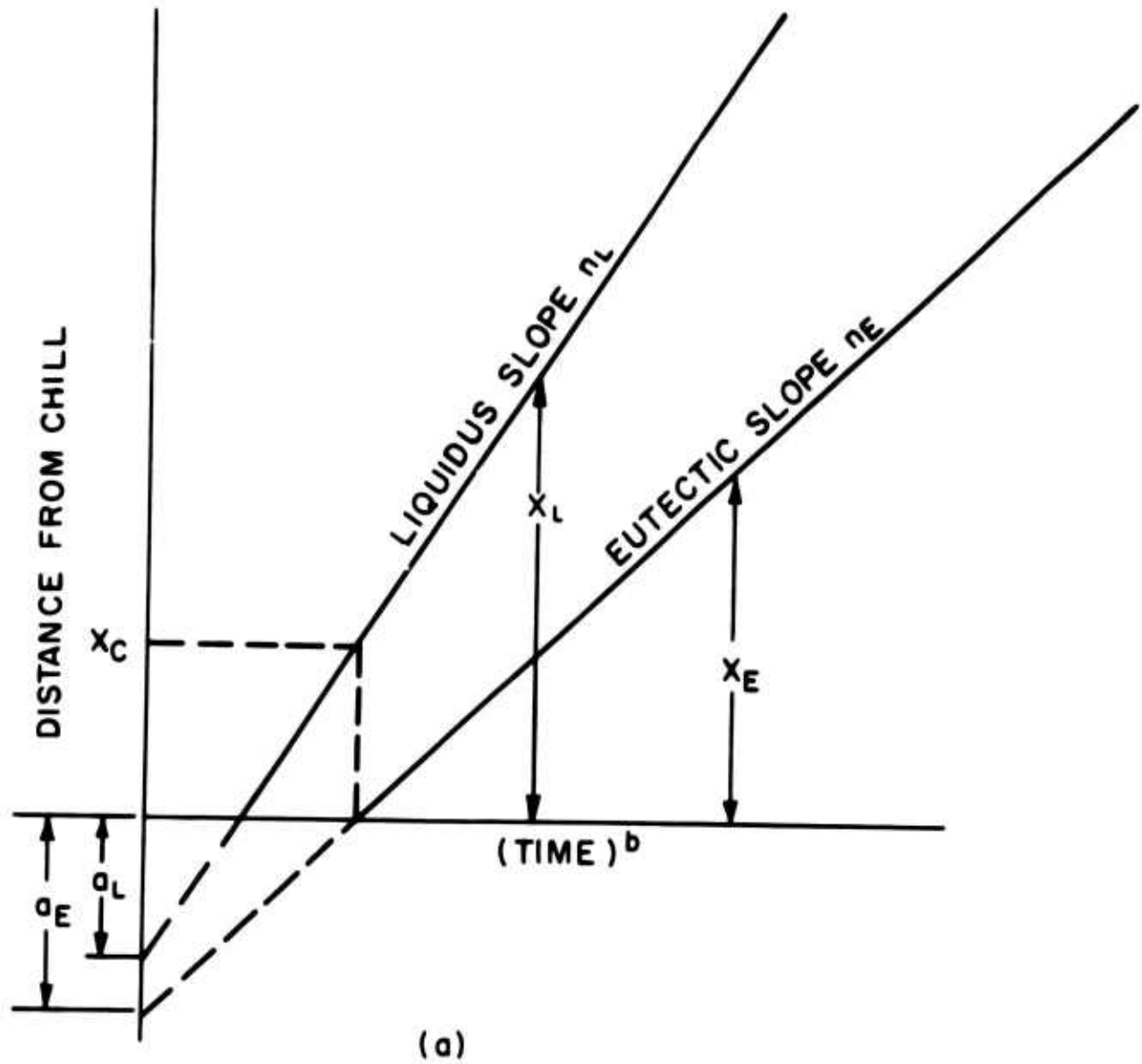
Figure 4(a): Liquidus and eutectic isotherm movement, interface resistance case, $n_L \neq n_E$.
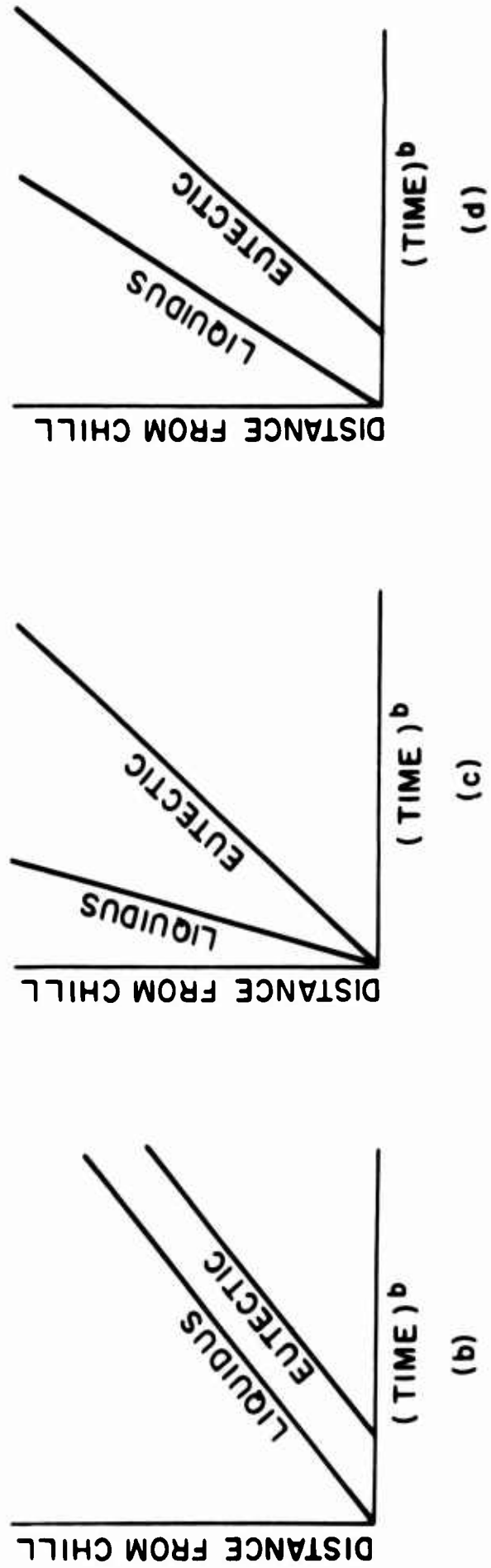
Figure 4: Liquidus and eutectic isotherm movement: (b) steady state, $n_L = n_E$ = constant, (c) no interface resistance, $a_L = a_E = 0$, (d) general case, $a_L \neq a_E$, $n_L \neq n_E$.

For analytic solution, it is now necessary to assume a distribution of fraction liquid, g_L' versus x' in the mushy zone. Reasonable alternatives include:

(1) A distribution as given by the steady state solute redistribution expression, equation (30). Such a distribution would clearly be correct for linear temperature distribution and small macrosegregation. This is sketched in Figure 5a.

(2) Linear g_L' versus x', assuming g_E constant and given by equation (30)(g_E = .0902 for aluminum-4.5 per cent copper), Figure 5b.

(3) Linear g_L' versus x', assuming g_L = 0 at x_E, Figure 5c.

An analytic solution for segregation based on condition (1) above would be quite complicated. A solution based on (2) is much simpler, and is given in part, in Appendix B for locations x > x_c where x_c is defined in Figure 4a as the location of the liquidus when the chill face reaches the eutectic temperature. For small g_E, condition (2) reduces to condition (3) which is by far the simplest for analytical solutions. The equation for (3) is written:

$$g_L' = \frac{x' - x_E}{x_L - x_E} \qquad (33)$$

Numerical examples in Appendix B show that for aluminum-4.5 per cent copper alloy, values of $\frac{v_x G}{\varepsilon}$ calculated from (3) vary by only a few per cent from those calculated from (2). Resulting calculated values of segregation are similar (within .02 per cent). Condition (3) is, therefore, used for the following.
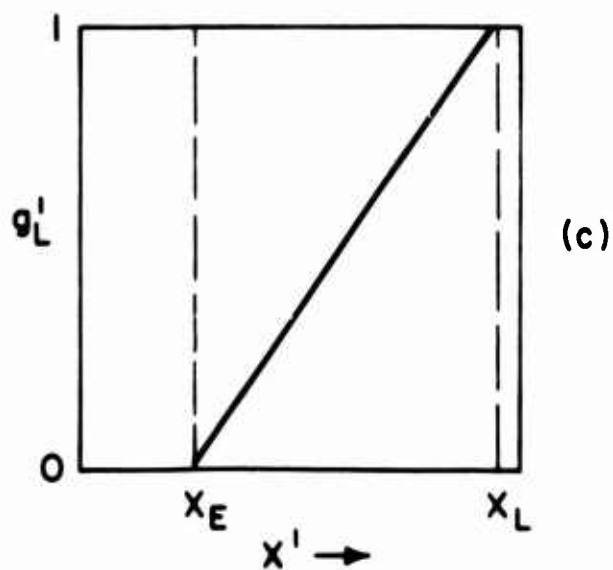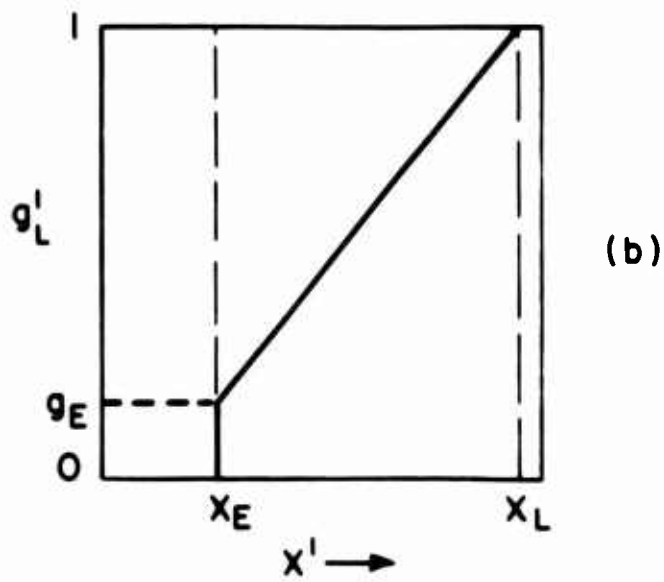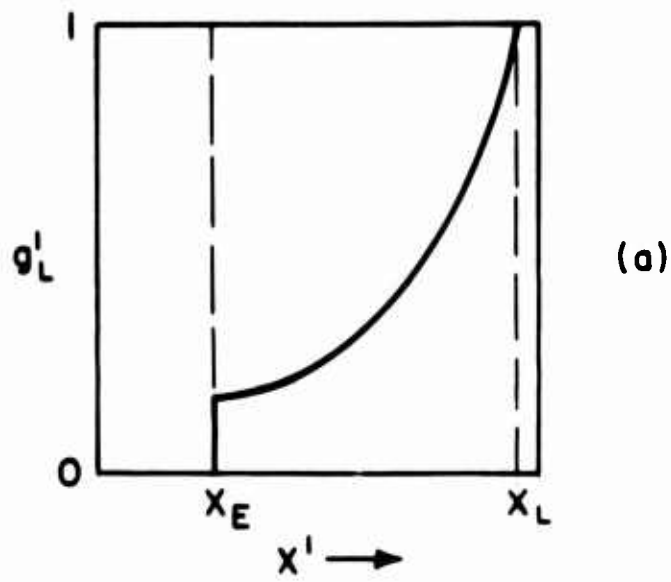
Figure 5: Distribution of fraction liquid in the liquid-solid region assuming (a) steady state solute redistribution, (b) linear g_L versus x' assuming g_E as given by steady state equation, (c) linear g_L versus x' assuming $g_E = 0$.

2. Macrosegregation, $x > x_c$.

Through manipulation of equations (22b), (32), and (33), an expression for $\dfrac{v_x G}{\epsilon}$ is readily obtainable (Appendix B) and is written:

$$\frac{v_x G}{\epsilon} = \frac{1}{2} \left(\frac{\beta}{1 - \beta} \right) \left(\frac{g_L n_q + 2}{g_L n_q + 1} \right) \tag{34}$$

where $n_q = \dfrac{n_L - n_E}{n_E}$

Combining equation (34) with (20) and integrating from $g_L = 1$ at $C_L = C_0$ to g_L, C_L yields the "solute redistribution expression" comparable to equations (28), (30) and (31):

$$C_L = C_0 g_L^{-(1-k)} \left[\frac{g_L n_q a + 1}{n_q a + 1} \right]^{-\frac{(1 - a)(1 - k)}{a}} \tag{35}$$

$$\text{where } a = 1 - \frac{\beta}{2}$$

and macrosegregation is readily determined graphically or analytically from (35) and (24 - 26).

3. Macrosegregation at $x < x_c$.

For locations $x < x_c$, a somewhat more complicated expression for $\dfrac{v_x G}{\epsilon}$ results than that of equation (34). This expression, derived in Appendix B is:

$$\frac{v_x G}{\epsilon} = \frac{x}{2} \frac{\beta}{1 - \beta} \left[\frac{2(x - x_E) + g_L n_q (x - 2x_E)}{(x - x_E)^2 (q_L n_q + 1)} \right] \tag{36a}$$

where

$$x_E = \frac{x + g_L a_E (n_q - 1) + a_L g_L}{g_L n_q + 1}$$

And C_L can now be determined as a function of g_L by combining equations (36) and (20) and integrating between the limits $g_L = 1$ at $C_L = C_0$ and g_L, C_L (Appendix B):

$$C_L = C_0 \left(\frac{N + Mg_L}{N + M} \right)^{-\frac{1 - k}{M}} \tag{37}$$

where

$$N = \frac{\beta x (2P - xn_q)}{2P^2} \tag{37a}$$

$$M = \frac{x\beta Q n_q + 2(1 - \beta)P^2}{2P^2} \tag{37b}$$

$$P = n_q x - a_E n_q + a_E - a_L \tag{37c}$$

$$Q = n_q x - 2a_E n_q + 2a_E - 2a_L \tag{37d}$$

It should be noted that N, M, P and Q are constants at any distance $0 < x' < x_c$.

Analytical solutions for solute redistribution between $x = 0$ to $x = x_L$ are obtained by solving equation (37) up to $g_L = g_L^c$ where g_L^c is the volume fraction liquid at location x_c when $x_E = 0$. After g_L^c is reached equation (35) is used by integrating between the limits $g_L = g_L^c$ at $C_L = C_L^c$ and C_L, g_L

$$C_L = C_L^c \left(\frac{g_L}{g_L^c} \right)^{-(1 - k)} \left[\frac{g_L n_q a + 1}{g_L^c n_q a + 1} \right]^{-\frac{(1 - a)(1 - k)}{a}} \tag{38}$$

4. Macrosegregation, Final Transient.

Consider macrosegregation in the last region to solidify of a unidirectional ingot of length L. Final composition in this region will, in general, be less than C_0 (for positive β, $k < 1$) as a result of draining away of solute-rich feed metal to feed shrinkage.

When the dendrite tips reach the ingot end $(x_L = L)$, at time $t = t_v^o$ subsequent solidification drains liquid back from the tips, voids result since no further supply of feed metal exists. The location x_v, of the end of the liquid at time t_v is:

$$L - x_v = -\int_{t_v^o}^{t_v} v_x dt \tag{39}$$

From which, by appropriate substitution, equation (39) can be solved to determine liquid fraction, g_L^v at x_v. This liquid fraction will all be drained from the volume element at x_v, leaving a void of volume $1 - g_L^v$. Finally, local solute redistribution in the ingot at x_v is the same for $g_L > g_L^v$ as in cases previously considered, but final composition is lower because of the voids present.

For the special case of $n_q = 0$, the critical value, g_L^v at x_v, needed to calculate macrosegregation (from Appendix C):

$$g_L^v = 1 - \frac{L - x_v}{(\beta)(x_L - x_E)} \tag{40}$$

5. Numerical Examples.

Some numerical examples of the foregoing are considered here, for unidirectionally solidified aluminum-4.5 per cent copper using the same value for constants as in previous examples.

(a) Constant Thermal Gradient.

Figure 6 shows composition versus distance from the chill for constant thermal gradient ($n_q = 0$), assuming a total length of mushy zone at steady state of 0.2 L where L is ingot length. Note the initial transient (where alloy composition is above C_0) is 0.2L in length. At the chill face, the maximum composition calculated earlier is reached (4.92 per cent copper). The final transient, resulting from depletion of feed metal, is shown on an expanded scale. In later graphs this zone is omitted for clarity.

(b) Thermal Gradient Decreasing with Time.

Figure 7 shows composition versus distance curves for several cases of varying n_q. Curve 1 shows segregation for a_L and $a_E = 0$, $n_q = 0.52$. (These are approximate values to be expected for aluminum-4.5 per cent copper alloy solidifying against a metal chill, no interface resistance as sketched in Figure 4c.) Note that overall composition of the ingot is imperceptibly higher than C_0 (approximately 4.53 as compared with $C_0 = 4.50$) and that no solute rich "initial transient" zone exists.
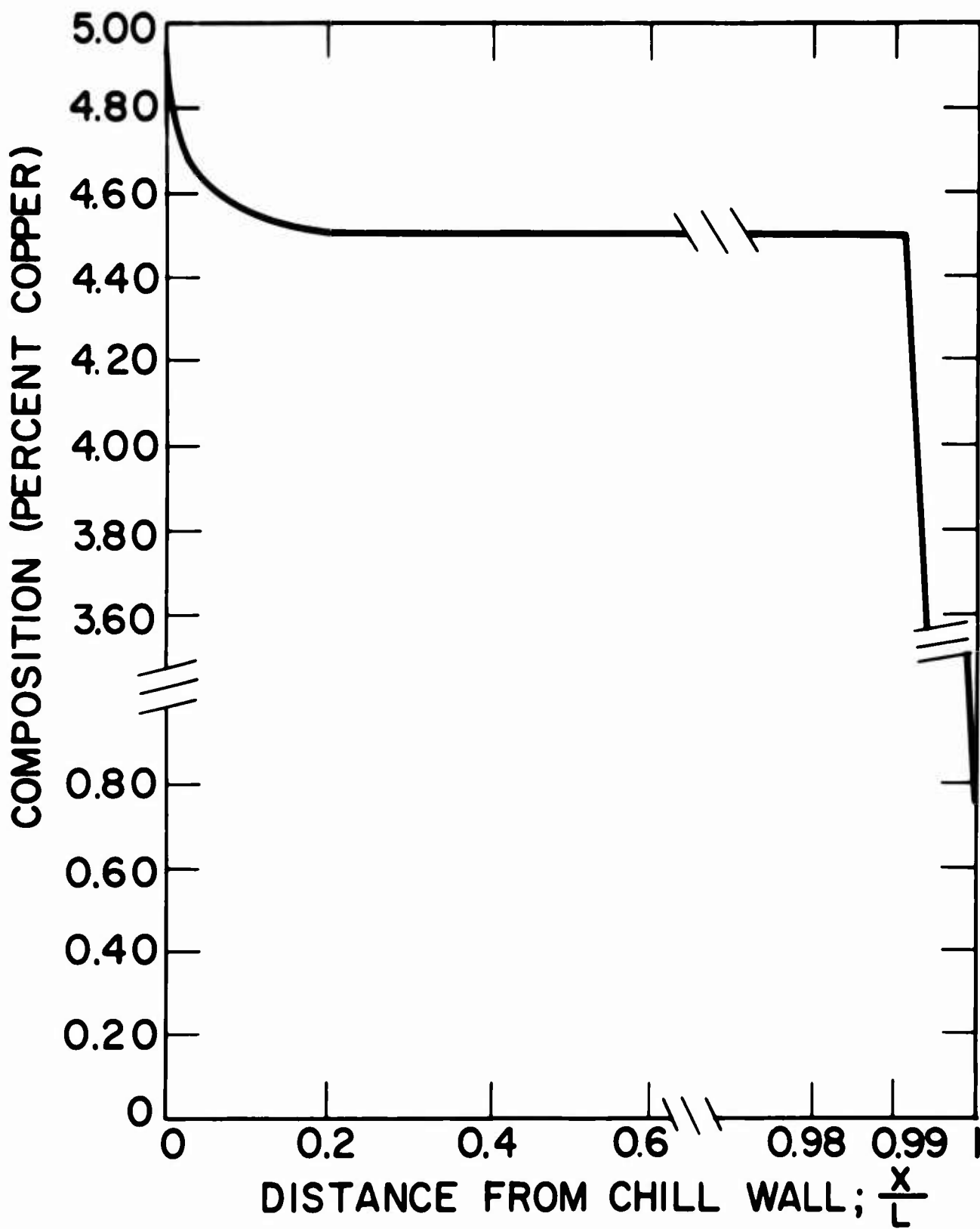
Figure 6: Composition versus distance from chill wall for constant thermal gradient ($n_q = 0$). Length of mushy zone at steady state is 0.2L.
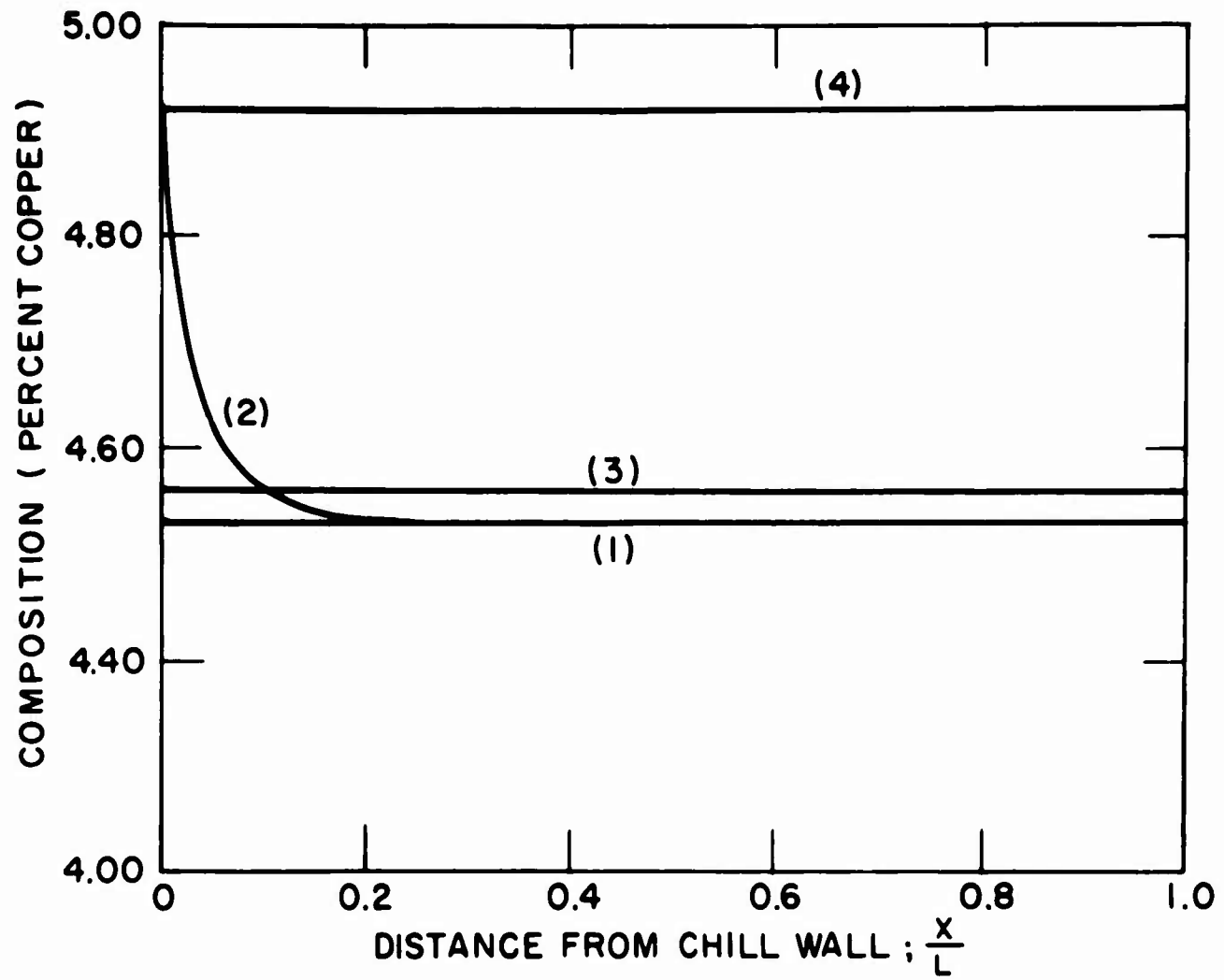
Figure 7: Composition versus distance from chill wall for varying thermal conditions: (1) $a_L = a_E = 0$, $n_q = .52$, (2) $a_L = 0$, $a_E = -2$, $n_q = .52$, (3) $a_L = a_E = 0$, $n_q \to \infty$, (4) $a_L = 0$, $a_E \to -\infty$, $n_q = .52$.

Curve (2) is identical to curve 1 except that reasonable values are employed for a_E and a_L for the case of moderate mold-metal interface resistance to heat transfer ($a_L = 0$, $a_E = -2$). As in the constant thermal gradient case surface composition again rises to the maximum chill face composition (4.92 per cent copper). Composition of the bulk ingot is unchanged (4.53 per cent copper).

It is possible to envission two other simple thermal cases. In one, excessively steep thermal gradients are maintained so $n_q \to 0$, $a_E \to 0$, $a_L \to 0$; here composition is maintained at exactly C_0 throughout. In a second, a_E and a_L remain zero so the chill face is brought instantaneously to the eutectic temperature T_E. Thereafter the chill face is held at T_E while the liquidus isotherm moves with a velocity proportional to t^b (i.e., $n_q \to \infty$). In this case, equation (24) becomes:

$$\frac{v_x G}{\epsilon} = \frac{1}{2} \left(\frac{\beta}{1 - \beta} \right) \tag{41}$$

and the solute redistribution equation is written as:

$$C_L = C_0(g_L)^{-\frac{1 - k}{a}} \qquad \text{where } a = 1 - \frac{\beta}{2} \tag{42}$$

Macrosegregation calculated from the solute redistribution expression (42) is shown as curve 3, Figure 7.

Finally, for the case of solidification under extremely shallow gradients ($a_E = \infty$), the limit of segregation calculated using equations

(36a) and (36b) is precisely the same as that at the chill face
(Figure 4, curve 4). This is most easily seen by insepection of
equation (20). At shallow gradient, and finite cooling rate, the
term $\frac{v_x G}{\epsilon}$ approaches zero, as at a chill face.

(c) Variable Thermal Gradients.

Consider unidirectional solidification with movement of isotherms
as sketched in Figure 8. Resulting composition is shown in Figure 9.
Region A is the initial transient, and final composition is similar
to that shown in Figure 6. In Regions B and F, $n_q = 0$ and final compo-
sition is C_0. Region D is drawn with $n_q = 2.5$ with the resulting
increase in composition (see Figure 10). Regions C and E are transient
zones between B-D and D-F respectively. The compositional variations
in these two transient regions are depicted schematically.

Macrosegregation in regions B, D, and F is readily calculated
from the solute redistribution equation (35) shown as Figure 10.
Figure 9 shows the final macrosegregation in the ingot. Note the
positive segregation (solute rich "band") at region C resulting from
decreasing thermal gradient. Similarly an increasing thermal gradient
will result in negative segregation (solute poor "band").

(d) Variable Ingot Cross Section.

Consider an ingot of design shown in Figure 11 solidifying
unidirectionally upwards with constant thermal gradient for liquid-
solid region is of length 0.2L for $x_E > 0$. The ingot is reduced,
on an area basis 10/1 at 0.5L.
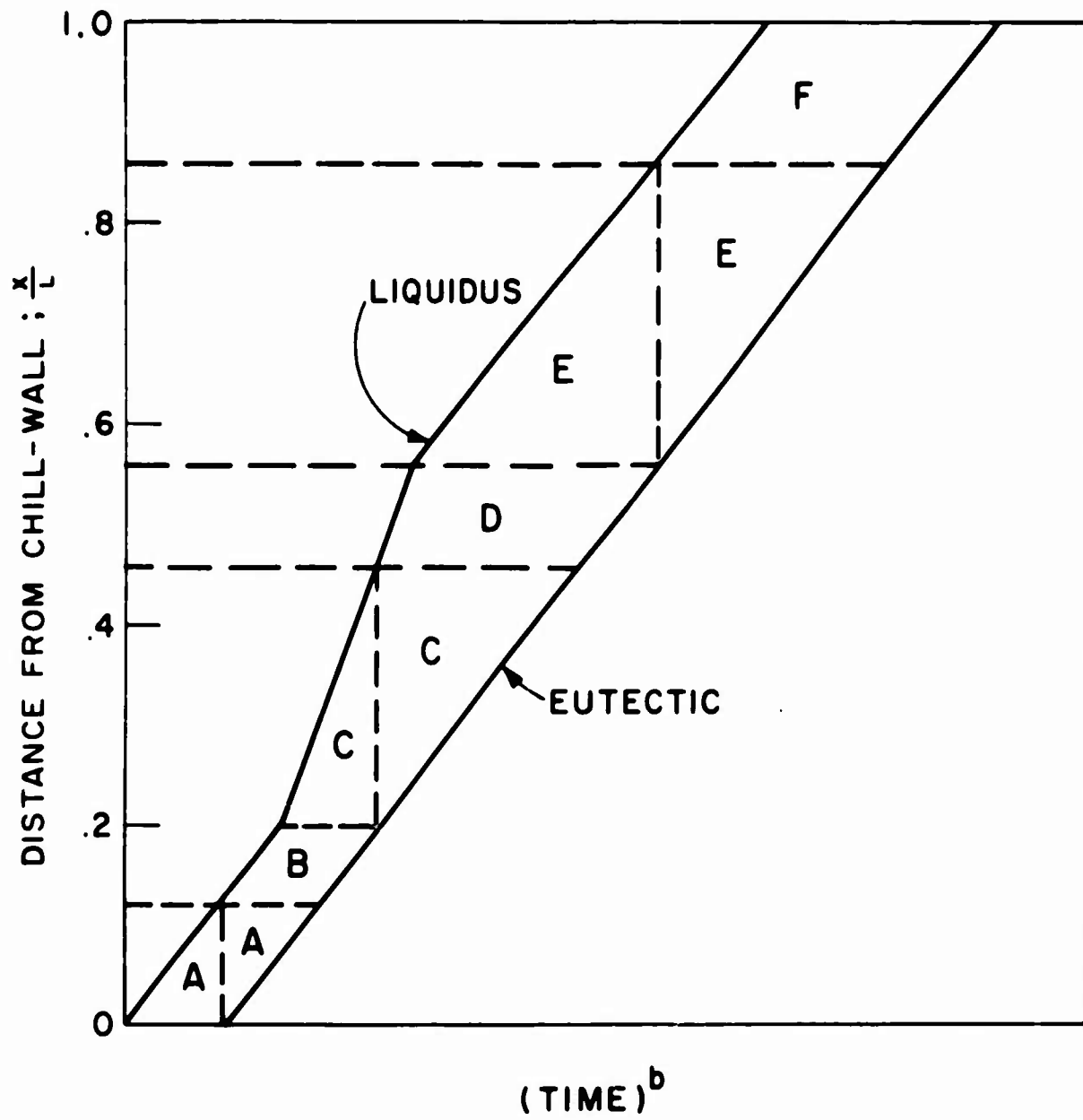
Figure 8:   Isotherm movement for a unidirectionally solidified ingot.
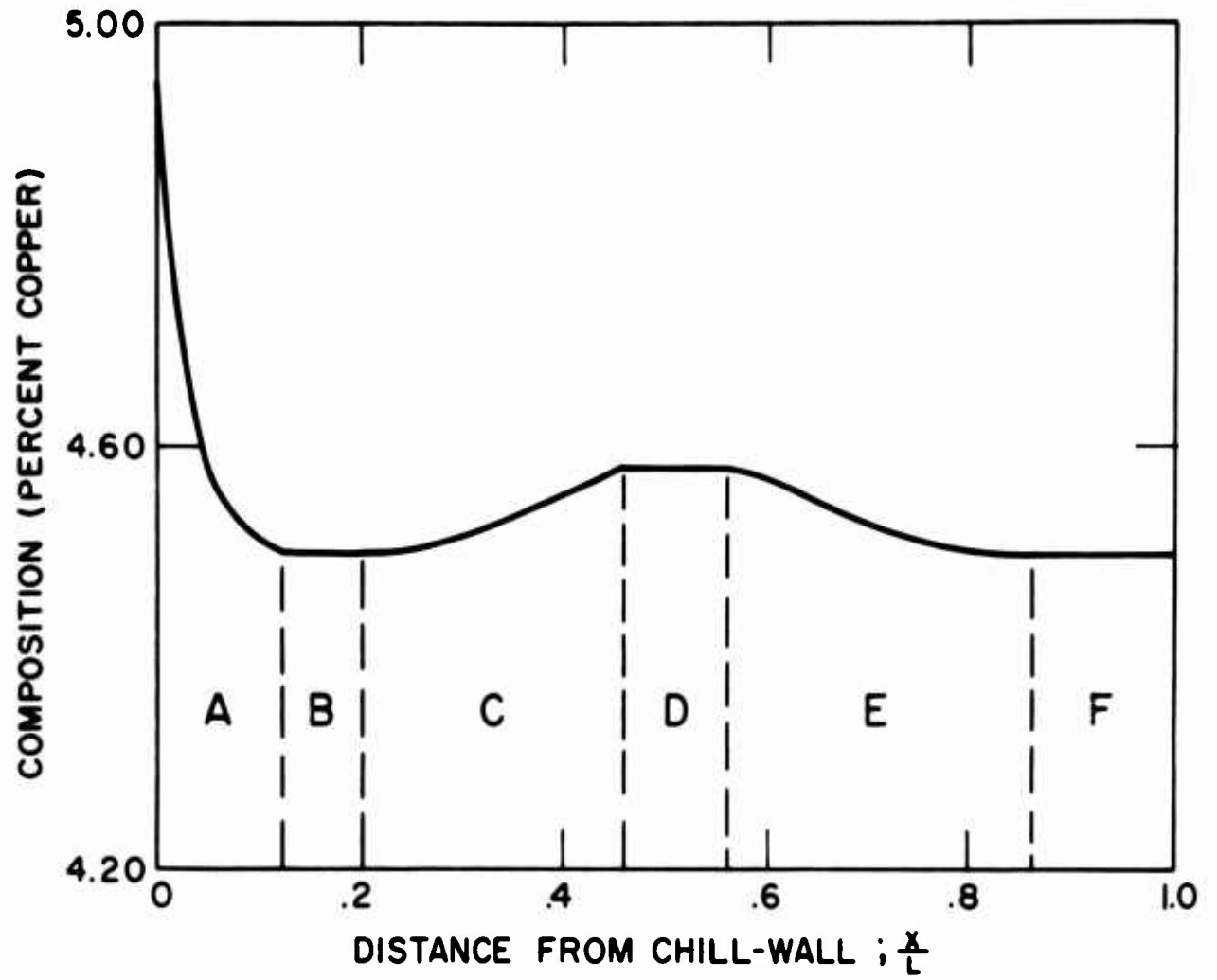
Figure 9: Composition versus distance from the chill wall for ingot with isotherm movement as shown in Figure 8.
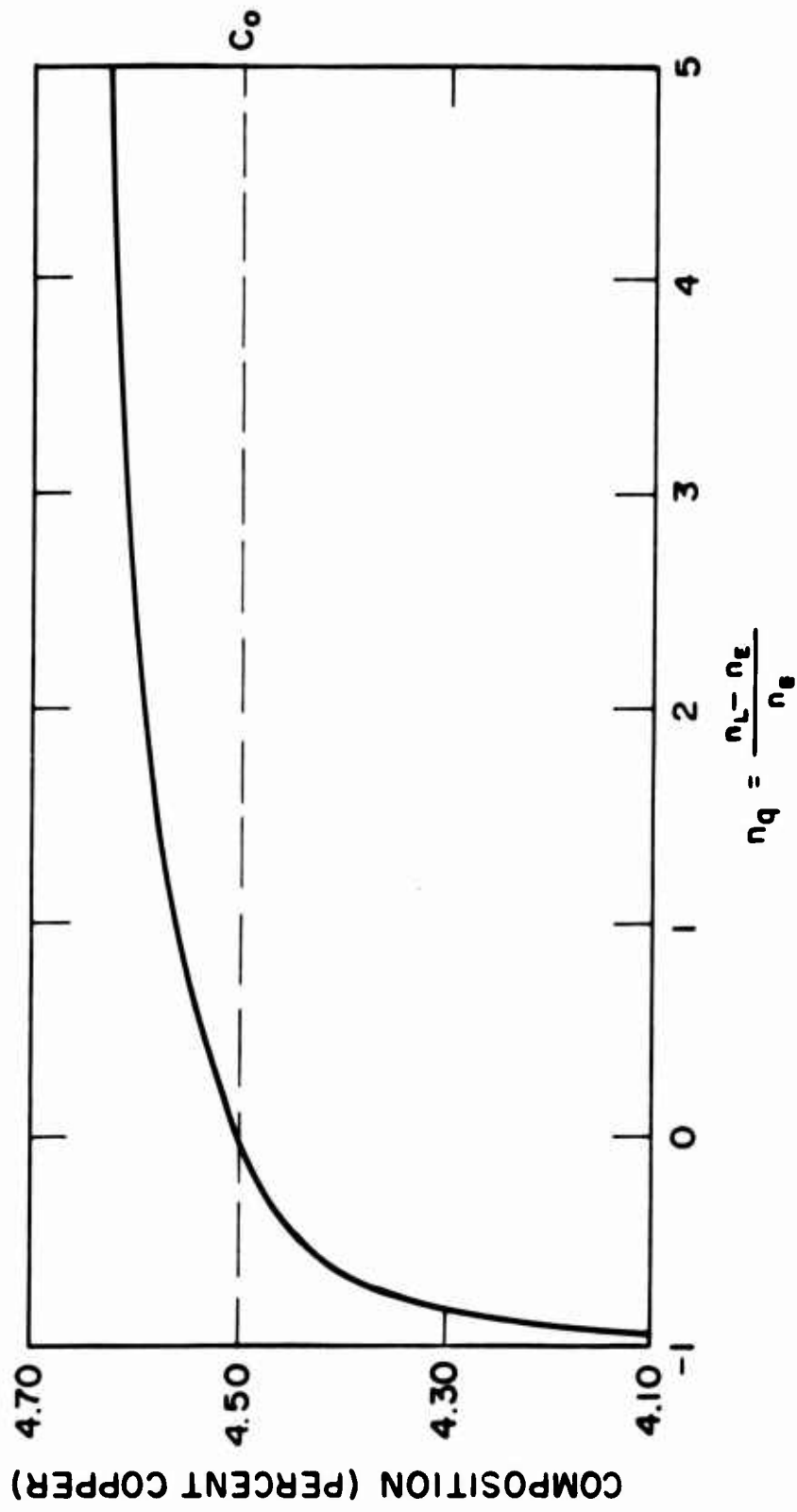
Figure 10: Effect of n_q on average composition for an aluminum—4.5 per cent copper alloy.

CHILL
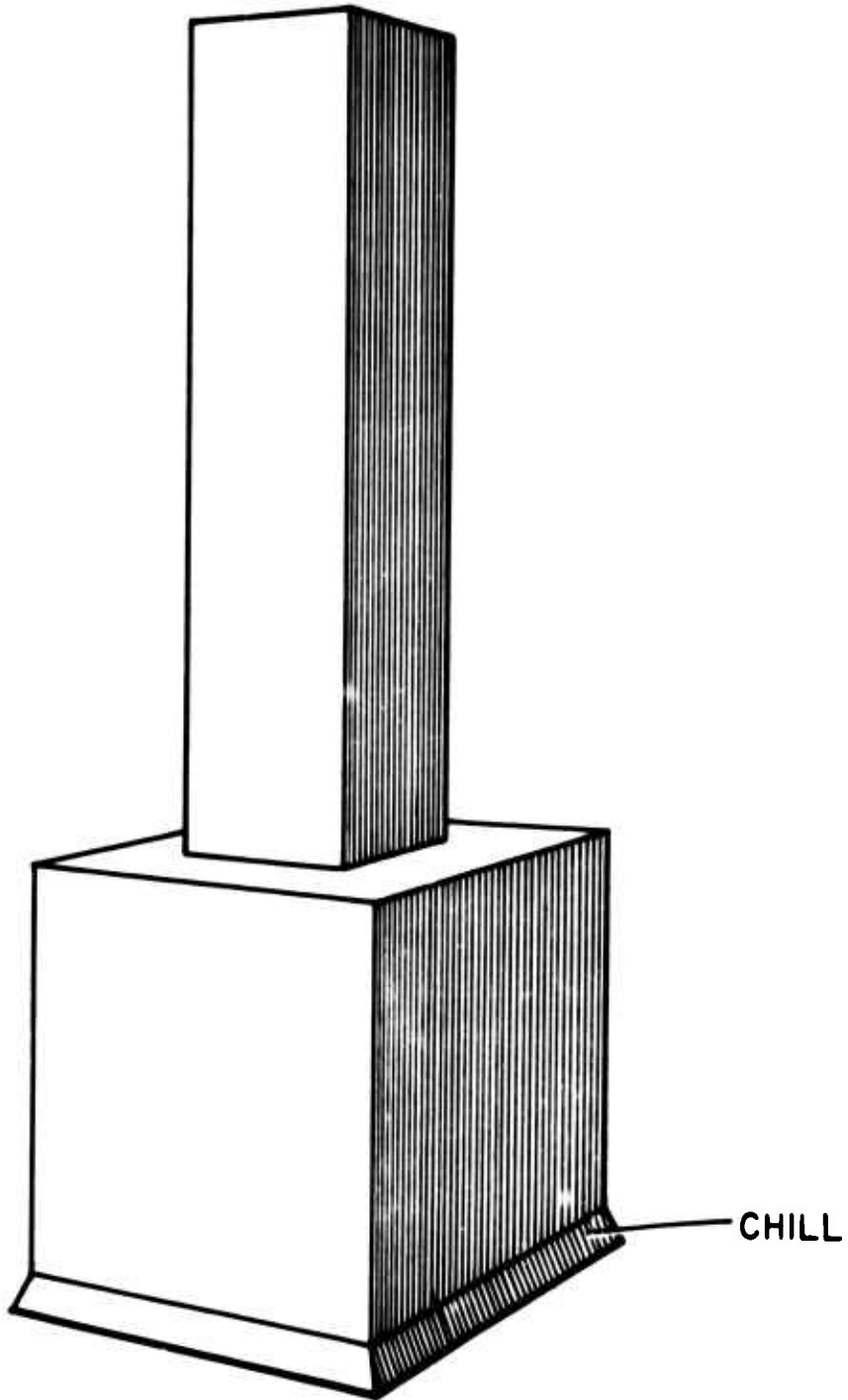
Figure 11: Sketch of reduced cross section ingot.

Final solid composition, Figure 12, is as in the comparable constant cross section ingot (Figure 6) up to $x/L = 0.5$. At $x/L = 0.5$, v_x, and hence $\dfrac{v_x G}{\epsilon}$ increases discontinuously by a factor of 10 (see equation 23). Hence, solid composition at $x/L = 0.5$ is given directly by Figure 3 for $\dfrac{v_x G}{\epsilon} \dfrac{1 - \beta}{\beta} = 10$ ($\bar{C}_S = 2.3$ per cent copper).

For the transient zone, $0.5 < x/L < 0.7$ a region exists where local solute redistribution is expressed, from equation (20), for $g_L > g_L^c$ where $\dfrac{v_x G}{\epsilon} \dfrac{1 - \beta}{\beta} = 10$ by:

$$g_L = \left(\frac{C_L}{C_0} \right)^{- \frac{1 + 9\beta}{1 - k}} \tag{43a}$$

For $g_L < g_L^c$, $C_L > C_L^c$, $\dfrac{v_x G}{\epsilon} \dfrac{1 - \beta}{\beta} = 1$ and equation (20) in the integrated form becomes

$$g_L = g_L^c \left(\frac{C_L}{C_L^c} \right)^{- \frac{1}{1 - k}} \tag{43b}$$

For $0.7 < x/L < 1.0$ final composition in the reduced cross section ingot, Figure 12, is again identical to that of the comparable constant cross section case, Figure 6, where $\dfrac{v_x G}{\epsilon} (1 - \beta) = 1$.

A second type of ingot of variable cross section is one in which cross section varies continuously. Consider, for example, the prism of Figure 13 in which

$$A' = \left(1 - \frac{x'}{L} \right) A_0 \tag{44}$$
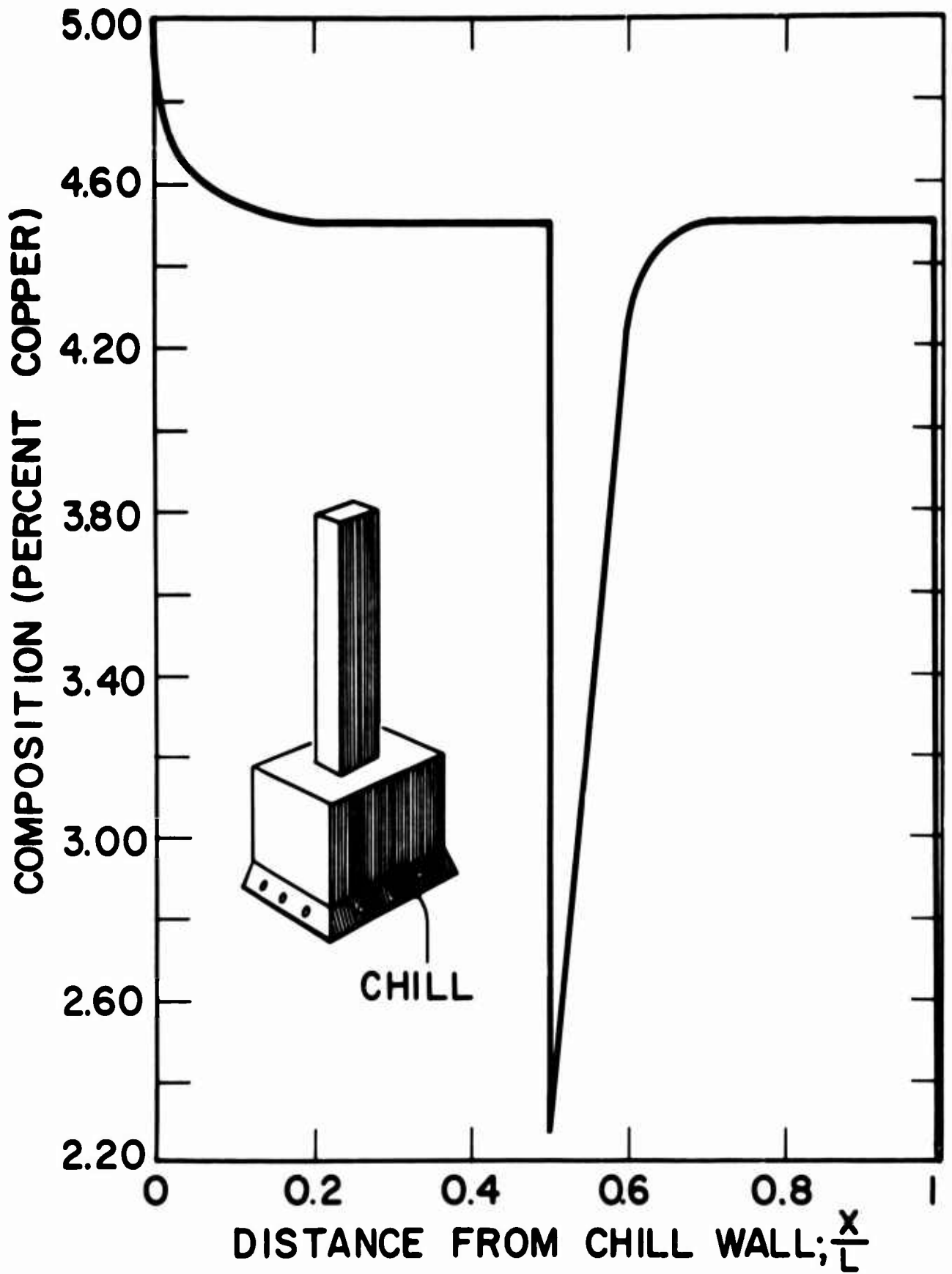
Figure 12: Composition versus distance from chill for ingot shown in Figure 11.
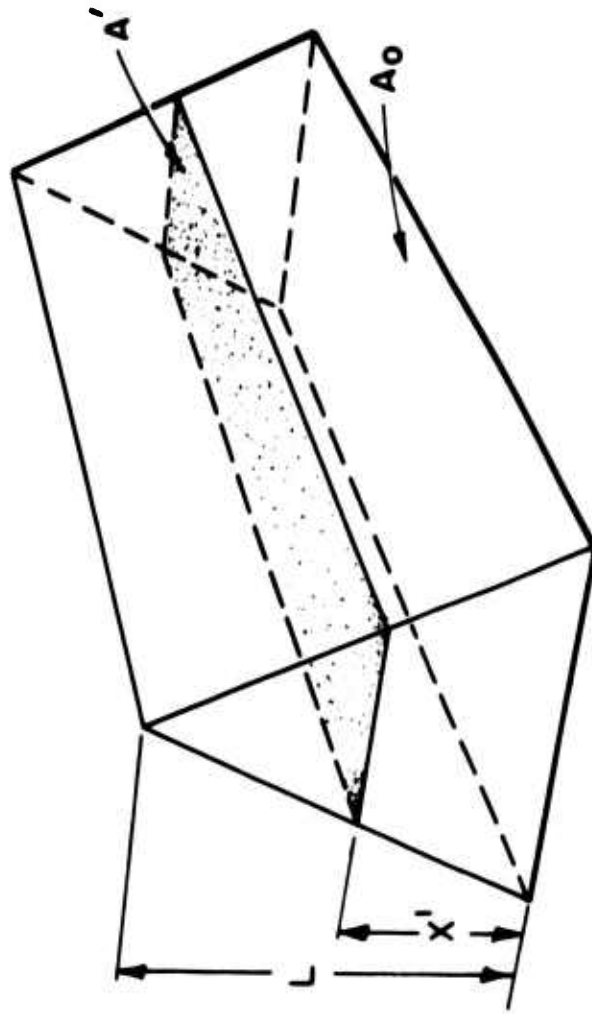
Figure 13: Sketch of prism ingot.

where: A' = cross sectional area at x'

A_0 = cross section area at chill face

Again assuming constant temperature gradient, $\dfrac{v_x G}{\epsilon}$ is calculated

from equation (23) which, for the assumptions used herein reduces

to, for $x > x_c$ (Appendix D)

$$\frac{v_x G}{\epsilon} = \frac{\beta}{1 - \beta} \left(\frac{1}{L - x} \right) \left[\frac{2L(x_L - x_E) + 2xa_T + a_T^2 g_L}{2(x_L - x_E)} \right] \qquad (45)$$

where $a_T = a_L - a_E$

Local solute distribution and macrosegregation are then calculated

as before by integrating (20) after substituting (45) and then

solving (26).

For $x < x_c$ equation (45) becomes

$$\frac{v_x G}{\epsilon} = \frac{\beta}{1 - \beta} \left(\frac{1}{L - x} \right) \left[\frac{x(2L - x)}{2g_L} \right] \qquad (45b)$$

and macrosegregation, is determined by a procedure similar to that for

the ingot of constant cross section (equations 36 - 38).

For $g_L > g_L^c$, $C_L < C_L^c$ equation (45b) is substituted in (20) and

integrated to solve for solute redistribution. When $g_L < g_L^c$, $C_L > C_L^c$

equation (45a) is used in (20) and integrated between appropriate

limits. The results are plotted as Figure 14.
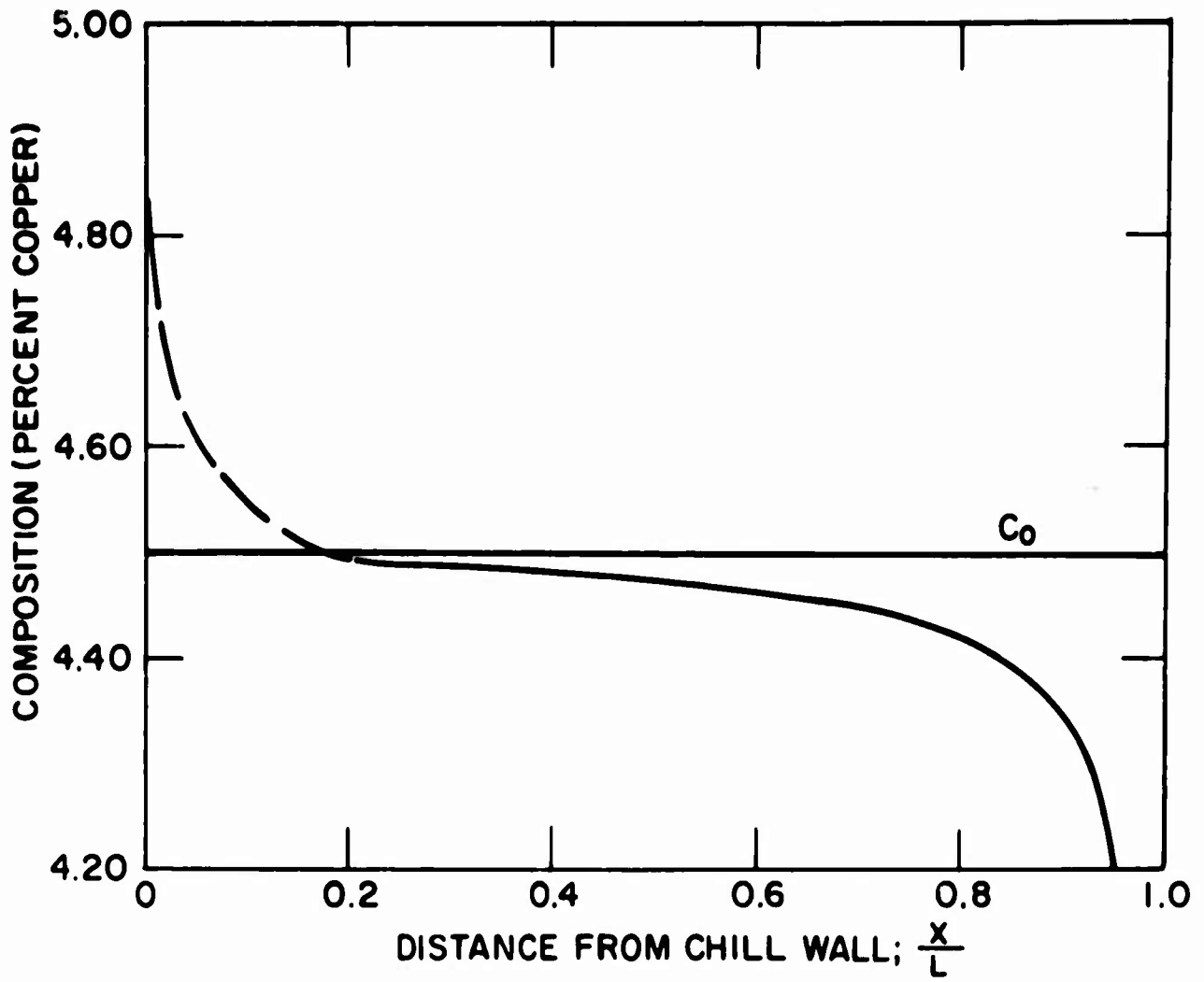
Figure 14: Composition versus distance from chill wall for prism ingot.

(e) Variable k, β.

To permit analytic solutions, the foregoing calculations have been made assuming constant k and constant β. In aluminum-4.5 per cent copper these factors are, however, not constant. Figure 15 shows k versus C_L; Figure 16 summarizes best available data on ρ_S and ρ_L versus C_L; Figure 17 shows β versus C_L, calculated from the data of Figure 15. Note that in this alloy, β is negative during much of solidification (negative β denotes expansion on solidification). However, a net flow of feed metal, negative v_x, still results throughout steady state solidification, because of thermal contraction of the liquid (i.e., the last term on the right of equation (12) is sufficiently large (negative) that v_x is negative even though the first term on the right is positive).

Figure 18 shows local solute redistribution at the chill face for aluminum-4.5 per cent copper, determined using the data of Figures 15 - 17 by graphical integration of equation (20). For comparison with the case of constant β (and hence constant ρ_S, ρ_L), the data are plotted as weight fraction solid, f_S, where:

$$f_S = \frac{\rho_S g_L}{\rho_S (1 - g_E) - \rho_{SE} g_E} \tag{44}$$

where: ρ_S and ρ_E = densities of the α phase and eutectic respectively (at just below T_E)

g_E = volume fraction eutectic
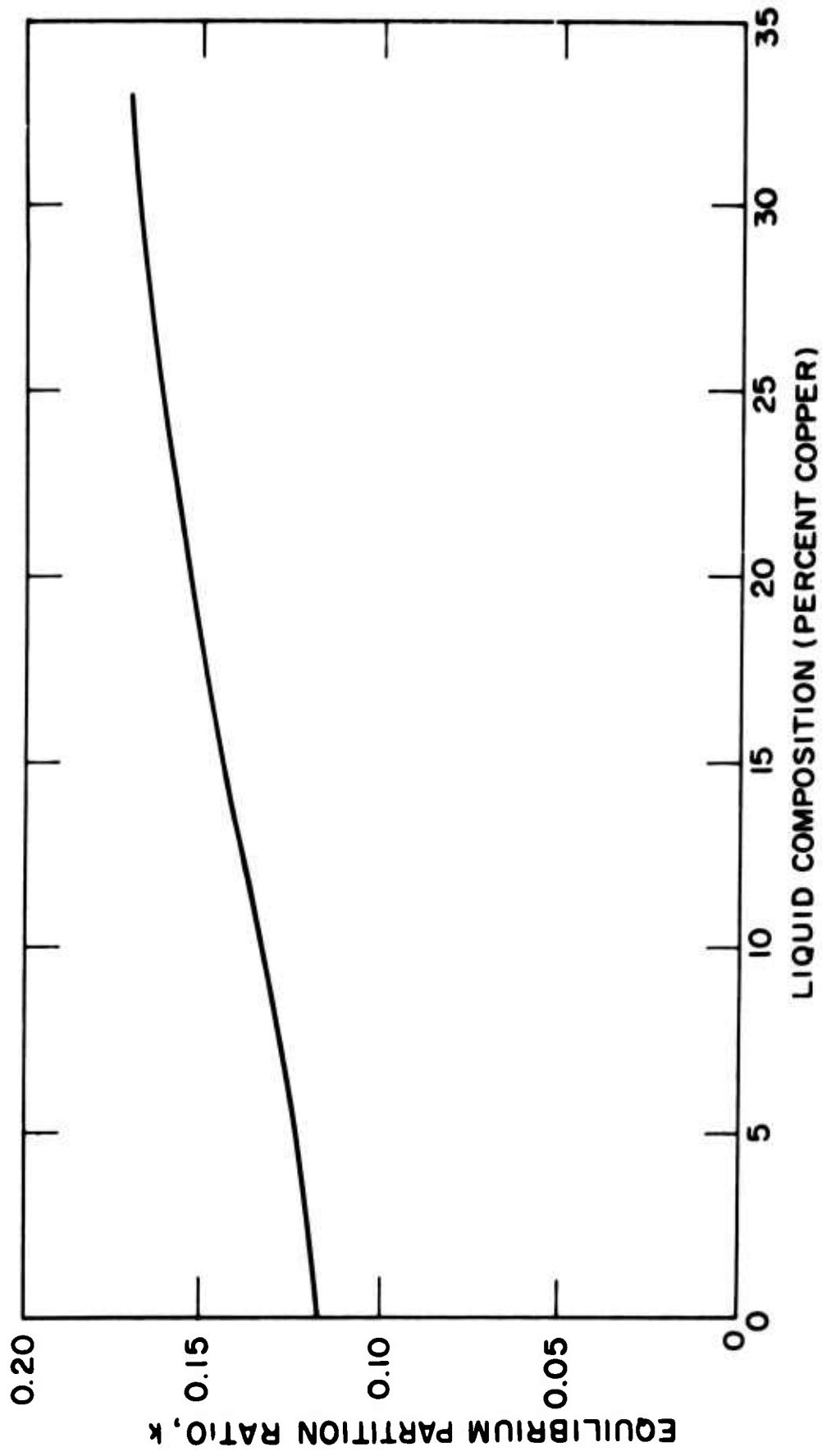
Figure 15: Equilibrium partition ratio versus liquid composition for aluminum rich, aluminum—copper alloy.[41]
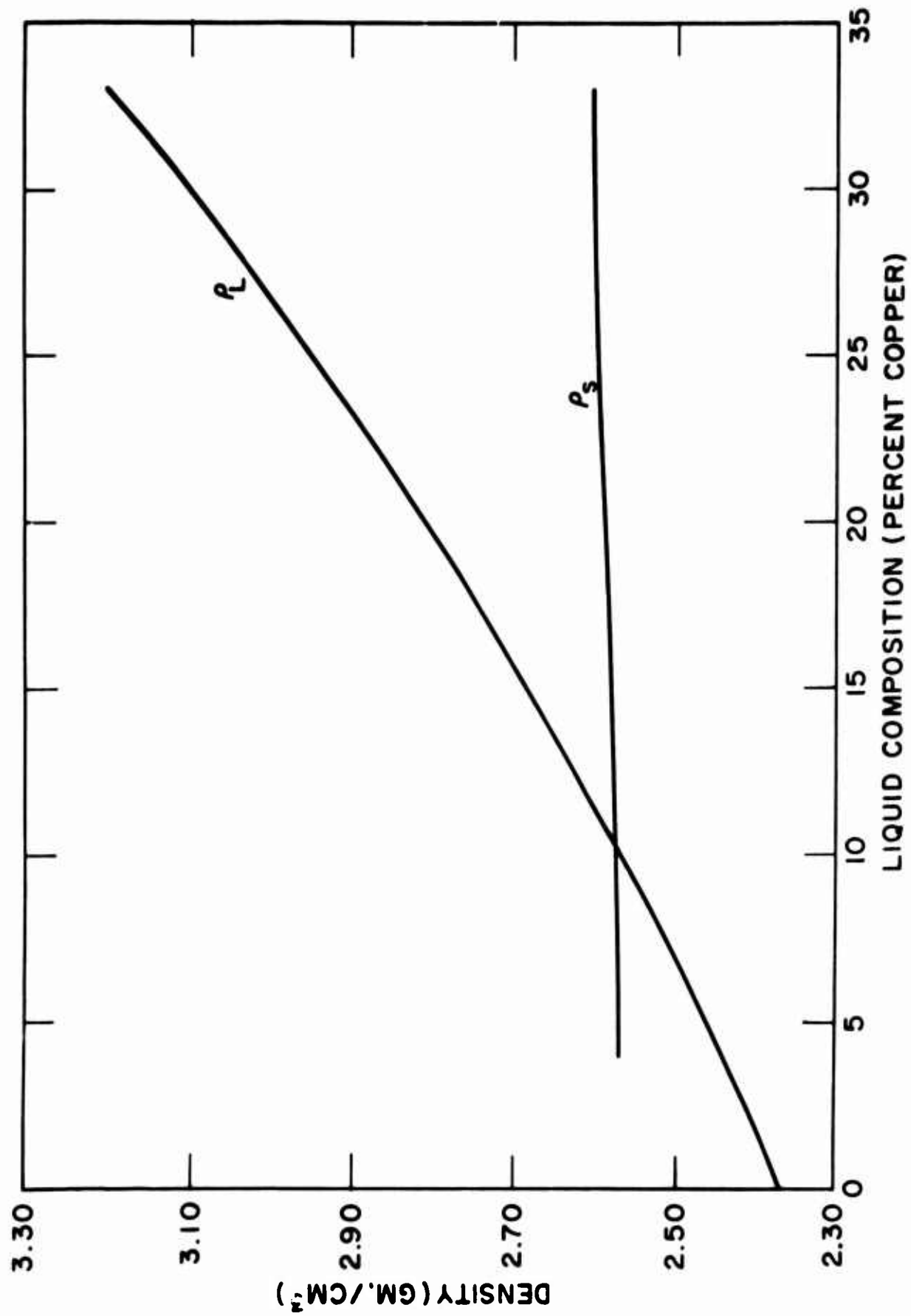
Figure 16: Liquid density (ρ_L) for aluminum rich aluminum-copper alloys and solid density (ρ_S) for an aluminum-4.5 per cent copper alloy.[41,42,45,46]
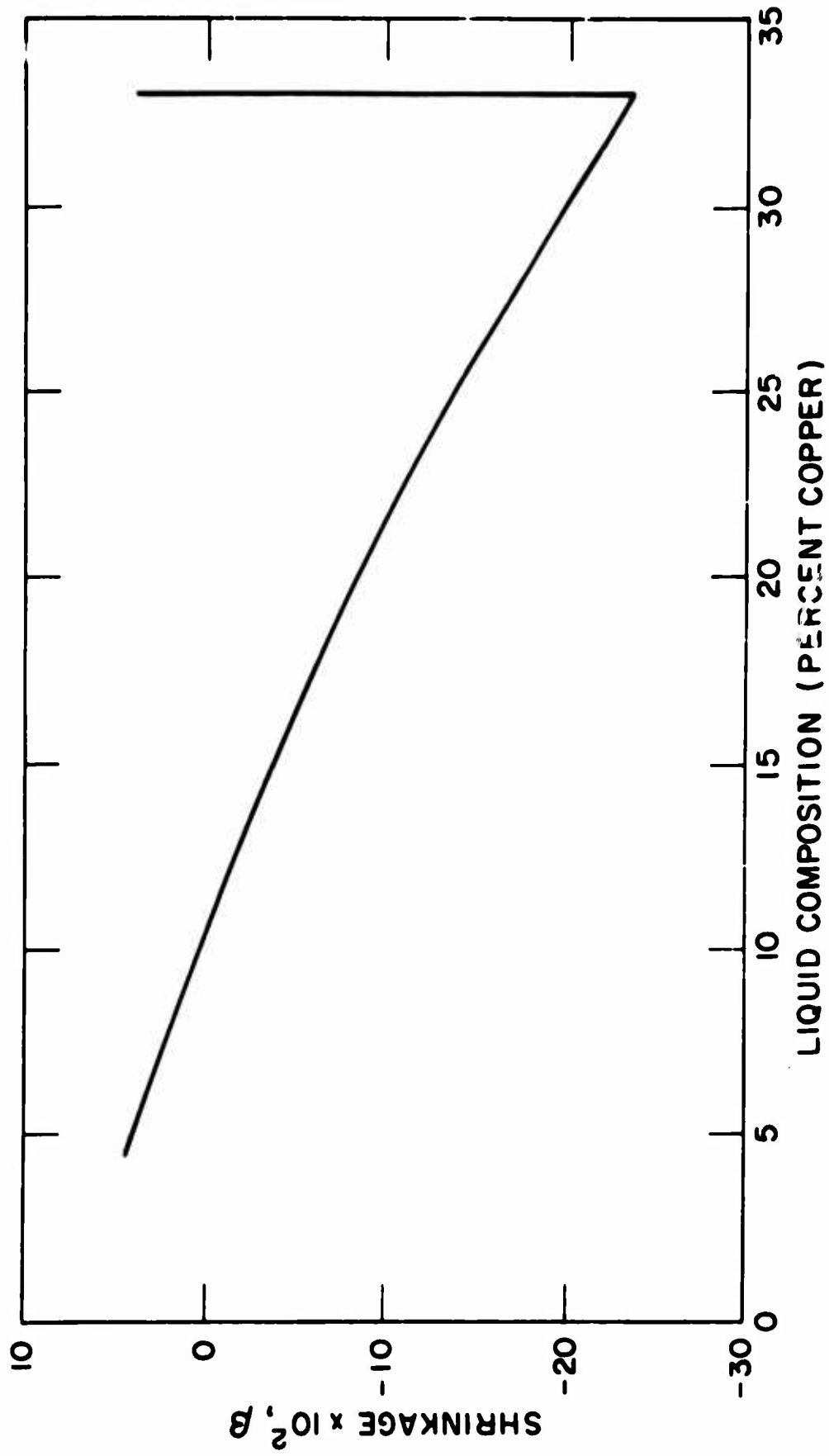
Figure 17: Solidification shrinkage for aluminum—4.5 per cent copper alloy.
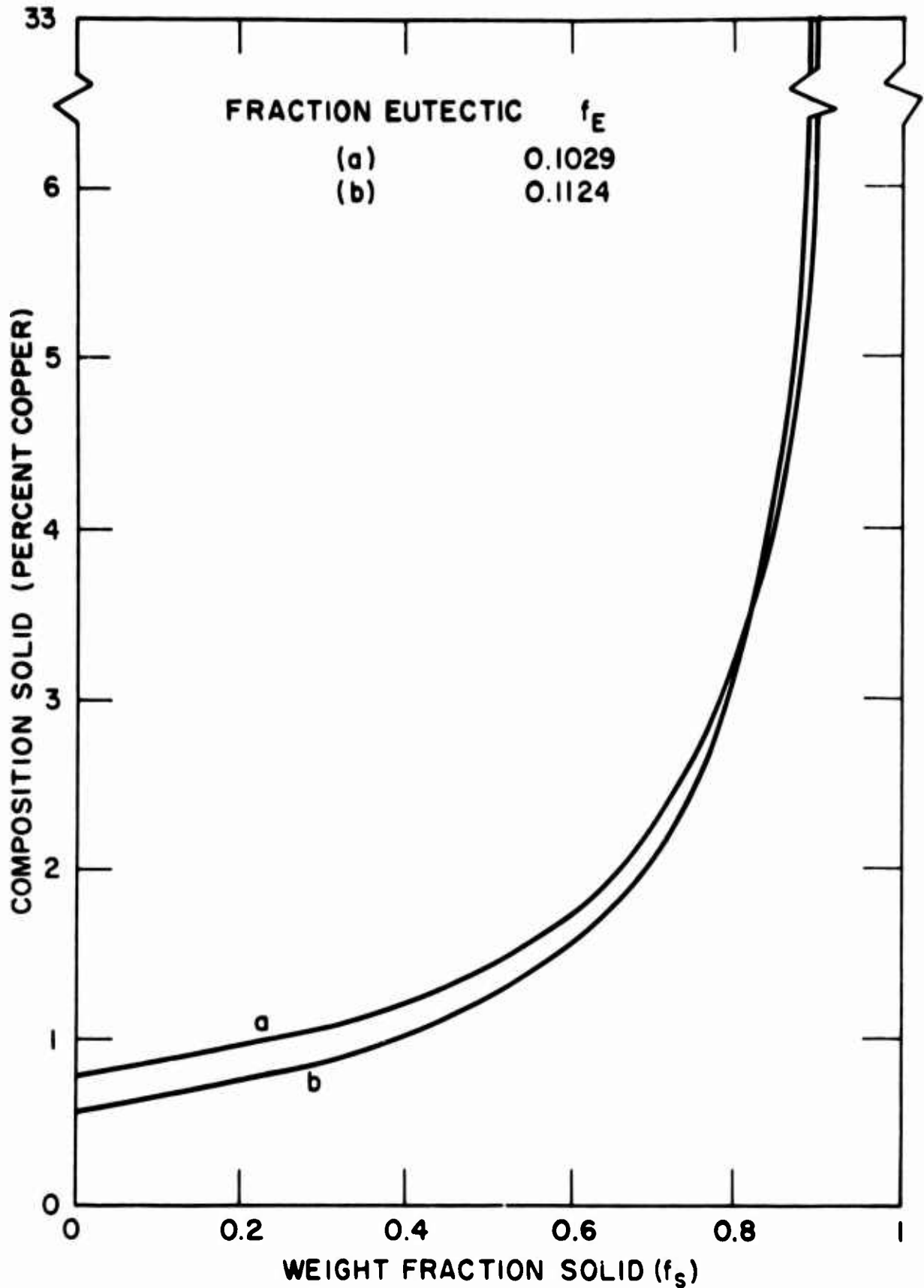
Figure 18: Steady state solute redistribution for two cases:
(a) constant, k, β direct calculation of weight = volume
fraction solid, and (b) variable k, β - calculation of
volume fraction, from density data Figure 16 conversion
to weight fraction.

Graphical integration of curve (b), Figure 18, gives a final chill face composition of 5.03 per cent. This curve, based on best available data for alloy constants, yields a final value of chill face composition close to that calculated by Scheil[6] using slightly different constants. The curve (a) in Figure 18 was calculated with constant k (k = .172), and constant β (β = .055), with the value of β chosen so that final chill surface composition is that calculated by Scheil (4.93). Note the similarity of curves (a) and (b), making reasonable the approximation used throughout much of this work, of constant β.

PART III: NON-UNIDIRECTIONAL HEAT FLOW

A. Introduction

The foregoing has been concerned only with cases where isotherms could be assumed planar, and heat flow unidirectional from the metal to a single flat mold wall. In this section we examine macrosegregation in castings or ingots in which heat flow is not unidirectional. Types of segregation include (1) centerline segregation, (2) negative "cone" of segregation, (3) positive segregation beneath risers (hot tops), and (4) others. It is assumed in most of the following, as before, that feeding is complete (no voids form during solidification). This however, is expected to be an increasingly poor assumption as thermal gradients decrease.

Figure 19 shows schematically solidification of an alloy in a metal mold. In Figure 19a, a fully liquid region remains at the ingot

center and in Figure 19b, at a later stage of solidification, this fully liquid zone has disappeared. It will be shown below that some centerline segregation will, in general, result from flow to feed shrinkage during and after the time of solidification sketched in Figure 19b. Also it will be shown that flow to feed shrinkage throughout most of solidification must result in negative segregation near the ingot base (negative "cone" of segregation).

Figure 20 is a sketch of a plate-type sand casting which may be made with, or without, a metal chill at the end of the plate opposite the riser. Figure 21 shows schematically the solidification of aluminum-4.5 per cent copper alloy in a 3/4-inch thick plate of this geometry. Temperature differences throughout most of the plate during solidification are small compared with the freezing range of the alloy, and so solidification proceeds in "mushy" manner as shown in Figure 21a. When a chill is placed at the end opposite the riser, longitudinal thermal gradients are introduced in the metal and solidification proceeds directionally towards the riser as sketched in Figure 21b. The two different types of solidification result in two distinctly different patterns of macrosegregation as discussed below.

As a final example of macrosegregation in non-unidirectional solidification, the case of segregation under a riser ("hot top") of insufficient size is considered. As example we will examine a cube, risered with a tall riser of square cross section, which is smaller than that of the cube, Figure 22. The small riser cools through the
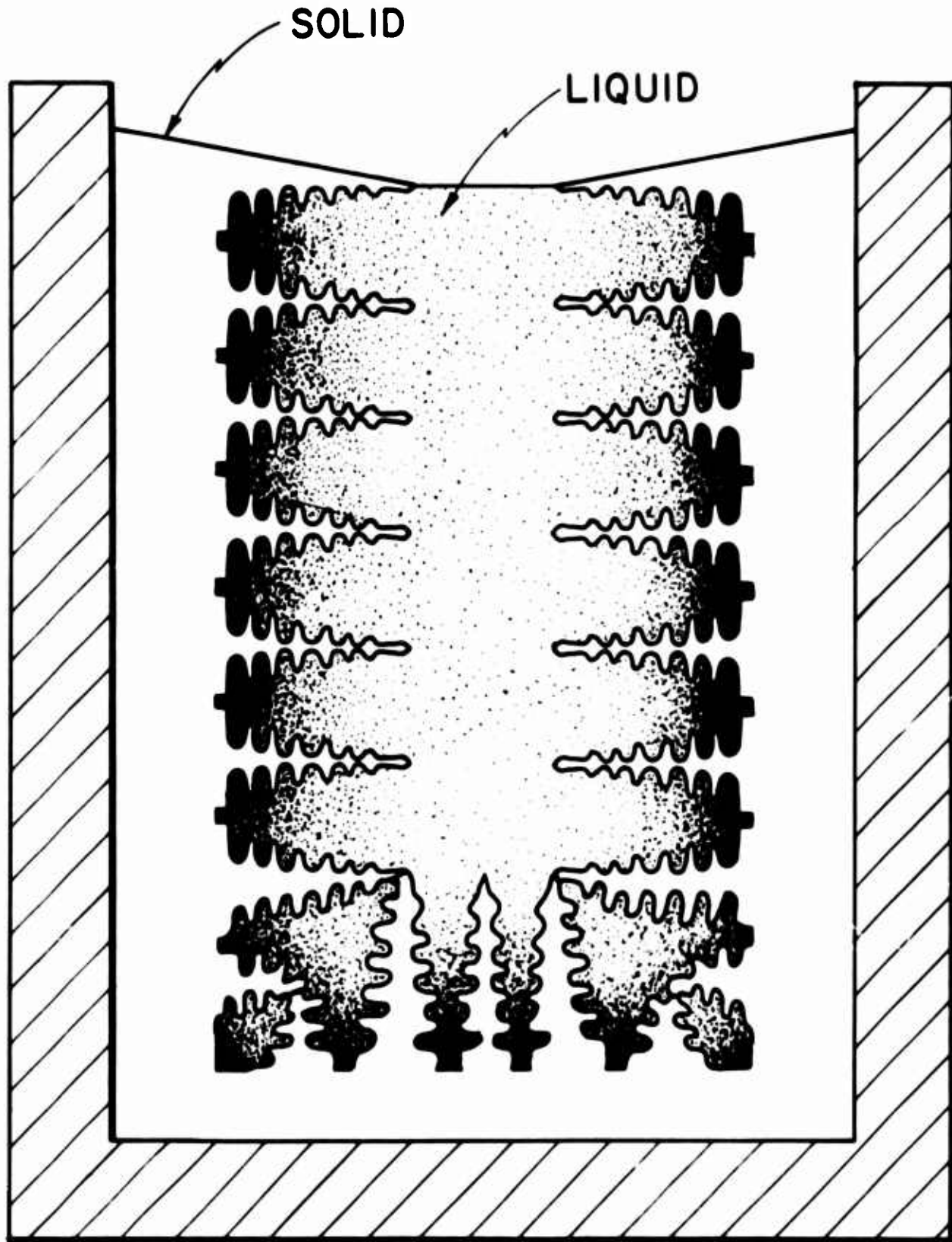
SOLID

LIQUID

Figure 19a: Sketch of ingot solidification in a metal mold showing liquid, liquid plus solid, and fully solid regions.
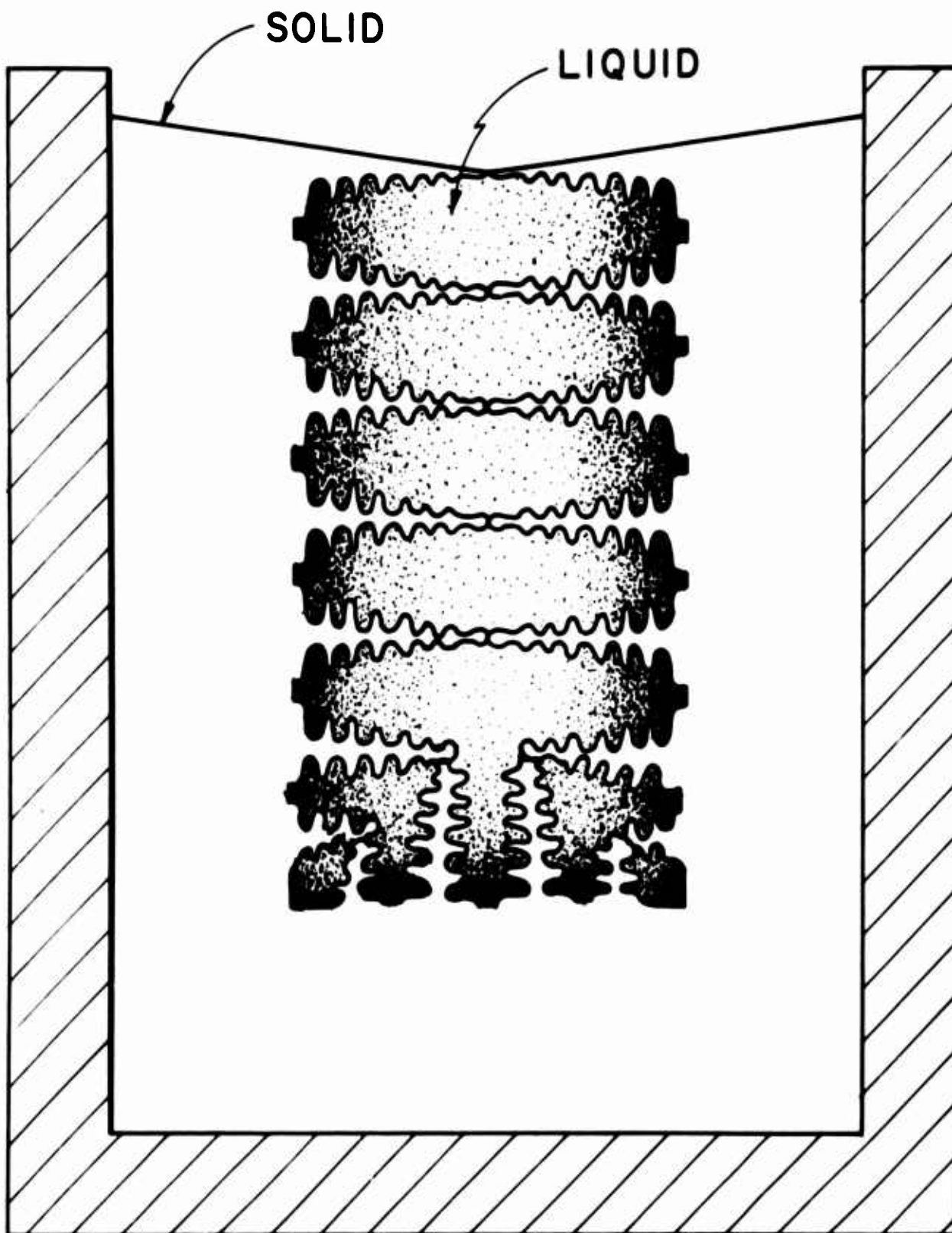
Figure 19b: Sketch of ingot solidification in a metal mold during late stages of solidification, after liquidus isotherms have met at the casting centerline.
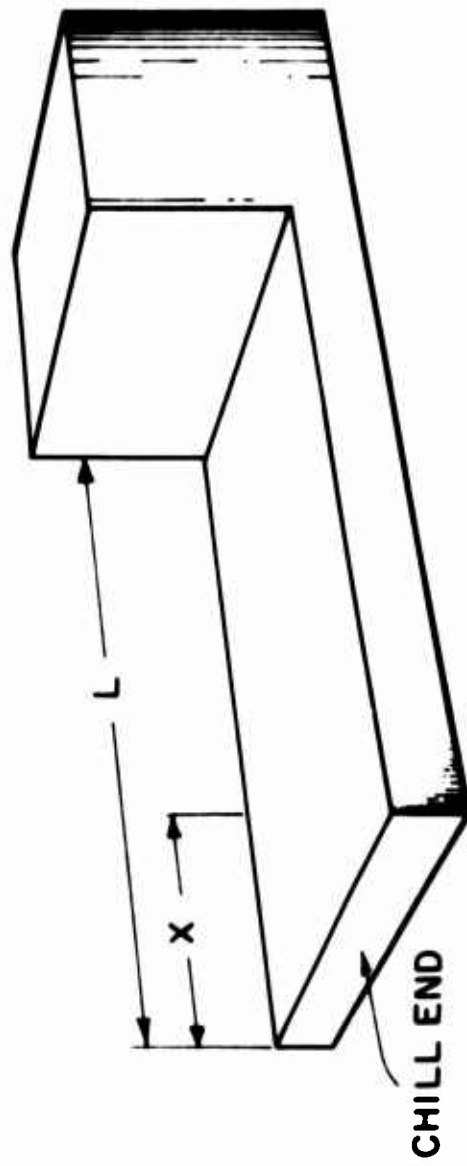
Figure 20: Plate type sand casting.
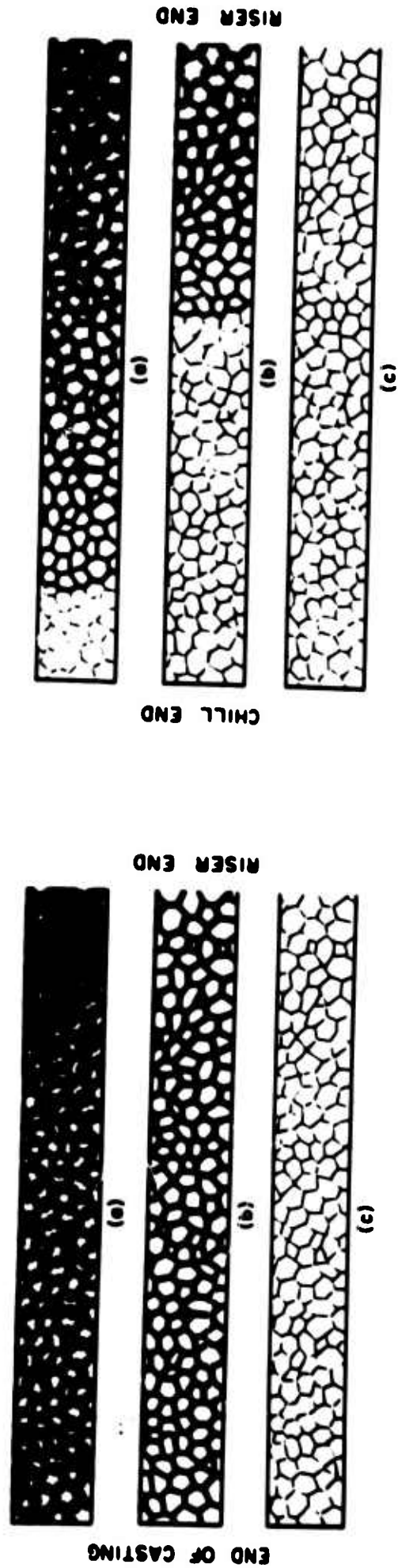
Figure 21: Schematic diagram of equiaxed solidification of sand cast plate. Left side, unchilled plate; right side end-chilled plate.

Plate 3/4" thick - (a) 1 minute after casting, (b) 4 minutes after casting, (c) 7 minutes after casting.
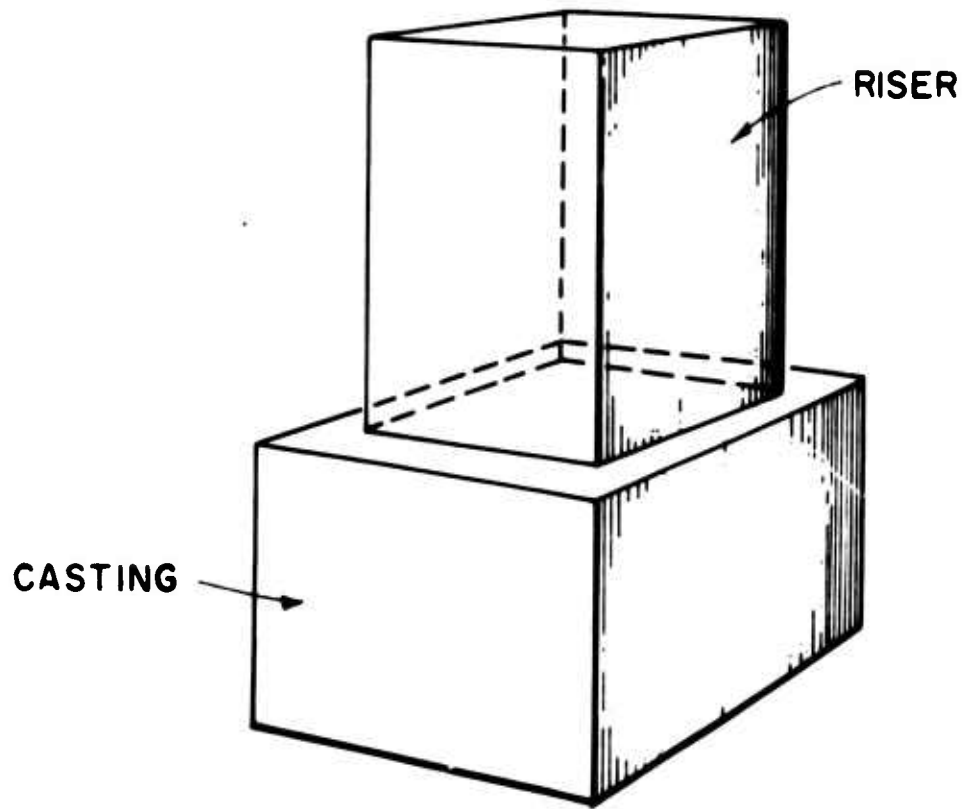
RISER

CASTING

Figure 22: Top risered cube casting.

solidification range somewhat more rapidly, than the casting and therefore contains somewhat more solid during most of solidification than does the casting. It will be shown below that this results in positive macrosegregation under the riser.

B. Centerline Segregation

1. No Contraction Strain.

Consider solidification from two flat parallel faces, so isotherms are planar and meet at the centerline, Figure 19. Before the centerline reaches the liquidus temperature, as in Figure 19a, liquid flow is expected to occur in the y vertical direction only in the region of no solid (region between the dendrite tips and the centerline) within the liquid-solid region, $v_y = v_z = 0$, and v_x is as in steady state unidirectional solidification.

When the liquidus isotherm reaches the centerline, Figure 19b, flow within the liquid-solid region must occur in the y direction. Three possible flow paths, with resulting segregation, will now be considered. In each, for simplicity, assumptions employed will include constant β, k, G, ε, and linear distribution of solid in the liquid-solid zone. Alloy used as example is again aluminum-4.5 per cent copper; n_q is assumed equal to 0 and at steady state the thickness of the mushy zone is 0.2L, where L is half thickness of this ingot.

(a) $v_y = 0$ within the liquid-solid zone except at $x' = L$. Here, all flow in the y direction is in a layer of vanishingly small thickness at the centerline. Hence, v_x at all locations up to $x' = L$ is exactly

as in steady state solidification, and G/ε is constant. Final local solute content is as in steady state solidification and no macrosegregation results at the centerline, curve (1), Figure 23.

(b) $v_y = 0$ at $x_L < L$; $v_x = 0$ after $x_L = L$. Here, the instant the liquidus isotherms reach the centerline, flow in the x direction is assumed to cease. If at this instant the fraction liquid at x' is g_L^c, then it is clear that for $g_L > g_L^c$, solute redistribution is as in steady state solidification, and for $g_L < g_L^c$, solute redistribution is at a chill face. Hence, local solute redistribution is calculated from:

$$g_L = \left(\frac{C_L}{C_0} \right)^{-\frac{1}{1-k}} \qquad \text{for } g_L > g_L^c \qquad (45a)$$

$$g_L = g_L^c \left(\frac{C_L}{C_L^c} \right)^{-\frac{1-\beta}{1-k}} \qquad \text{for } g_L < g_L^c \qquad (45b)$$

and segregation is calculated as before, and shown as curve (2), Figure 23.

(c) $v_y = 0$ at $x_L < L$; $v_y = f(g_L)$ for $x_L > L$. While cases (1) and (2) represent limits on centerline segregation which can occur in the examples chosen, v_y, and hence v_x and segregation can generally be expected to lie between the extremes chosen. For example when $v_y = f(g_L)$ solute content in the final transient region will at all locations lie between case (1) and case (2). At the beginning of the transient region composition will be C_0 while at the centerline it is the same composition as case (2) where no flow has occurred in the x
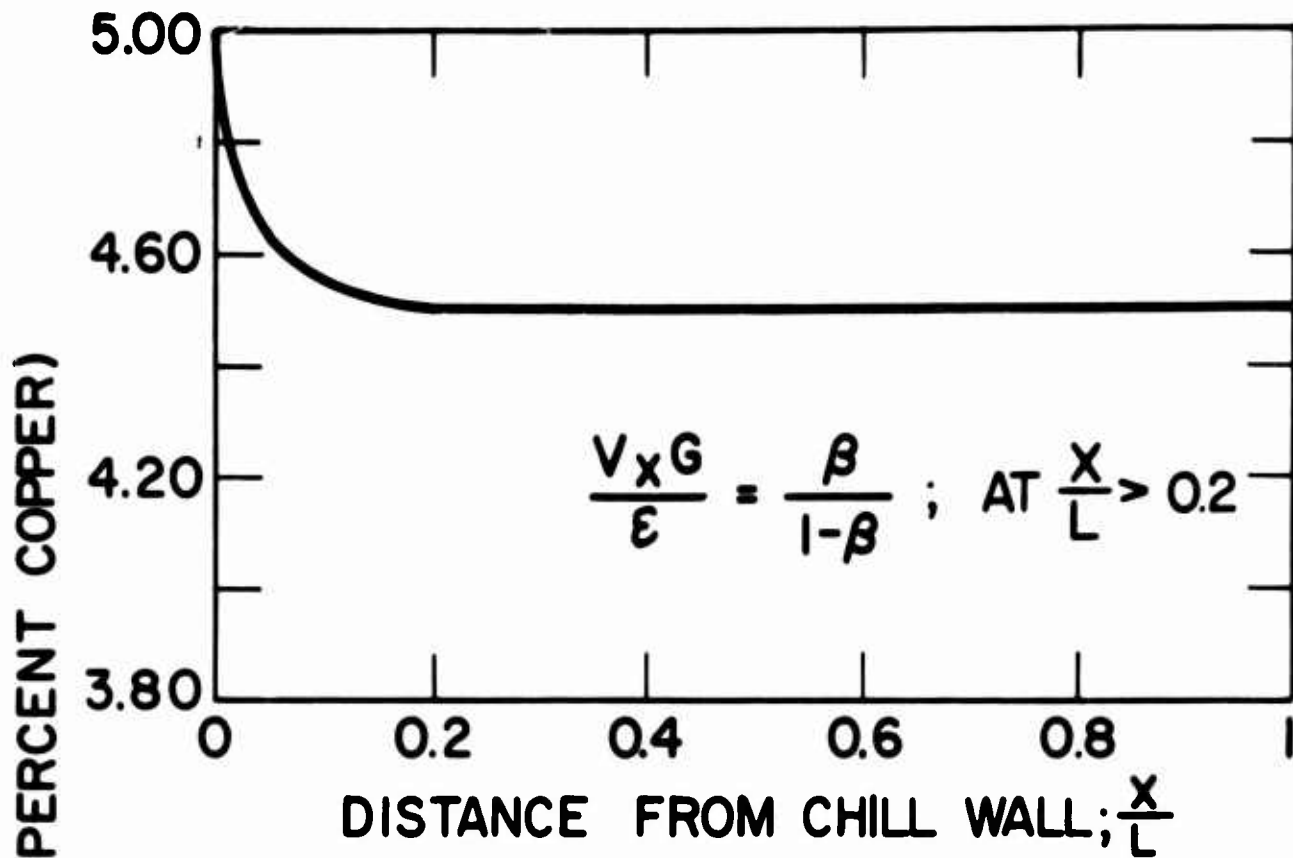
(a)
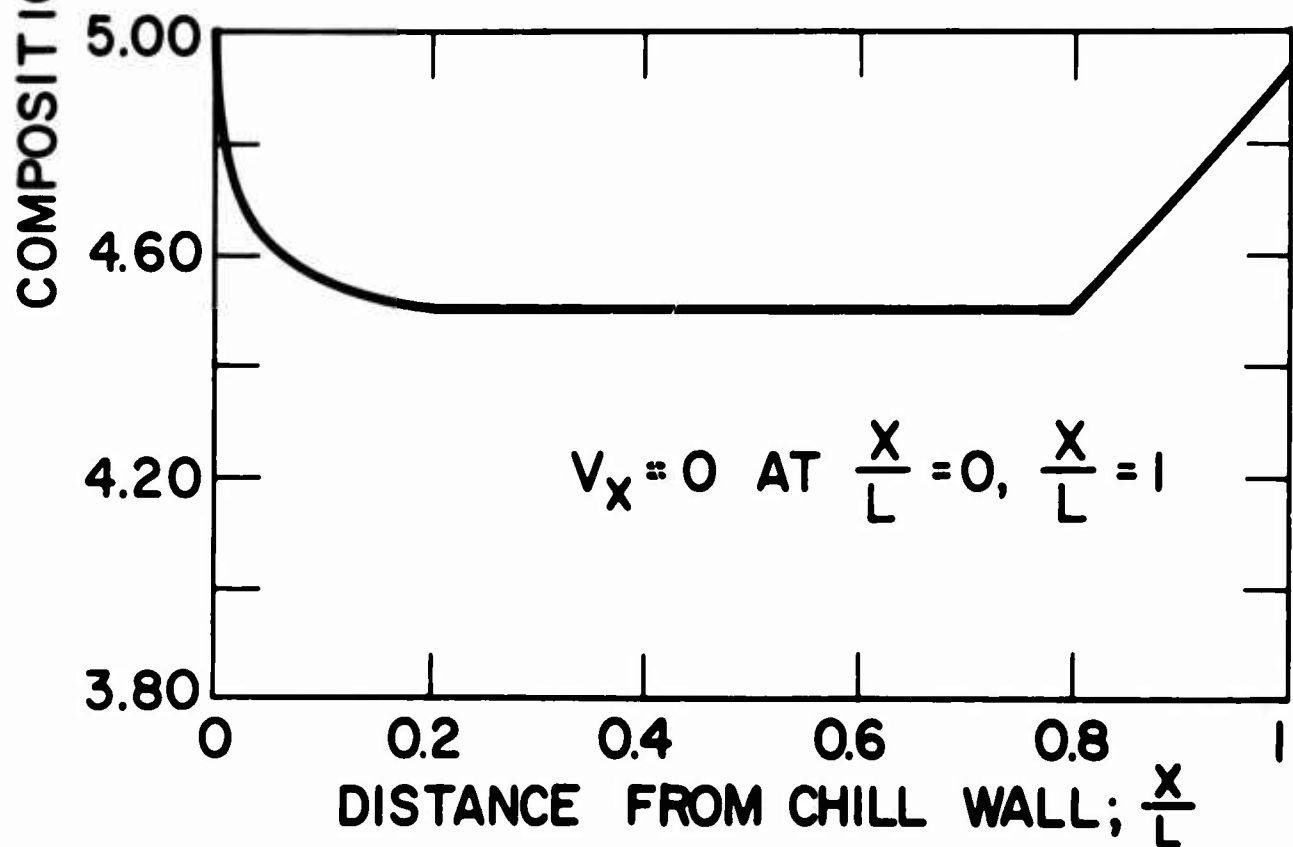
(b)

Figure 23: Final composition versus distance for two cases of ingot mold solidification. (a) Steady state $v_y = 0$, within the liquid-solid zone except at $x' = L$. (b) Steady state $v_y = 0$ at $x_L < L$; $v_x = 0$ after $x_L = L$.

direction. The shape of the curve in between these two points, however, is determined by the dependence of v_y on g_L. Solution requires detailed consideration of fluid flow within the porous medium.

2. Contraction Strain.

In the foregoing, movement of solid during solidification has not been considered. Such movement might occur by (a) floatation or settling, (b) contraction or other strain. Contraction strains can result in internal fissuring and/or "filled hot tears" at any location, x, y, z in an ingot; one example of this is at the ingot centerline, considered below.

Consider the case examined in the preceding section of solidification with planar isotherms from two flat parallel faces meeting at a centerline as shown in Figure 19; except that "fissuring" will occur from thermal contraction of the already solidified metal, at the casting centerline, $x' = L$. When the centerline just reaches the liquidus temperature, solid begins to form and is drawn away from the centerline at a velocity v from thermal contraction; hence, the "volume element" associated with this solid is also drawn away at velocity v'. At subsequent temperatures T below the liquidus, other volume elements form at the centerline, in liquid of composition $C_L^\circ > C_0$ (for $k < 1$).

For the volume element which forms at the centerline at temperature T below the liquidus (when the liquid composition at the centerline is

raised to $C_L^\bullet$), equation (20) is written:

$$\int_1^{g_L} \frac{dg_L}{g_L} = - \int_{C_L^\bullet}^{C_L} \left(\frac{1-\beta}{1-k} \right)\left(1 + \frac{v_x G}{\varepsilon} \right) \frac{dC_L}{C_L} \qquad (46)$$

The final position of the volume element at the end of solidification $(t_L + t_f)$ is:

$$\Delta L = \int_{t_L}^{t_L + t_f} v'dt \qquad (47)$$

where: t_L and t_f are times for initiation and completion of solidification at x

Δ_L = distance from casting centerline

If the only strain is from thermal contraction and the strain is small:

$$v = \int_{x = 0}^{x = x_E} Tdx' \qquad (48)$$

where: T = temperature at x

α = linear coefficient of thermal contraction at T

Qualitative conclusions from the foregoing are that thermal contraction can cause segregation at the centerline (or elsewhere) in the solidifying ingot. Segregation resulting from this contraction is additive to that resulting from solidification contraction.

Equations (46) and (48) can be used to evaluate thickness of segregated zone, and g_L and C_L at any location within the zone during solidification. Hence, final segregation at the centerline is readily calculated as above.

Consider, for example, the unidirectionally solidification aluminum-4.5 per cent copper alloy used as example above, constant k, β, G, ε linear distribution of solid in the liquid-solid zone (with z). Assume near the region in question fluid flow (to feed thermal contraction and shrinkage) occurs only by (a) flow down the ingot centerline, parallel to isotherms, and (b) flow perpendicular to isotherms at locations other than the centerline.

Hence, $\dfrac{v_x G}{\varepsilon} = \dfrac{\beta}{1 - \beta}$ so equation (31) becomes:

$$g_L = \left(\frac{C_L^{\circ}}{C_L} \right)^{-\frac{1}{1 - k}} \qquad (49)$$

Figure 24 plots C_S versus g_S for three values of C_L°, (a) $C_L^{\circ} = C_0 = 4.5$ per cent copper, (b) $C_L^{\circ} = 20$ per cent copper, and (c) $C_L^{\circ} = 33$ per cent copper.

Assume now thermal contraction was such that each volume element moved .001 cm/per cent increase in solute at the centerline. Hence, a segregated centerline results of thickness (.001)(33) = .033 cm in which the average composition varies linearly from 4.5 per cent copper to 33 per cent, Figure 25.
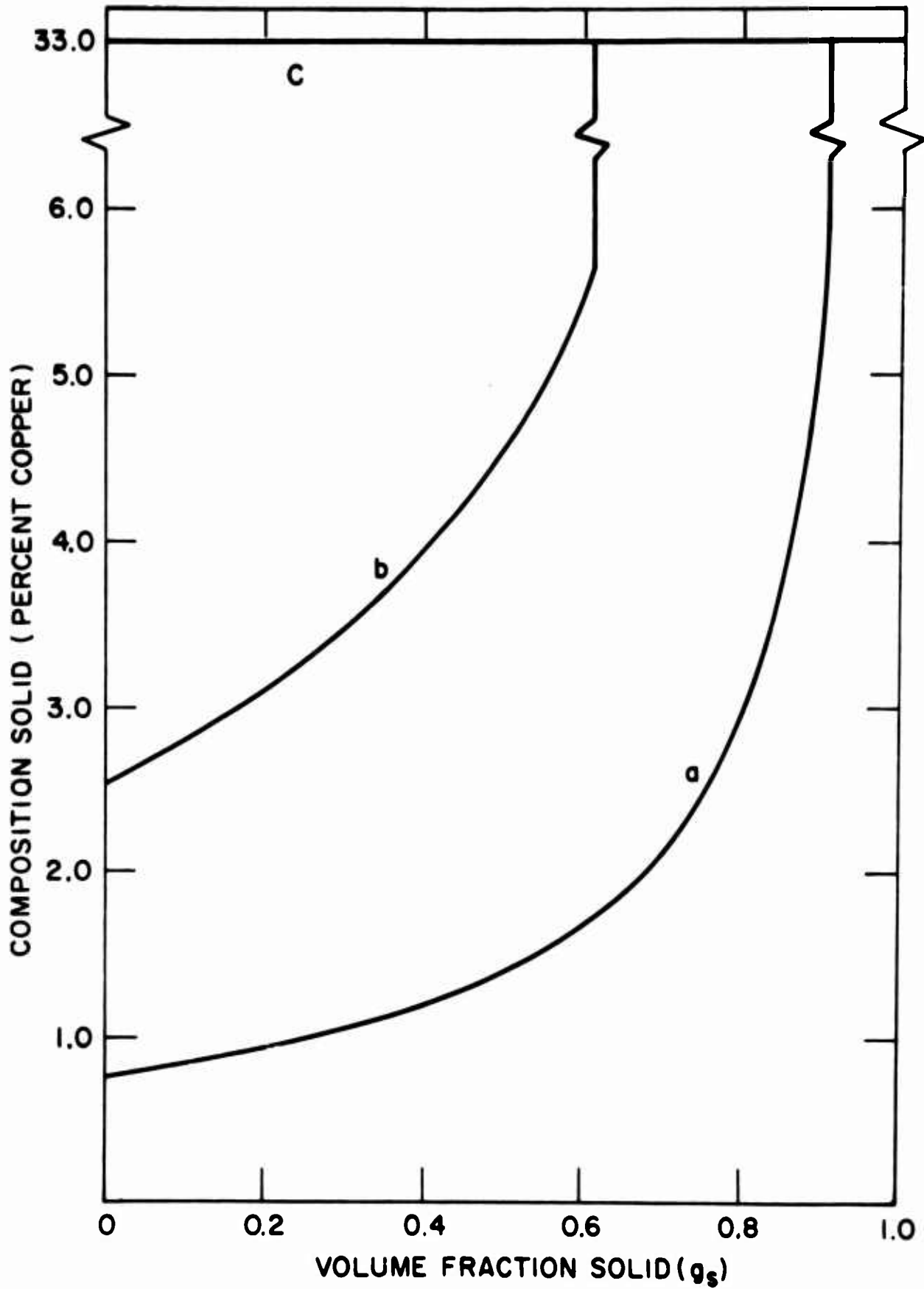
Figure 24: Solid composition, $\bar{C}_S$, versus volume fraction solid, g_S, for three values of C_L°; (a) $C_L^\circ = C_0 = 4.5$ per cent copper, (b) $C_L^\circ = 20$ per cent copper, (c) $C_L^\circ = 33$ per cent copper.
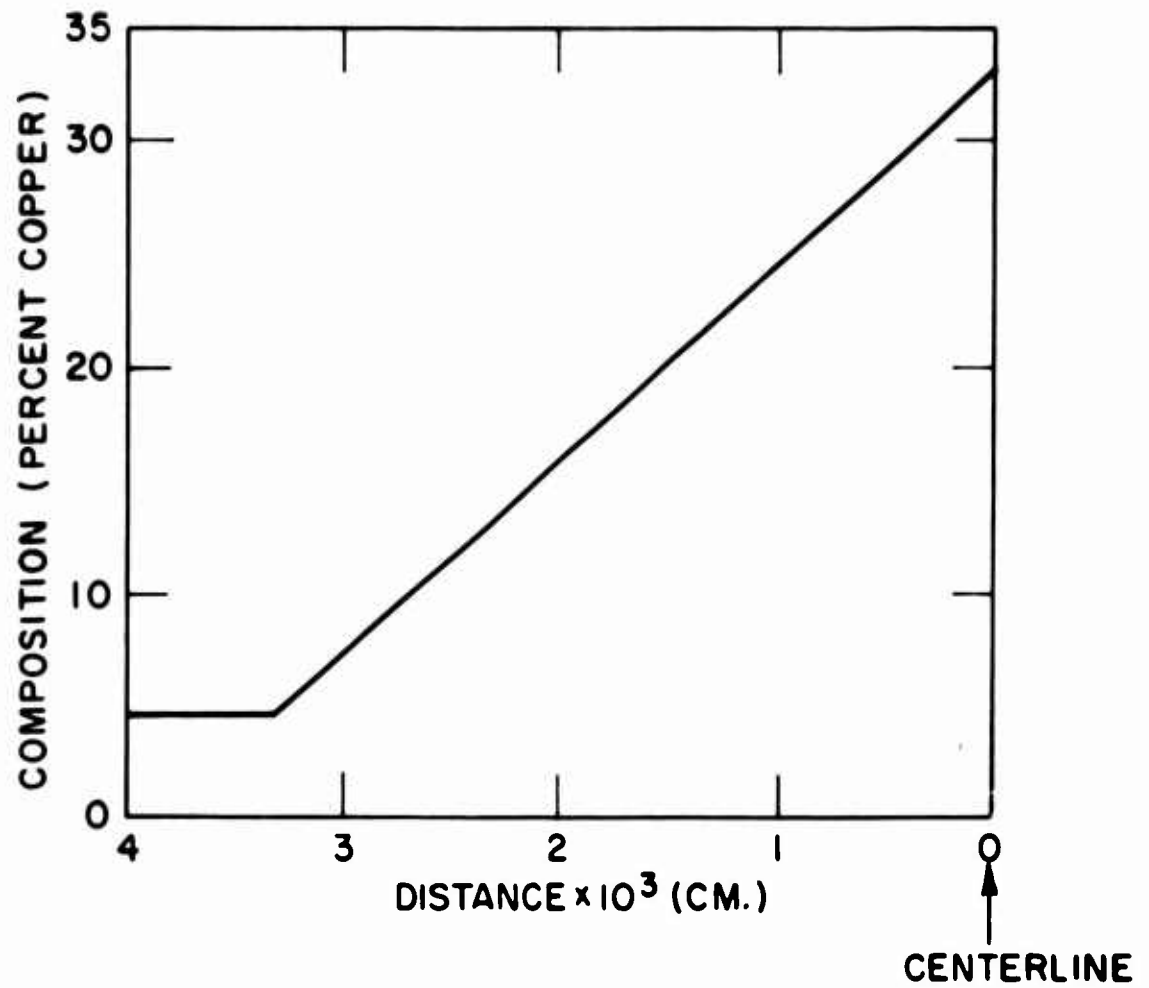
Figure 25: Centerline segregation resulting from thermal
con'raction of .001 cm/per cent increase in solute
at the centerline.

C. Negative "Cone" of Segregation at Ingot Base

Consider solidification of the bottom portion of the ingot illustrated in Figure 19. Assume as limiting case that

(1) at the periods of solidification represented by Figure 19a, feed metal flows into the bottom "cone" (represented by the dendrites growing vertically) only from the fully liquid region, and

(2) after the dendrites growing from the sidewalls reach the centerline, flow into the "cone" is all through a small channel at the apex of the cone.

Now, assume an ingot of long rectangular cross section (long dimension perpendicular the planr of the paper). The "cone" then is a prism, and hereafter referred to as such. Moreover, fluid flow into this prism is exactly as in the prism ingot discussed earlier (Figure 13) and final composition within the prism is expected to be as given in Figure 14. Note that compositions particularly near the apex, are substantially below nominal, in qualitative agreement with experiments on large ingots which show what is commonly termed the "negative cone" of segregation.

D. Macrosegregation in Sand Cast Plates

In sand castings temperature gradients within the solidifying metal are generally small, because of the low heat diffusivity of the mold compared with that of the metal. Where these are negligible, and where feeding is complete, the term $\dfrac{v_x G}{\varepsilon}$ in equation (20) is zero.

For the plate shown in Figure 20 solidification is sketched in
Figure 21. Significant macrosegregation is expected through the
plate, approaching the maximum expected at a chill face in unidirec-
tional solidification (as temperature gradient in the longitudinal
direction goes to zero, assuming complete feeding). In the region
near the riser, some thermal gradients are expected, and hence, some
reduction in final composition in this area is also expected.
Figure 26 illustrates this schematically for aluminum-4.5 per cent
copper alloy.

In the end chilled plate, Figure 21b, steep longitudinal gradients
are introduced by the chill, and although some heat is lost to the
cold sand mold, isotherms are expected to be essentially planar, and
perpendicular to the longitudinal (x') direction. Since the isotherms
are assumed planar, relations developed in earlier sections for
"unidirectional solidification" apply here as well. Movement of the
isotherms, however, is expected to depend on plate geometry and heat
diffusivity of the mold as well as on rate of heat removal through
the chill. Figure 26 illustrates composition distribution expected
assuming (1) movement of isotherms throughout most of the plate is as
in unidirectional solidification from a metal chill, no interface
resistance, but (2) isotherms approach each other near the riser end
of the plate.
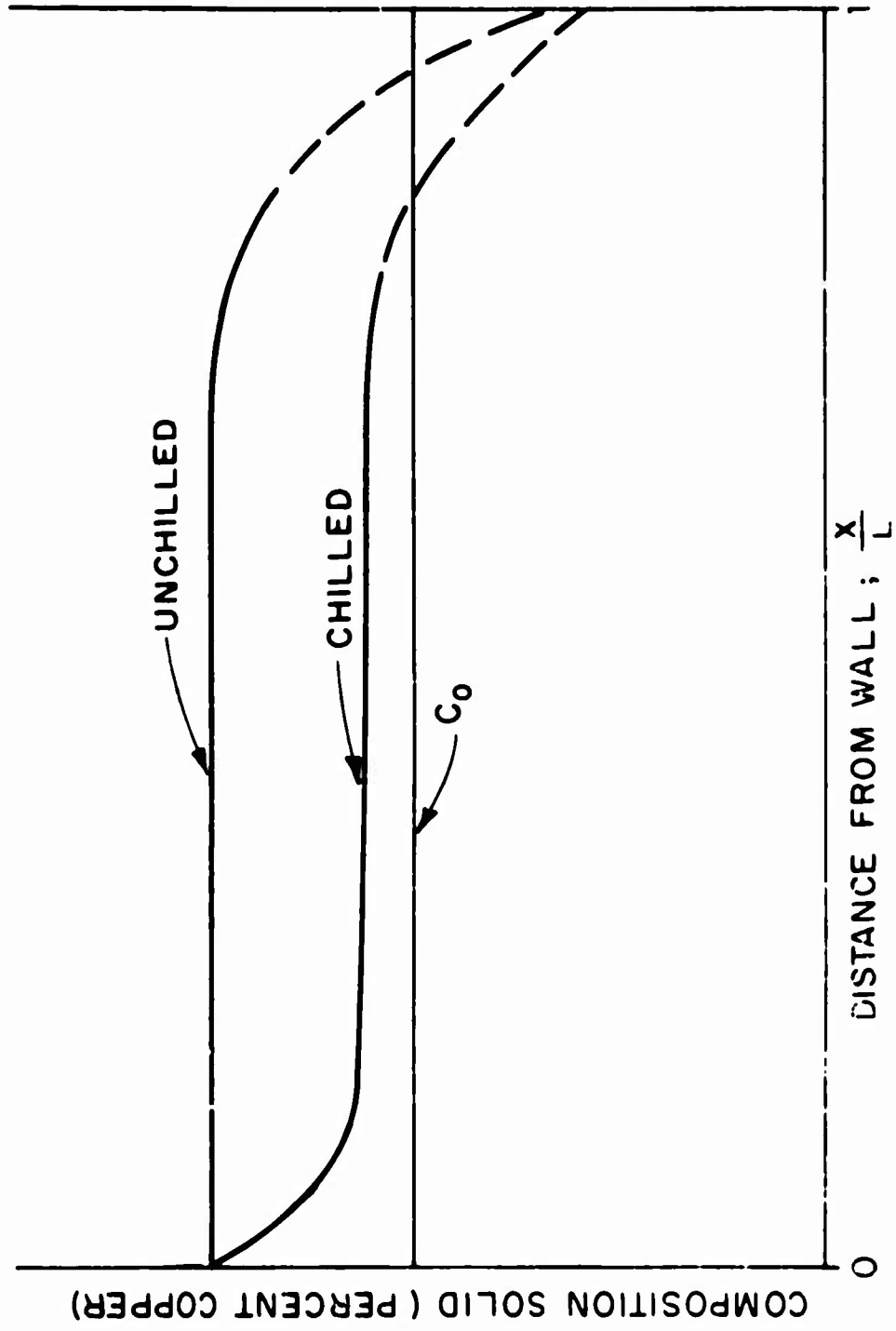
Figure 26: Schematic diagram of composition versus distance in a sand cast plate and a chilled, sand cast plate.

E. Under Riser Segregation Positive Segregation Near "Hot Top"

For one example of under riser segregation consider the risered sand cast cube of Figure 22. Here, the riser chosen is inadequate to feed the cube and at any time during solidification the metal in the riser area will contain more solid than the metal in the casting, Figure 27.

Thermal gradients are assumed small in the horizontal (y and z) directions of casting and riser. The thermal gradient is also assumed small in the x direction except in the region between the casting and riser. To illustrate the problem simply, assume temperature difference between bulk riser and bulk casting are constant during solidification, and the temperature gradient in the vicinity of the casting and riser junction is constant.

Consider first solidification in the bulk riser, well away from the casting riser junction; here, $G = 0$. Since v_x and ϵ are finite $\frac{v_x G}{\epsilon} = 0$ and maximum segregation, as at a chill face, is expected (provided no pores form), except in the region at the top of the riser where negative segregation occurs as a result of liquid depletion.

Similarly, while feeding occurs, solute redistribution in the bulk casting must be as at a chill face (at locations well away from the casting-riser junction). However, at some critical fraction solid, g_S^c which must occur not later than when the riser reaches T_E, its non-equilibrium solidus, all feeding is expected to cease. Final composition in the bulk casting is therefore expected to be less than
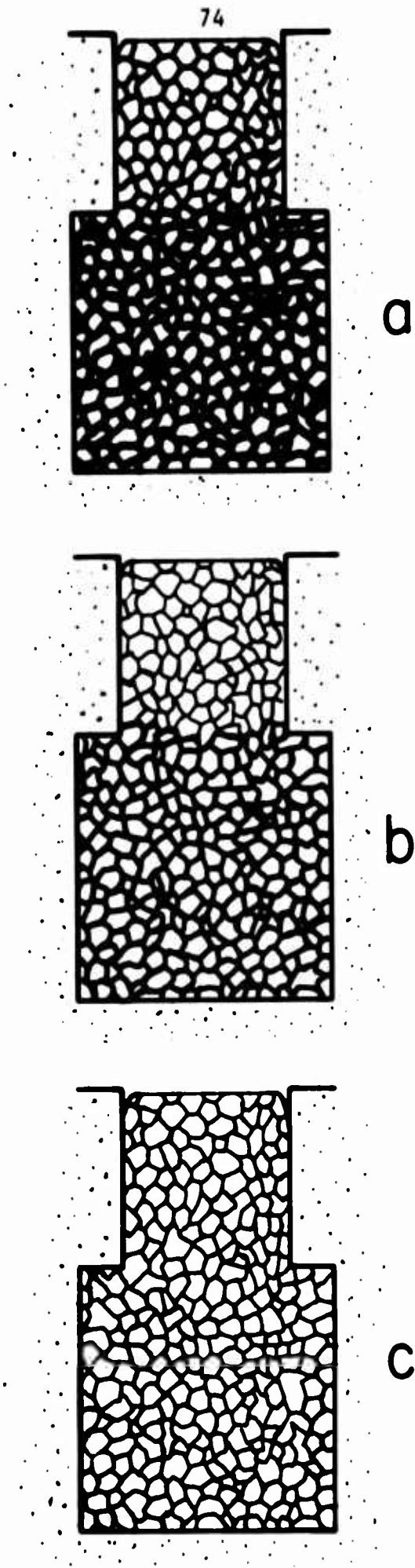
Figure 27: Sketch of solidification for cube casting of Figure 22.

the chill face maximum, by an amount determined by the time during solidification when feeding ceases. This composition will however, be at least slightly greater than C_O.

In the region at, or just below, the riser-casting junction, we expect composition to be significantly higher than in the bulk casting. This is because, as long as flow occurs in this region, it is flowing up a temperature gradient; hence $\dfrac{v_x G}{\varepsilon}$ is positive and compositions in excess of the chill face maximum are possible. Compositions in excess of the chill face maximum must result as long as there is a net flow of solute up a temperature gradient, and this flow continues to the last stages of solidification.

III. EXPERIMENTAL RESULTS AND DISCUSSION

In this section, results are presented from experiments designed to illustrate and substantiate certain aspects of the general macrosegregation expression previously developed. In particular, consideration is given to the parameter, $\dfrac{v_x G}{\epsilon}$ in equation (20)

$$\frac{dg_L}{g_L} = - \left(\frac{1 - \beta}{1 - k} \right)\left(1 + \frac{v_x G}{\epsilon} \right) \frac{dC_L}{C_L} \tag{20}$$

This solute redistribution expression is for the case of unidirectional heat flow, but where fluid flow is not necessarily unidirectional.

As previously discussed for a particular alloy system and composition, values can be assigned which effectively average k and β over the complete solidification range, even though they are usually functions of C_L. Using the values β = .055 and k = .172 as the constants for this particular alloy composition, consideration can then be given to the effect of solidification variables on the parameter $\dfrac{v_x G}{\epsilon}$. The following experimental results are presented to show how variations in this parameter can cause compositional changes throughout a casting or ingot.

A. Unidirectional Heat and Fluid Flow

  1. Constant Cross Section.

Consideration is first given to experimental results on four ingots of constant cross section where both heat and fluid flow are

unidirectional. The ingots were made using the experimental set up described in Appendix E. Ingots 1 - 3 are of square cross section 7.5 cm per side, 20 cm high. Ingot number 4 is circular 11.5 cm in diameter and 20 cm high.

(a) Ingot Number 1.

Ingot number 1 was cast and solidified on a water cooled chill. Furnace temperature was maintained high enough to obtain a completely columnar casting structure. Cooling curves for the ingot are shown in Figure 28. From these curves Figure 29 was constructed, showing liquidus and eutectic isotherm movement as a function of time. It is interesting to note that even though a water cooled chill was used, after 720 seconds the mushy zone extends the entire length of the casting. That is, at the same time the metal at the chill first becomes completely solid, initial solid is forming at the top. This means that at least the initial stages of solidification, at all locations, is under the initial transient conditions previously considered (i.e., $x < x_c$).

Calculation of composition up the length of the ingot using only thermal data was done as described in Appendix G. Agreement between this and the experimentally determined curve (using fluorescent analysis for chemical analysis, see Appendix F) is shown in Figure 30.

Calculated agreement becomes poor at distances greater than 10 centimeters from the chill. It can be seen from the thermal data of Figure 28 that at this location gradients become shallow (typically
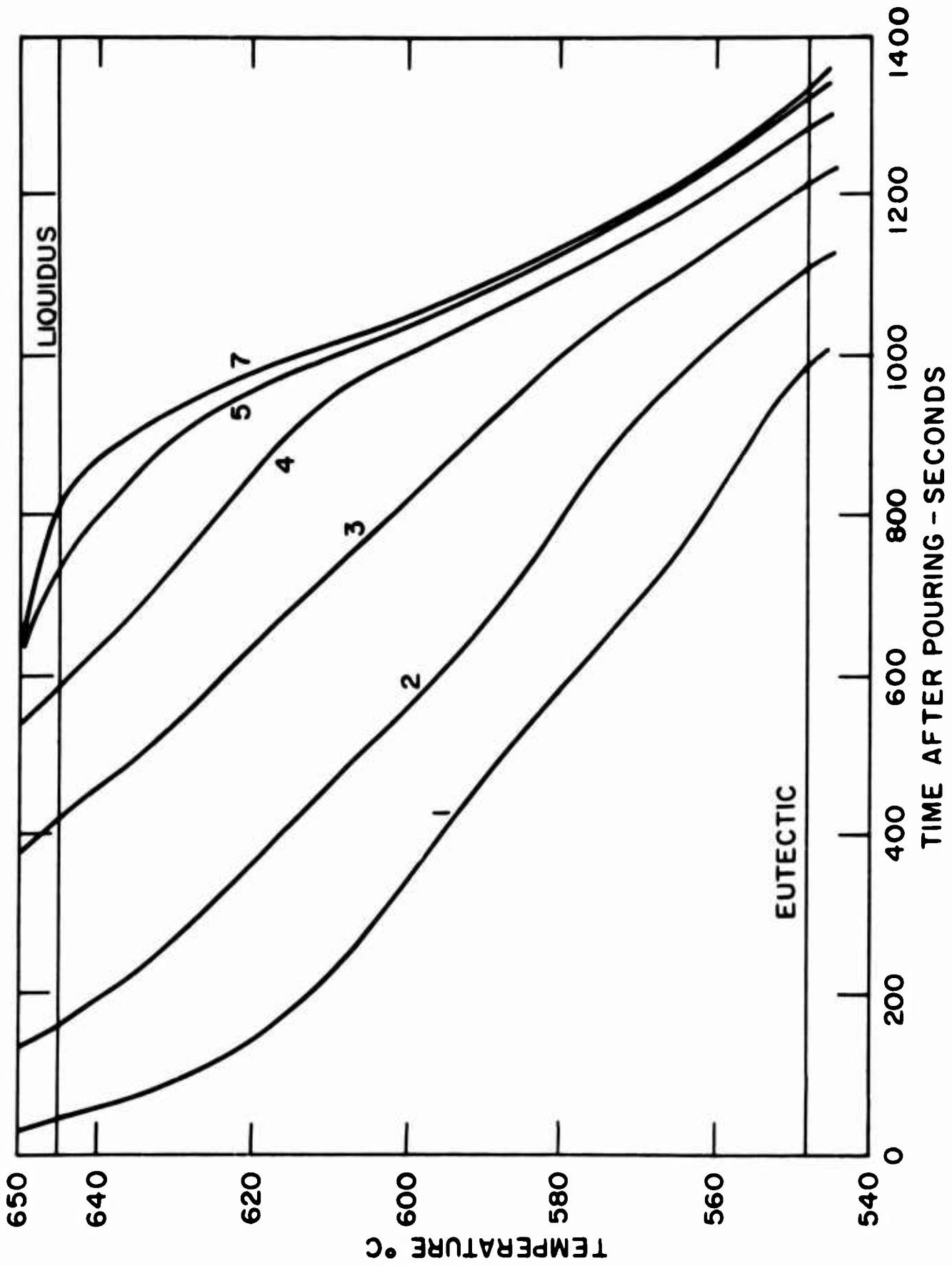
Figure 28: Cooling curves for Ingot No. 1 at locations 1, 2, 3, 4, 5 and 7 inches from the chill.
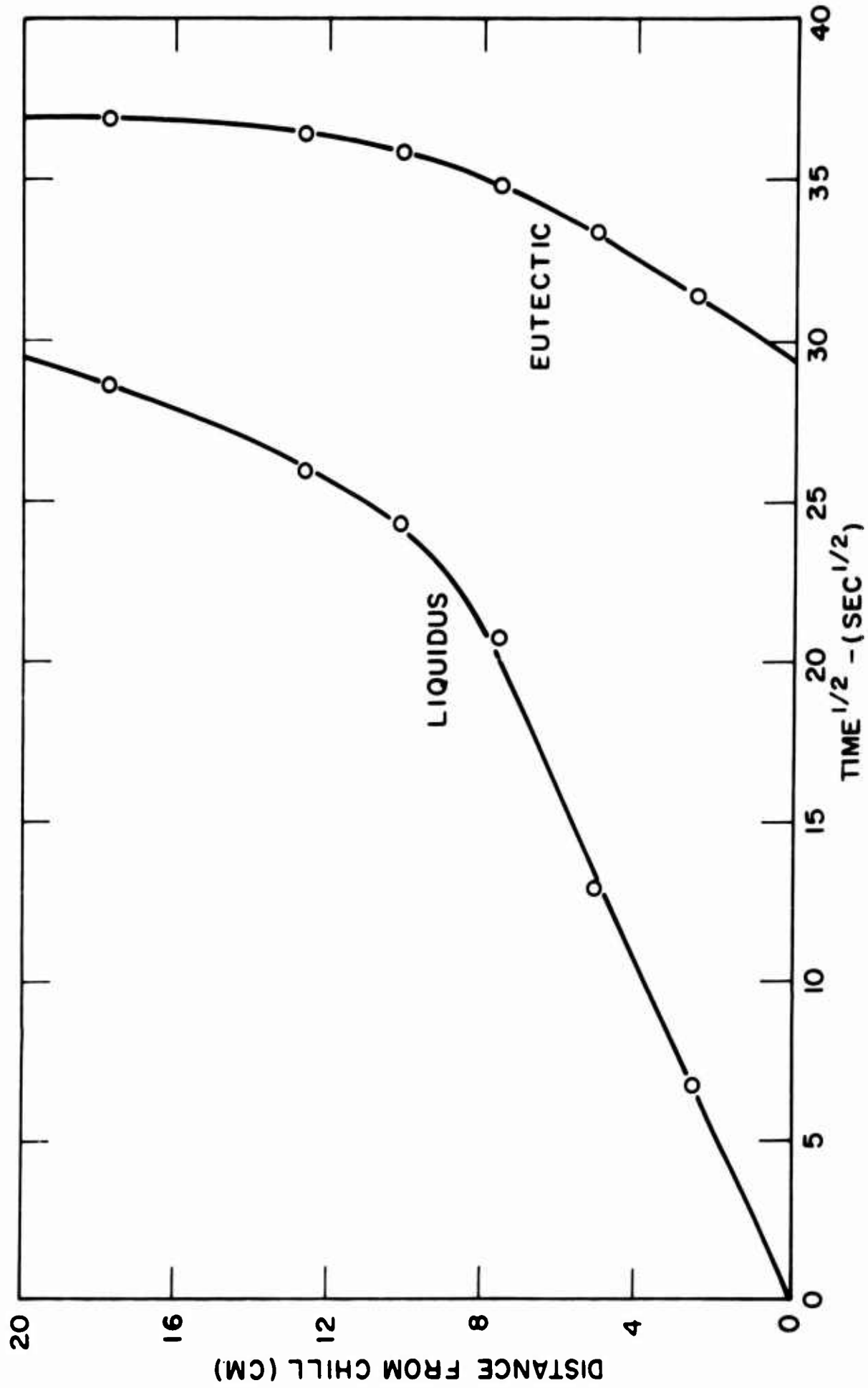
Figure 29: Liquidus and eutectic isotherm movement for Ingot No. 1.
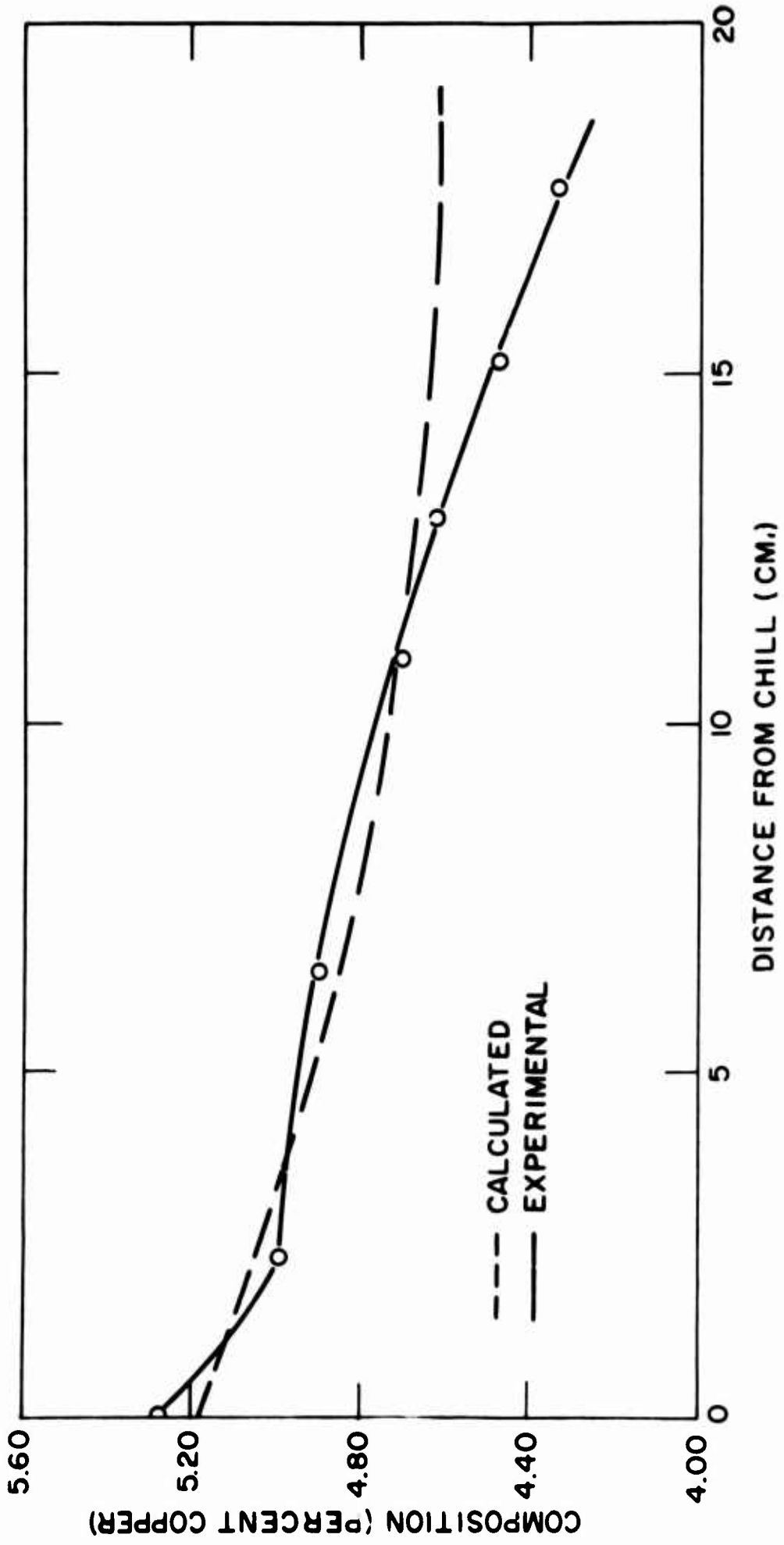
Figure 30: Experimental and calculated (from thermal data) solid composition versus distance from chill in Ingot No. 1.

2 - 5°C/cm), a condition which can lead to porosity and therefore
lower composition.

(b) Ingot Number 2.

Ingot number 2 was also cast and solidified against a water
cooled chill. Furnace temperature was lower than for the preceding
ingot, and resulted in an equiaxed ingot structure, even though heat
flow was unidirectional. Insufficient thermal data is available for
complete analysis, but liquidus and solidus isotherm movements were
recorded. An initial transient of about 5 centimeters (Figure 31)
exists which is seen from the increased composition at locations
less than 5 cm, Figure 32.

In the region after the initial transient, n_q (equation 34),
which reflects the relationship between isotherms, changes very little.
At locations greater than 5 cm, n_q varies from .8 to 1.0. Figure 10
shows that within this range of n_q values composition is not expected
to vary more than .03 per cent and within experimental limits should
be relatively constant. This is the case in the region from 5 to
about 15 cm from the chill where composition is about 4.68 per cent
copper. It is also expected (Figure 10) that within this region
(i.e., 5 - 15 cm, n_q = .8 - 1.0) average composition will be slightly
greater than C_0. For this ingot C_0 is 4.60 per cent copper, less than
the composition in the 5 - 15 cm range (4.68 per cent). Toward the
top of casting (greater than 15 cm) composition begins to drop off
since solute must be conserved.
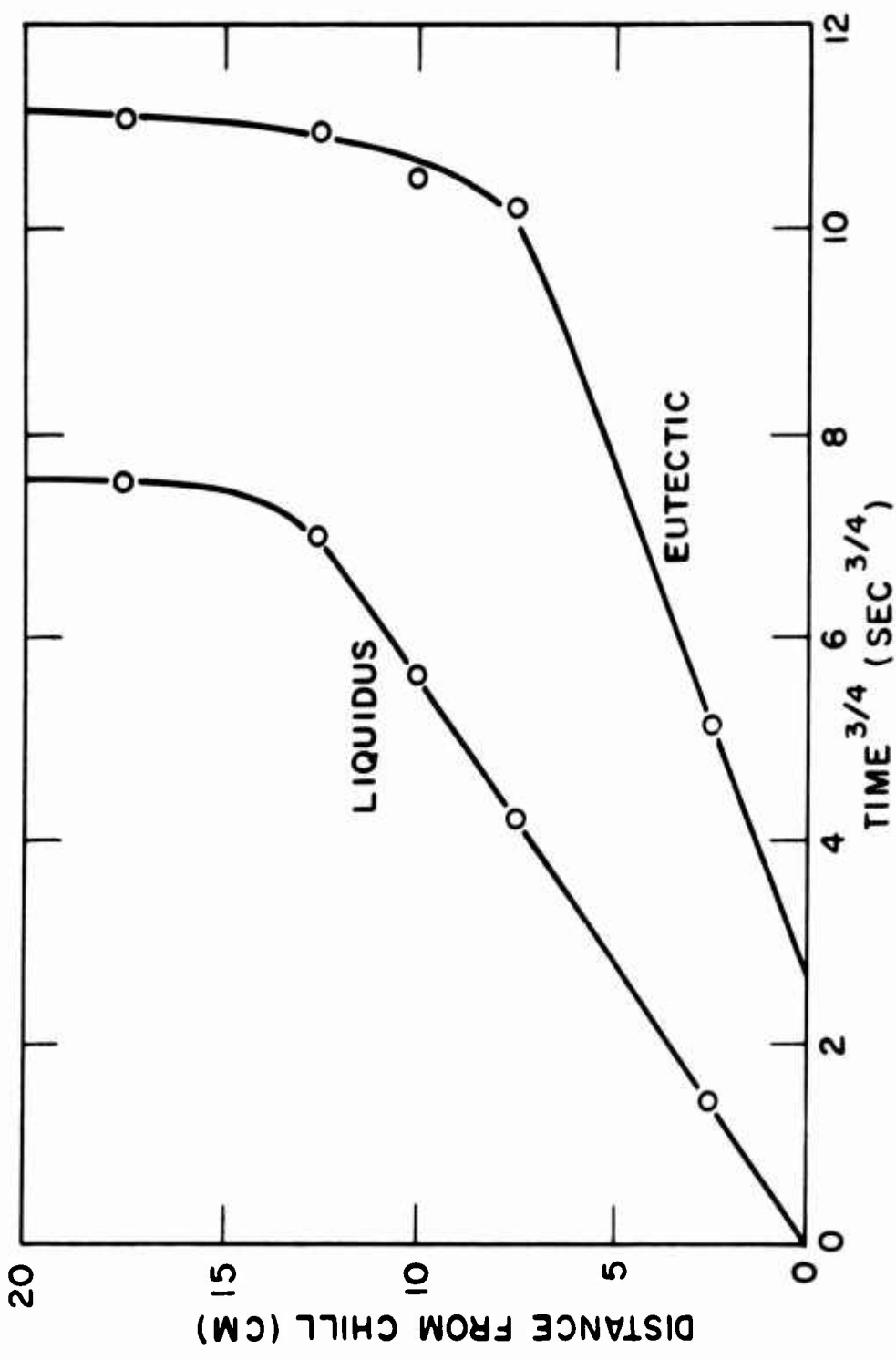
Figure 31: Liquidus and eutectic isotherm movement for Ingot No. 2
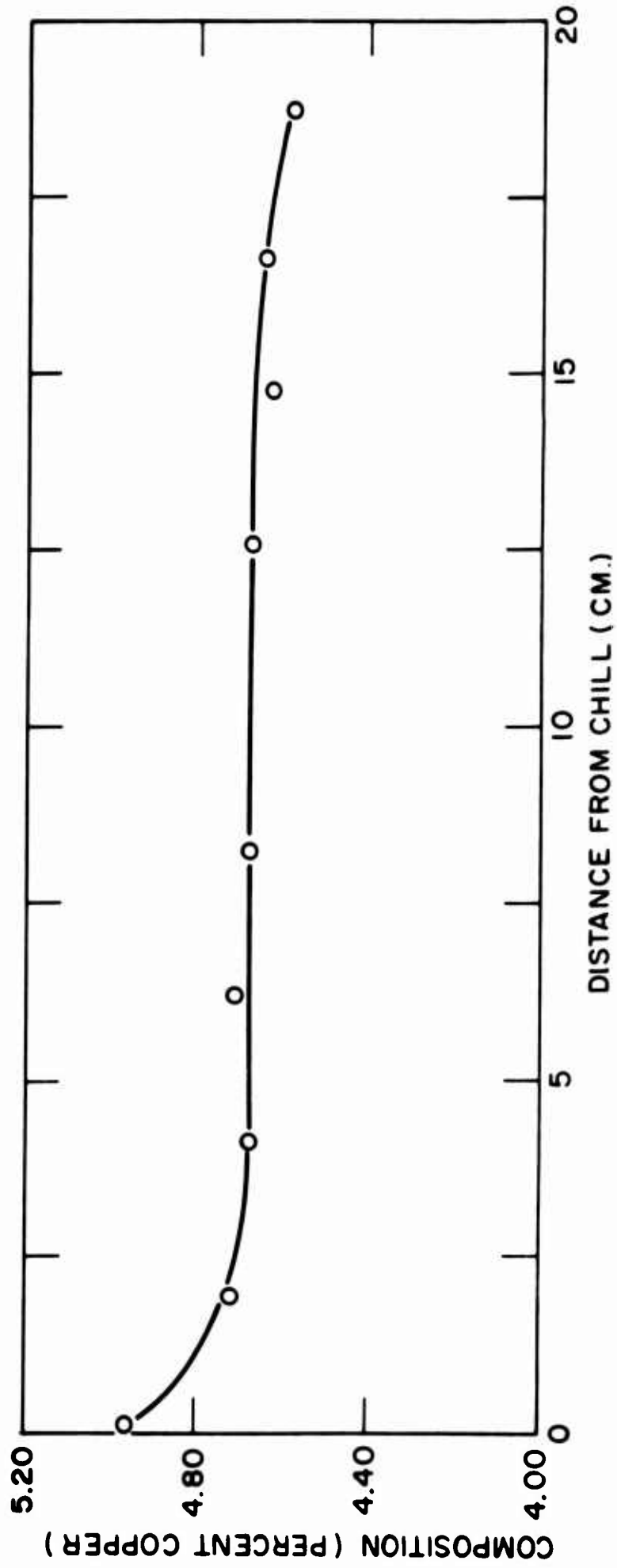
Figure 32: Solid composition versus distance from the chill in Ingot No. 2.

(c) Ingot Number 3.

Ingot number 3 was cast and solidified against a chill which had both air and water for a coolant. Figure 33 presents the experimental and calculated (from thermal data) composition curves. At locations greater than 15 centimeters where gradients are shallow and porosity forms, agreement between experimental and calculated curves breaks down. The general method used for calculating the curve is outlined in Appendix G.

(d) Ingot Number 4.

Ingot number 4 was cast against a chill and air cooled to start solidification. After the liquidus had extended 2.2 - 2.5 cm into the casting, before the liquid at the chill reached the eutectic temperature, the air was replaced by a water coolant. The resulting thermal curves for some typical isotherms are shown in Figure 34. Resulting composition near the chill face is shown in Figure 35.

When comparison is made between the liquidus and eutectic isotherms the initial transient ($x < x_c$) extends almost 4 cm into the casting. This precludes quantitative comparison in this region of the liquidus and eutectic isotherm slopes to obtain n_q because use of equation (34) requires $x > x_c$. Also, complete analysis as in ingots 1 and 3 was not possible due to insufficient thermal data in the critical region. However a qualitative comparison can be made between the liquidus isotherm and an isotherm less than 100 per cent solid (eutectic). For example consider the liquidus and 30 per cent solid isotherms in
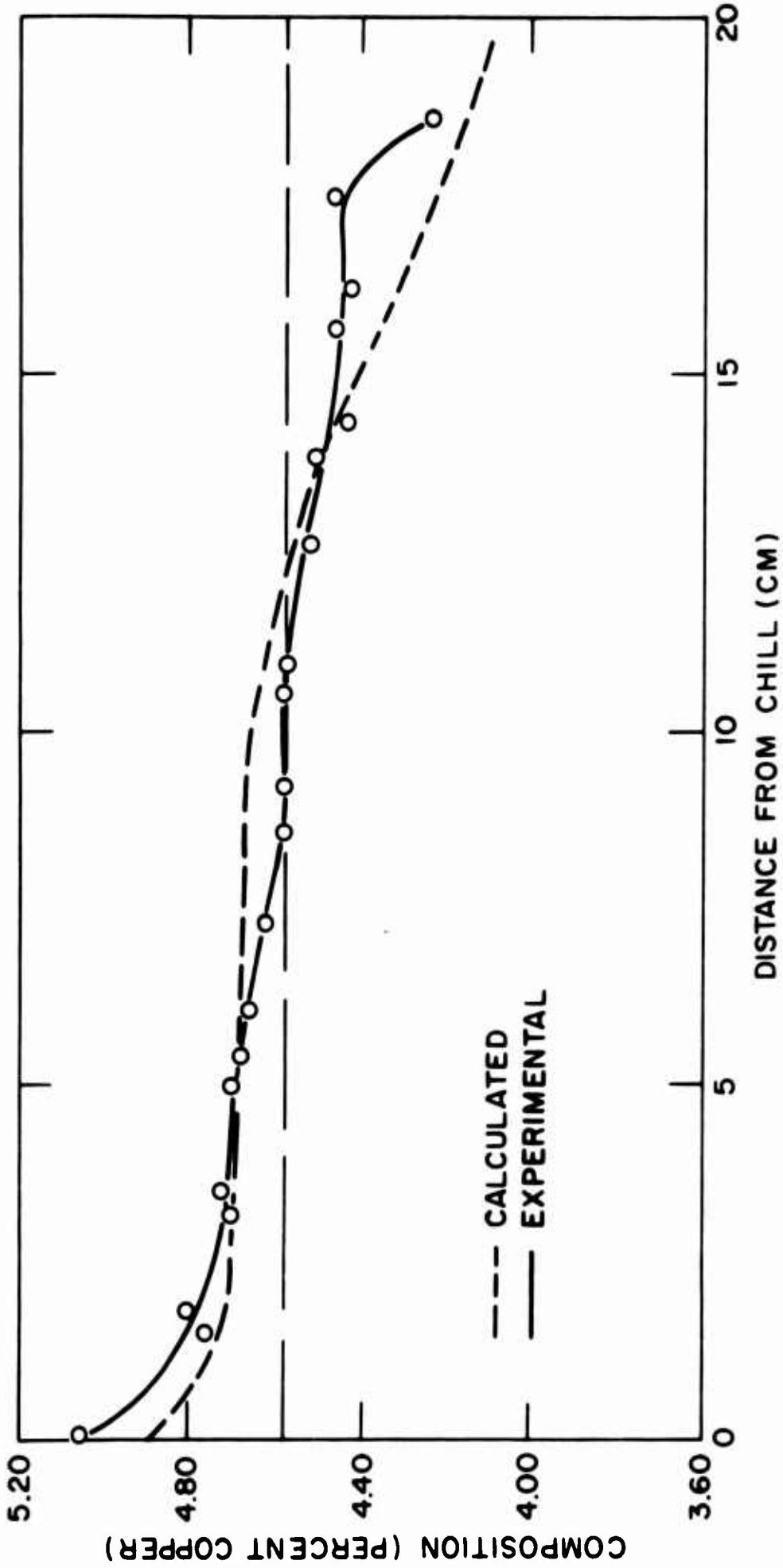
Figure 33: Experimental and calculated (from thermal data) solid composition versus distance from chill in Ingot No. 3.
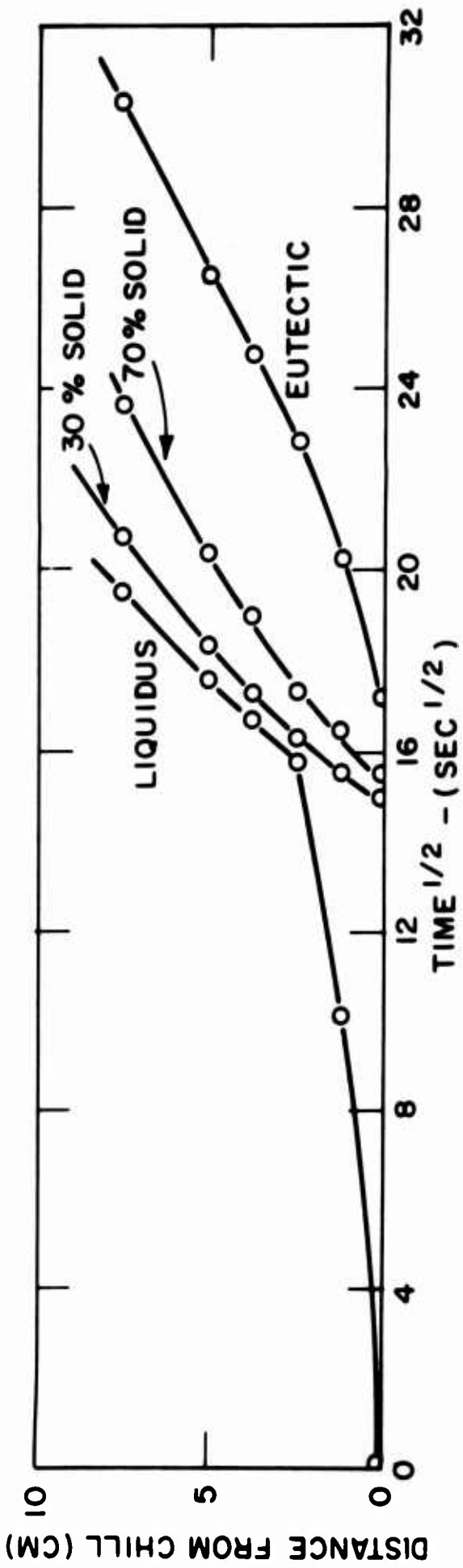
Figure 34: Thermal curves for some typical isotherms in Ingot No. 4.

6.40
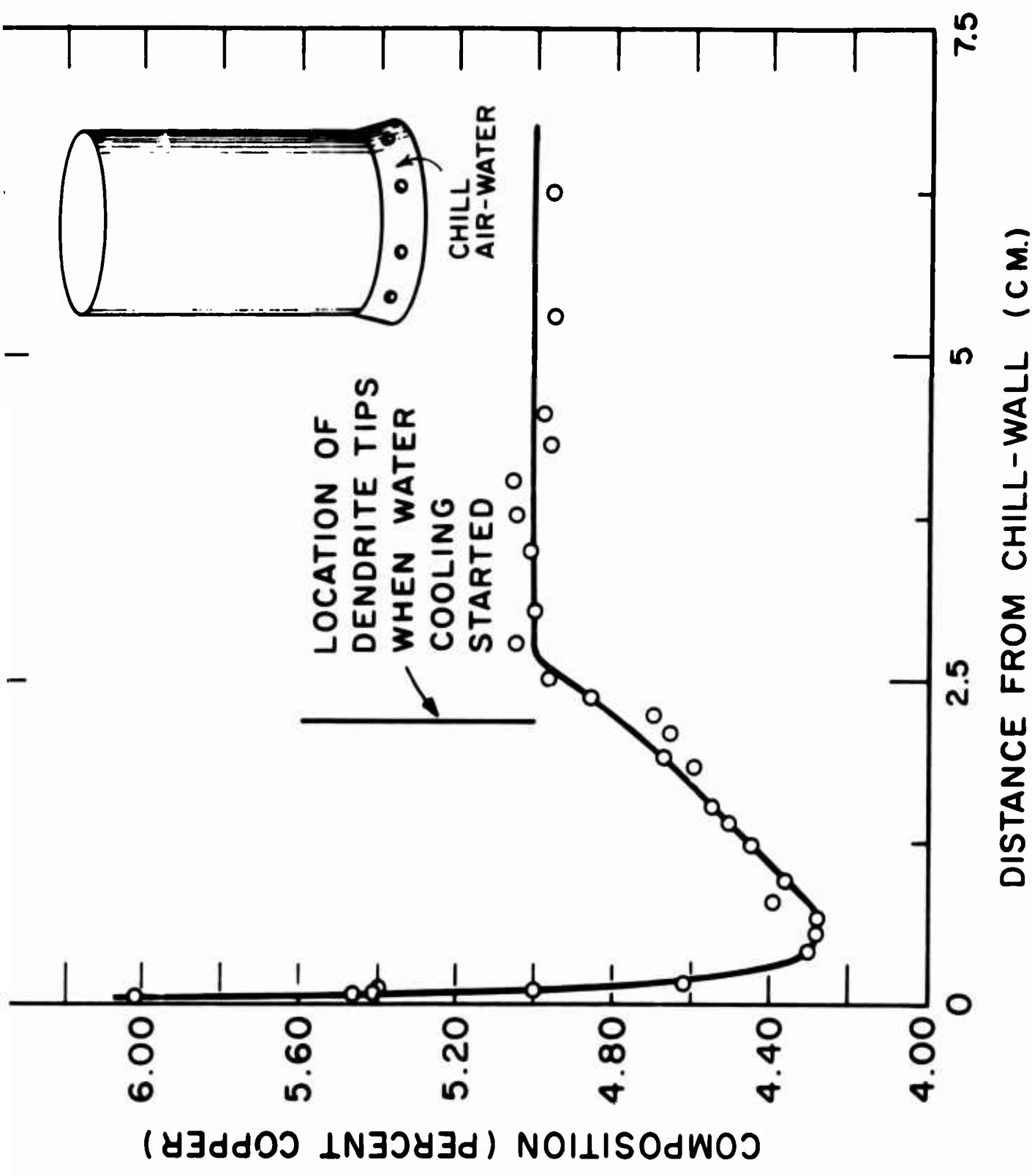
Figure 35: Solid composition versus distance from the chill in Ingot No. 4.

Figure 34. We can define n_{qx} as:

$$n_{qx} = \frac{n_L - n_x}{n_x}$$

where n_x = slope of an isotherm movement line where
$0 < x < 100$ per cent

Now n_{qx} can be calculated which will give a qualitative indication of whether compositions should be greater or less than C_0 even though quantitative results are not available. In the region where x is less than 2.5 cm comparison between the liquidus and the 30 per cent solid isotherm slopes gives n_{qx} as -.9. The maximum negative deviation possible between two isotherms is -1, therefore significant negative departure from C_0 is expected in the region up to 2.5 cm. After $x = 2.5$ cm the relationship between the liquidus and all other slopes becomes about the same; that is, n_q becomes constant which predicts a constant composition (Figure 35).

2. Reduced Cross Section.

The next group of castings were reduced in cross section as shown in the schematic diagram, Figure 11. While the castings will be considered again in a later section, attention in this portion is directed only at the effect of the reduction on composition through the central portion of the ingot. That is consideration is given to a section 3/4 inch by 3/4 inch extending from the chill surface to the top of the casting through the geometric center.

Figure 36 shows the composition variations up the length of
an ingot in the center section where area reduction is 9/1. As
expected there is a sharp minimum at the intersection of the large
and small sections (see theoretical section, Figure 12, variable
ingot cross section). To the left of the intersection there is no
change from ∞ to zero slope as in the theoretical case (Figure 12).
This is because the theoretical model assumes constant v_x at any
location y from the chill. In the actual ingot, just below the
reduction, v_x will be greatest at the center of the ingot (i.e.
absolute value) and decrease toward the edges. This will be
considered further in a later ingot, where extensive thermal data was
available.

An experiment was next conducted similar to the previous, but
with the area change 2/1; results are presented in Figure 37. For
this ingot, P equals 2 (Figure 3) with a predicted minimum composition
at the intersection about 4.1 per cent copper. Experimental value is
4.16 per cent. The general shape of the composition curve is similar
to that of the previous figure, except for a secondary minimum about
12 cm. This may be related to a sudden velocity increase at this
location when the final liquid solidifies just below the intersection.
This, however, would require verification by thermal analysis and has
not been done.

The final ingot presented in this section is a repeat of the 9/1
reduction ingot made with thermocouples cast in place so that
experimental and theoretical curves could be compared with curves
calculated from the thermal data. Figure 38 shows the measured
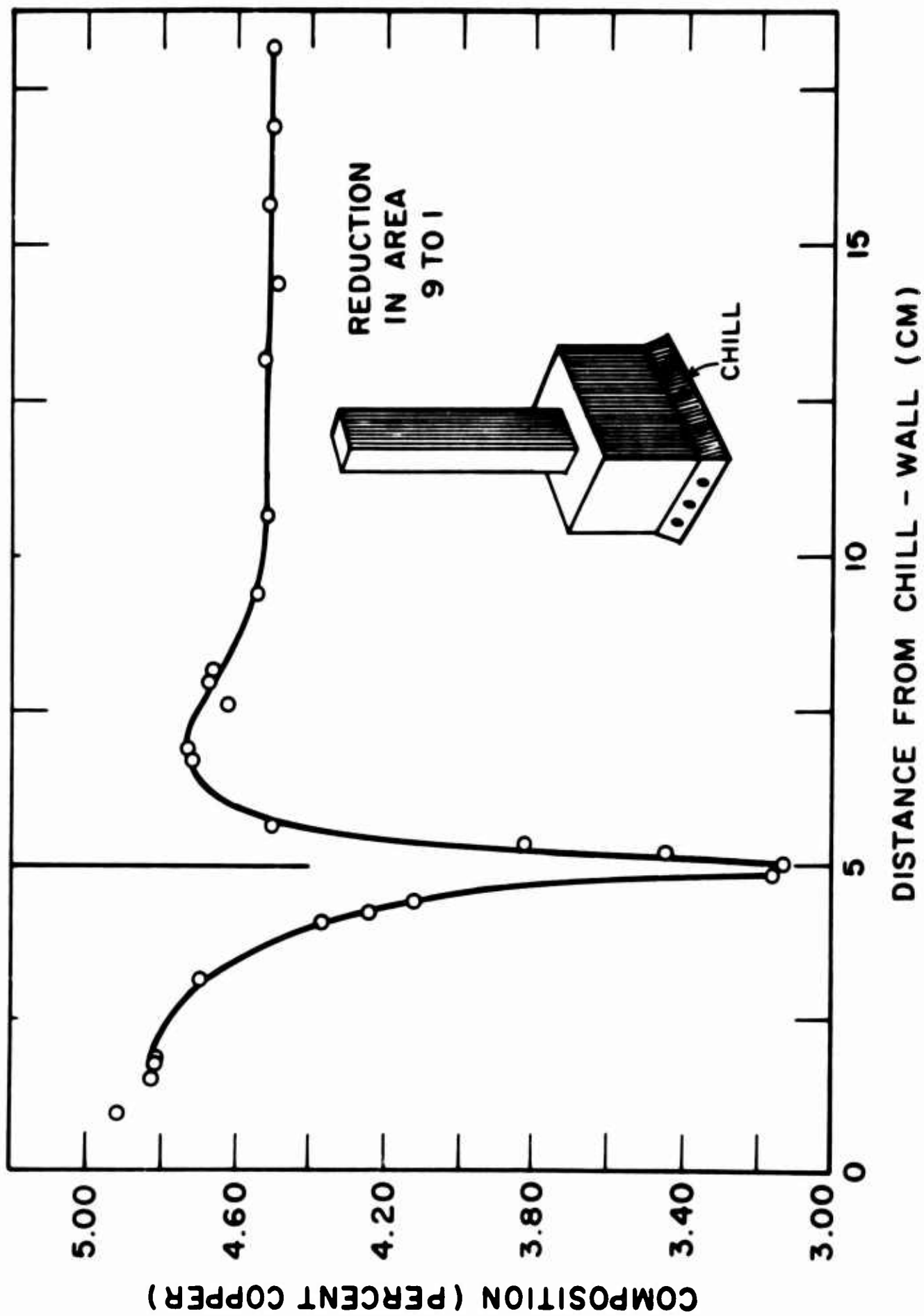
Figure 36: Solid composition versus distance from the chill in an ingot of 9 to 1 reduction in area (no thermal data).
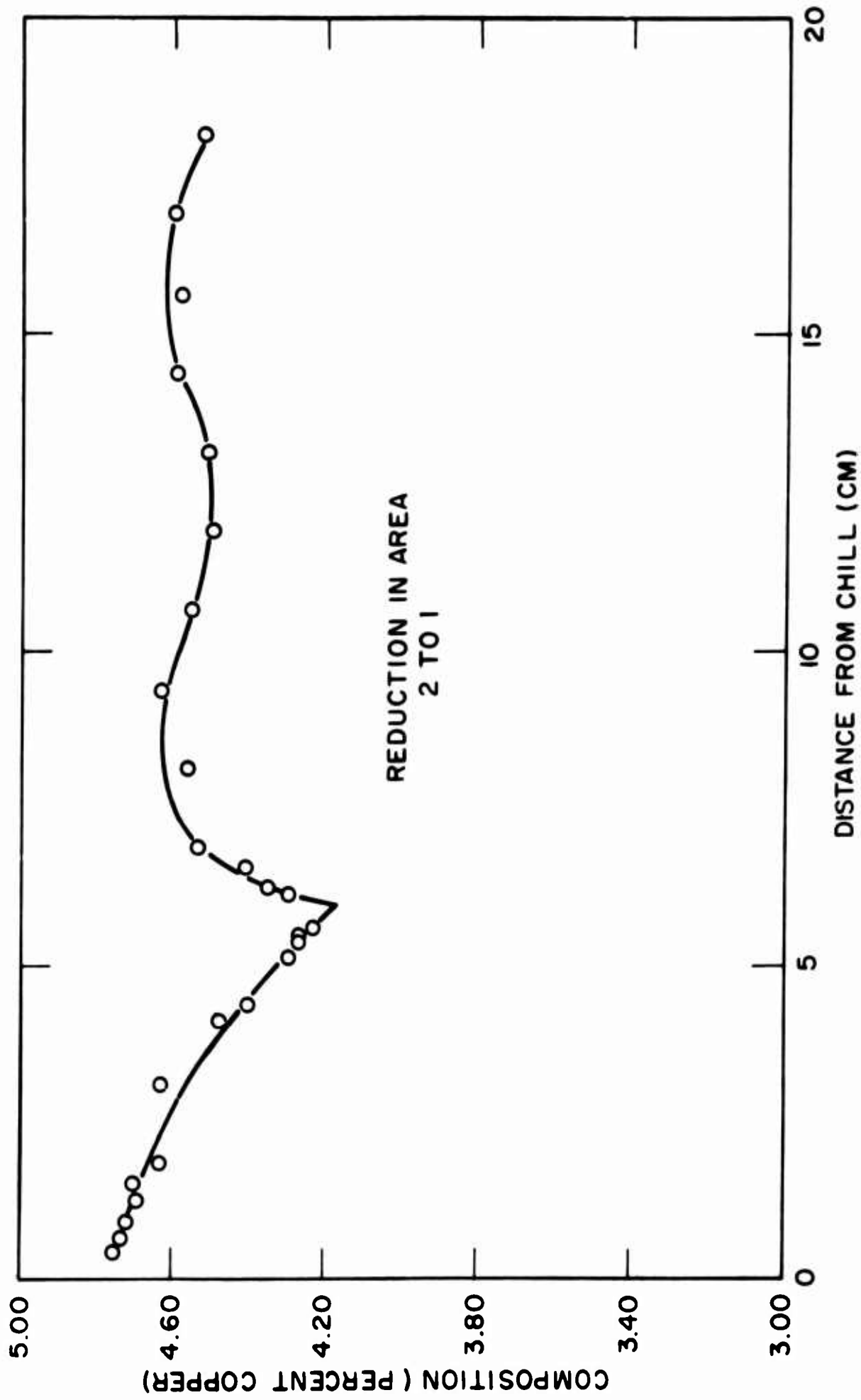
Figure 37: Solid composition versus distance from the chill in an ingot of 2 to 1 reduction in area.

composition using fluorescent analysis. Figure 39 shows the
theoretical curve for a 4.5 per cent alloy solidifying with a mushy
zone 0.2L at steady state. This curve had previously been presented
in Figure 12. The curve as presented in Figure 39b was calculated
using thermal data from the actual ingot, as described in Appendix G.
The sharp breaks at the reduction in area of the theoretical and
calculated curves are due to the assumption that v_x is constant at
a given time over the entire y-z plane at a given distance x from
the chill. This requires discontinuous change in v_x at the reduction.
In the actual case this is not to be expected since it would require,
just below the reduction, that feed metal flow in a thin layer across
the top of the large section and then down, so that v_y and v_z equal
zero at all locations except precisely at the junction. Experimental
data from this ingot, presented in Figure 40, show that final solid
composition just below the junction is much lower near the center of
the casting than it is toward the edges. This clearly results from
finite v_y and v_z, and is discussed in a later section.

As a final example of the effect of section reduction on
composition, partial results of an ingot with metal plates to divert
fluid flow are presented in Figure 41. The plates are spaced so they
extend half the width into the casting (total width 7.5 cm). The
side of the casting with the plates will be considered in a following
section. On the side with no plates, the minimum composition occurs
at approximately 4 cm from the chill. The 2/1 reduction in area from
the inserted plates occurs at 5 cm. That the expected minimum occurs
below the reduction seems possible since from fluid flow considerations
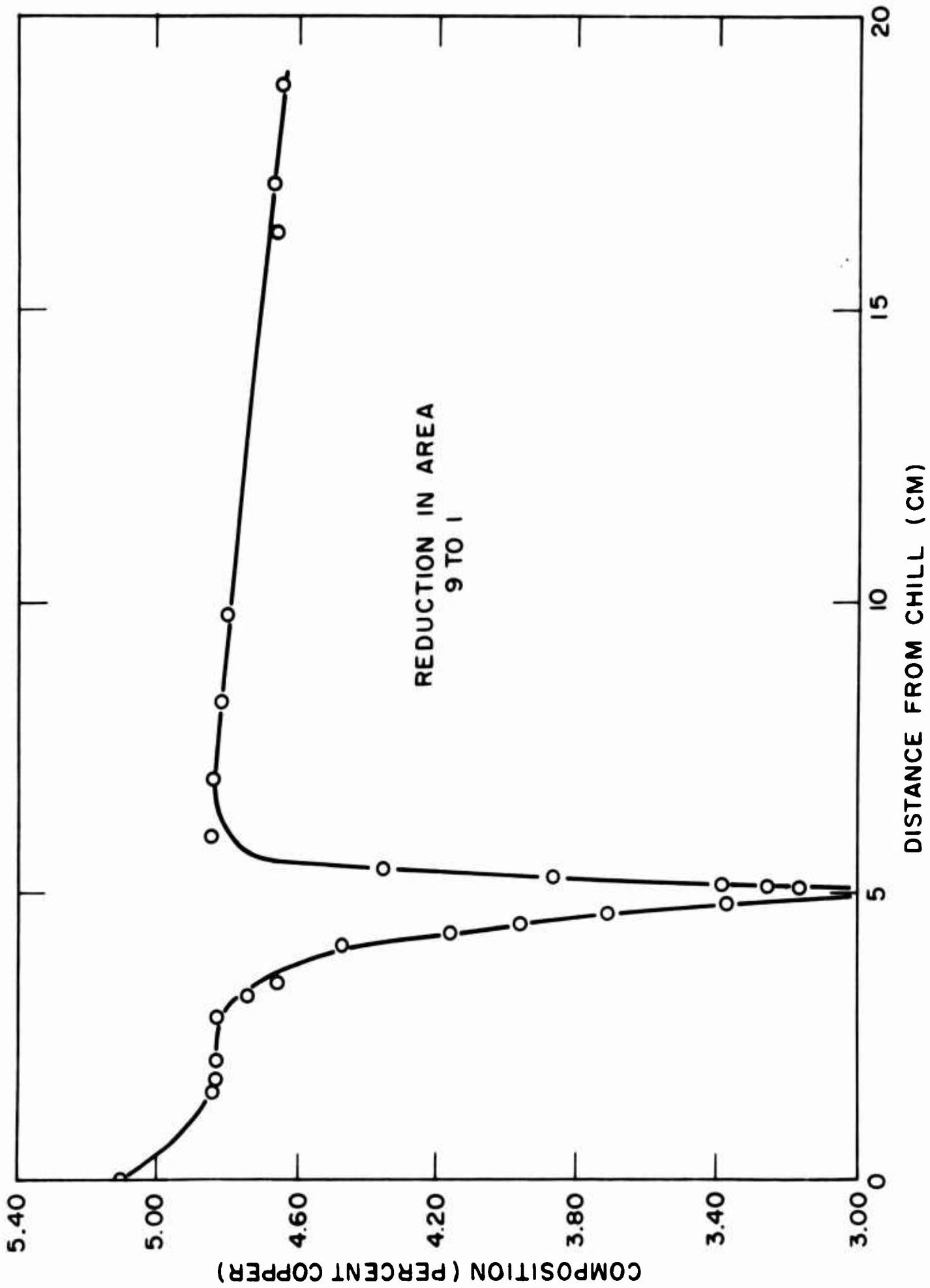
Figure 38: Solid composition versus distance from the chill in an ingot of 9 to 1 reduction in area (thermal data, Appendix G).
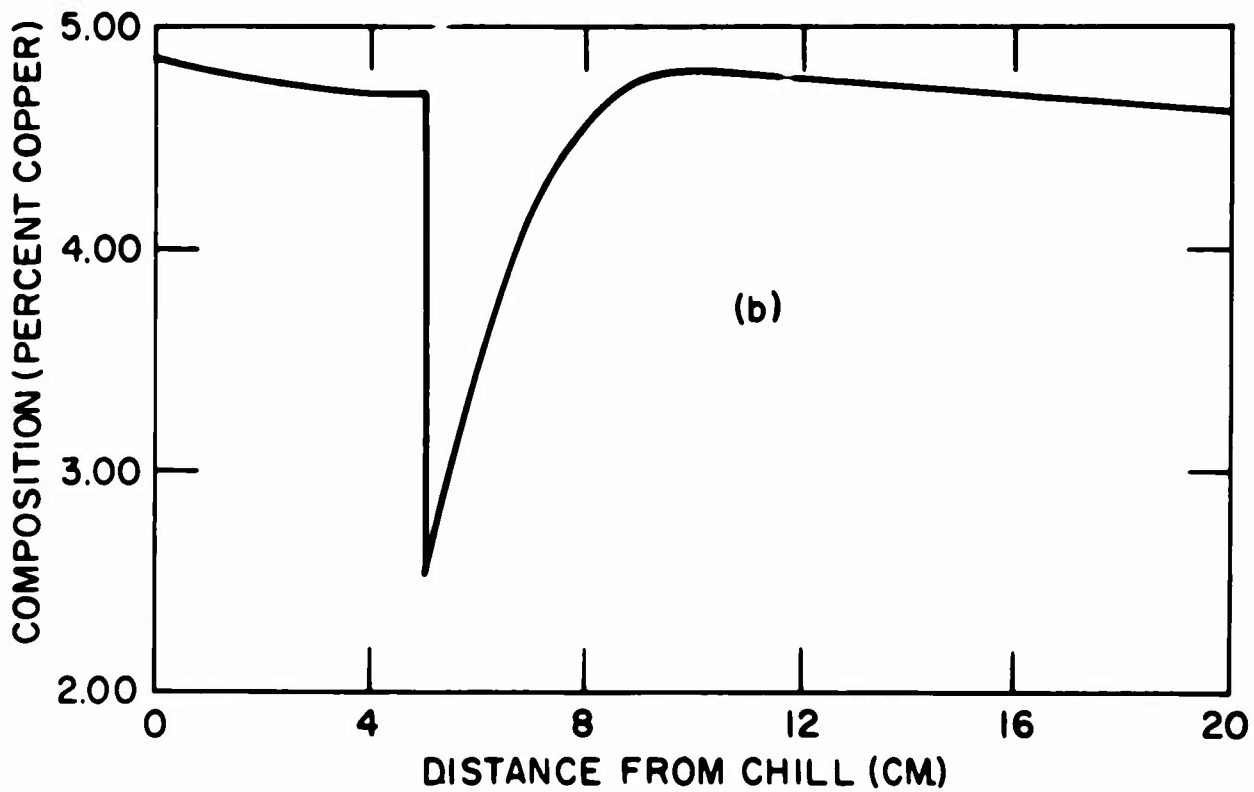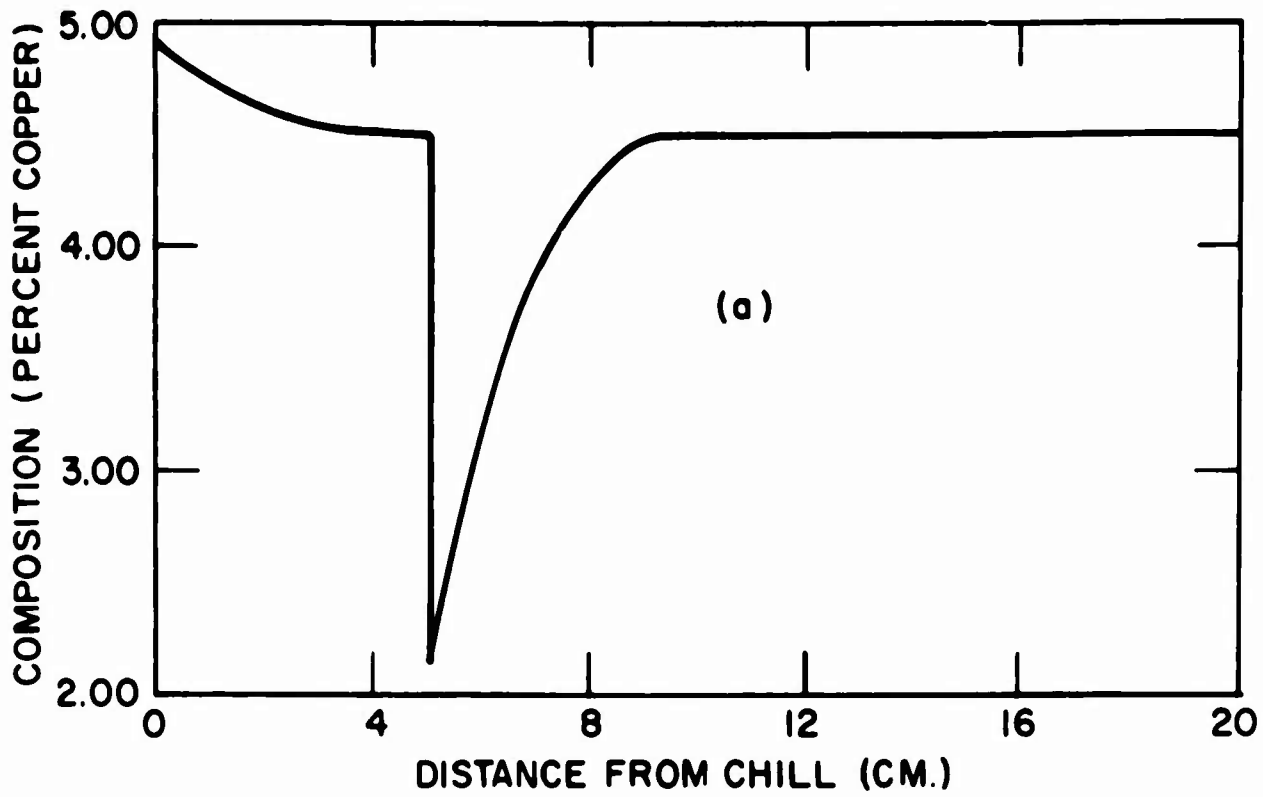
Figure 39: Composition versus distance from chill for reduced section ingot. (a) Theoretical – C_0 = 4.5 per cent copper, 10/1 reduction. (b) Calculation from experimental data C_0 = 4.68 per cent copper, 9/1 reduction.
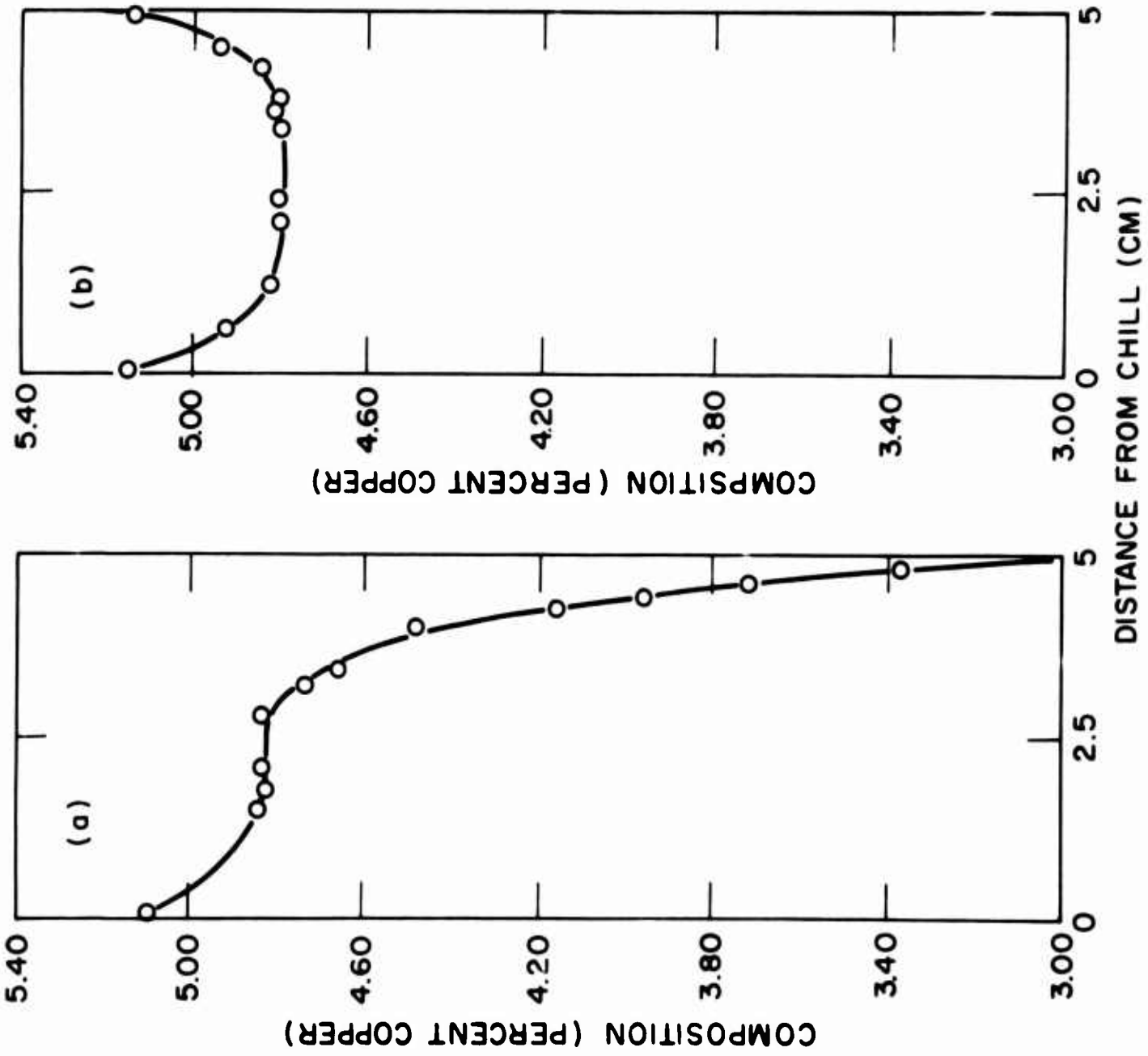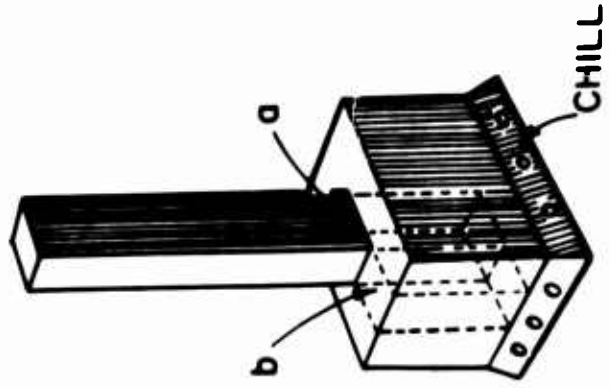
Figure 40: Solid composition versus distance from the chill at two locations in the bottom portion of an ingot of 9 to 1 reduction in area.
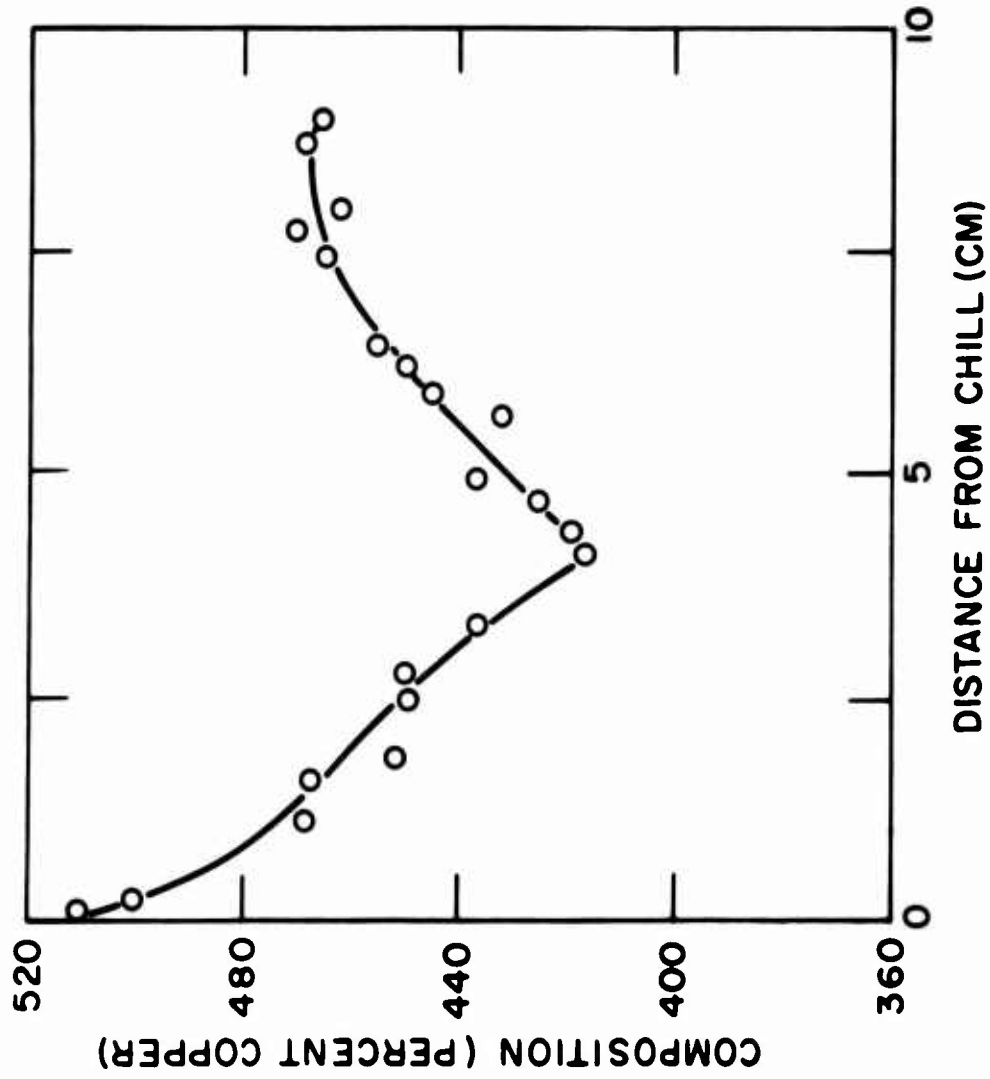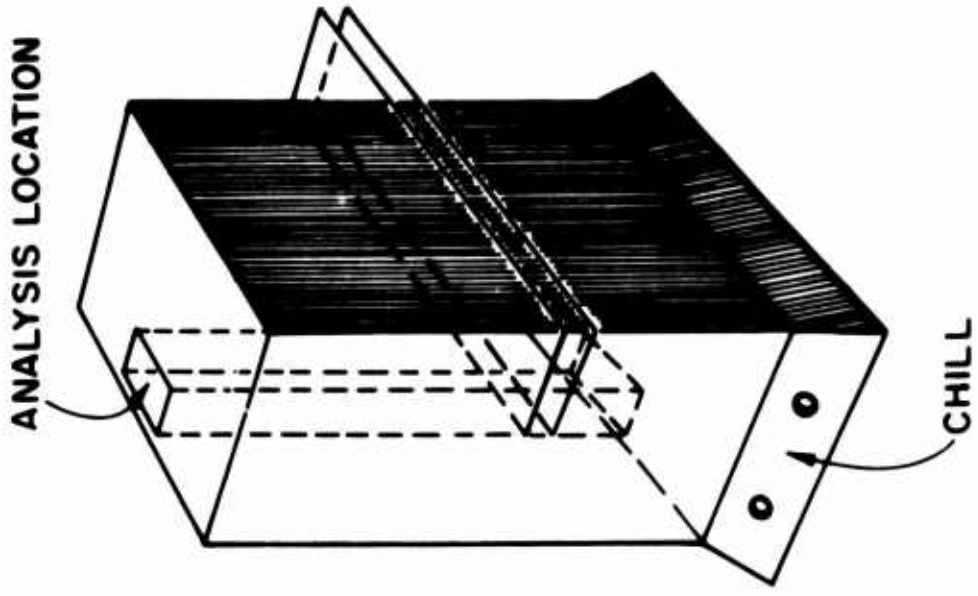
Figure 41: Solid composition versus distance from the chill in an ingot with horizontal plates (as sketched) extending half the width into casting. Composition determined on side without plates.

the plates may act similar to an orifice with the maximum in velocity occurring slightly downstream from the reduction.

The 2/1 reduction is the same as in one of the reduced section ingots previously discussed, Figure 37. In fact the shapes of the two composition curves are very similar.

If comparison is made of Figures 36, 37, and 41 it can be seen, as expected from Figure 3, that the minimum composition is a function of the area reduction.

B. Unidirectional and Bi-Directional Heat Flow; Non-Unidirectional Fluid Flow

In the theoretical section v_x was discussed as a part of the parameter, $\frac{v_x G}{\epsilon}$. When $v_x = 0$ the general macrosegregation equation (20) reduces to that for solidification at a chill face. This is the maximum composition obtainable in unidirectional solidification (in the absence of melting and solidification) and for an aluminum-4.5 per cent copper alloy is 4.92 per cent copper. The minimum composition is $kC_0 = .77$ per cent copper for 4.5 per cent = C_0 which will be approached as v_x approaches minus infinity. For solidification where both heat and fluid flow are non-directional v_x can become positive and local compositions greater than 4.92 per cent copper are possible. In general, for solidification where heat flow is unidirectional and no melting and resolidification occurs, as v_x increases negatively from zero, local average composition will decrease.

1.   Unidirectional Heat Flow, Non-Unidirectional Fluid Flow.

For unidirectional solidification v_x refers to that component of fluid flow which is perpendicular to isotherms (parallel to heat flow). In this section three castings will be considered in which v_x values and the resulting compositions varied considerably.

The first experimental ingot considered is shown in Figure 42. The "ingot" comprises the bottom portion of the mold cavity (3.8 cm, by 15 cm by 10 cm high). The hot top is as shown, feeding through a neck at one end of the ingot. Ingot, neck, and hot top are "perfectly" insulated so all heat flow is downwards, out through the water-cooled base plate.

The ingot is designed to simulate heat and fluid flow in solidification of a slice of a large ingot. Specifically, the base of the ingot is intended to represent the mold wall, the "top" of the ingot represents the centerline, and flow occurs left to right from the neck, as it would downwards from the hot top of a large ingot.

Solidification in the portion of the ingot near the base is as in a simple, constant cross section, unidirectionally solidified ingot. This is confirmed by the final segregation seen in this region (at locations 4.5, 6.1 and 7.6 cm from the chill, Figure 43). At any given location along the casting, composition is essentially the same at all three distances from the chill.
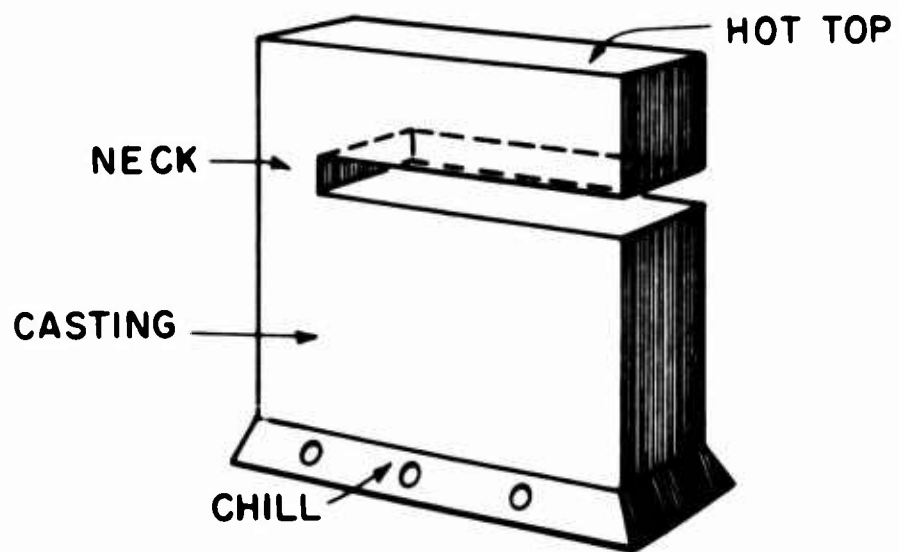
Figure 42: Simulated centerline ingot.
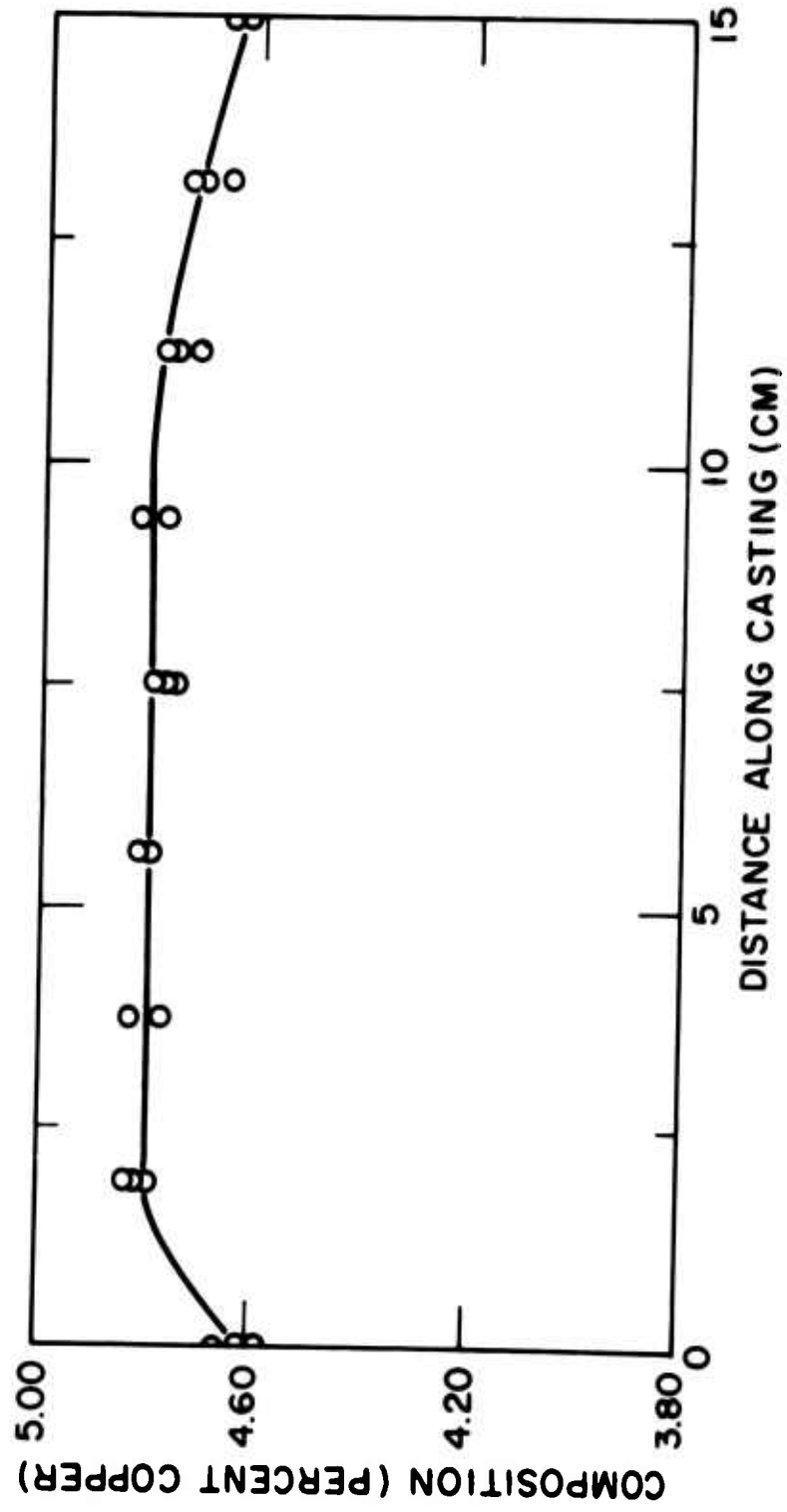
Figure 43: Solid composition along the simulated centerline ingot at locations 4.5 , 6.1 and 7.6 cm from the chill.

As the dendrite tips approach the ingot top some differences in flow behavior are to be expected:

(1) fluid flow can no longer be perpendicular to isotherms throughout the ingot if solidification shrinkage is to be completely fed, (2) downward flow in the vicinity of the neck must be much greater than that in a classical unidirectional ingot at a similar distance from the chill. In addition, it may be expected that isotherms in the vicinity of the neck may become crowded relative to the rest of the ingot, and alter G/ϵ; this, however, did not significantly affect solute redistribution in the similar ingot of Figure 40, in which any change in movement of isotherms did not appreciably affect calculate segregation.

Figure 44 shows the composition along the ingot at locations 7.9 and 9.8 cm from the chill (i.e., 2.1 and 0.2 cm from the casting top). Remarkably strong macrosegregation results, where compositions near the ingot top vary systematically by as much as .83 per cent which is nearly 20 per cent of the base alloy composition (aluminum-4.7 per cent copper alloy).

Most notable feature of the data is the low solute region below the neck. This would be predicted from (2) above. In addition the composition of the ingot top at locations removed from the neck appears to be above C_0; this would be expected (in the case of complete feeding) since the flow here cannot be perependicular to isotherms. That is, v_x is approaching zero and lies between zero and the steady
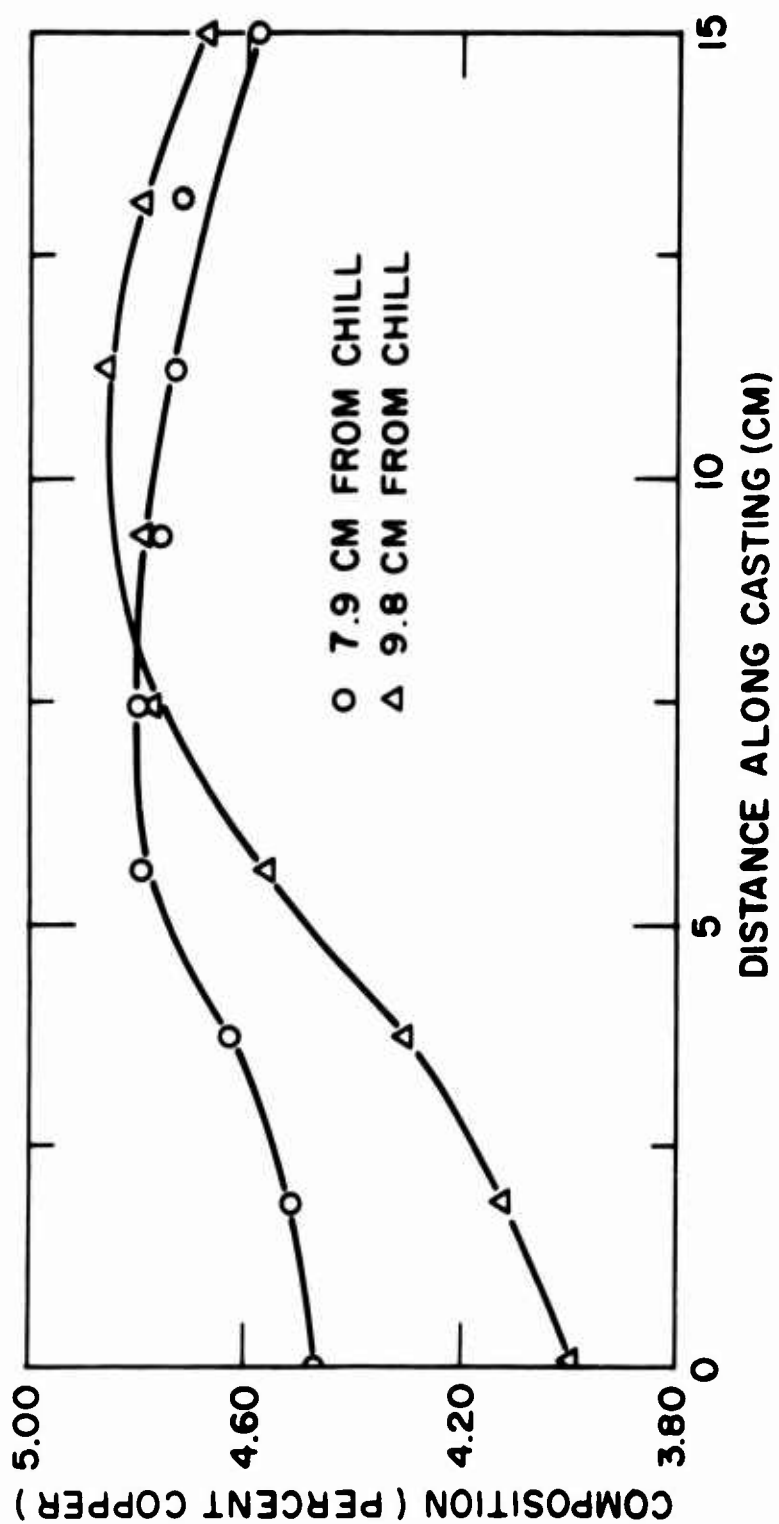
Figure 44: Solid composition along the simulated centerline ingot at locations 7.9 and 9.8 cm from the chill.

state value. This will be discussed further in the centerline
segregation portion.

The second example considered in this section is the portion of
the previously described ingot that had stainless steel inserts.

Figure 45 shows composition as a function of distance from the
chill for that portion of the ingot shown which had the plates to
restrict fluid flow. The decrease in composition near the chill,
with increasing distance from the chill, is as expected in usual
unidirectional solidification, the minimum at 2.5 cm, however, is
lower than expected; it is not clear why this is so.

It is interesting to note, by comparing Figures 41 and 45, that
the minimum in the section with the plates occurs at a different
distance from the chill than minimum in the other portion of the
ingot. At the location where the right portion reaches a minimum
(at 4.40 per cent copper) the left portion is about the same composi-
tion. The left side (without plates), however, continues to decrease
to a minimum of 4.16 per cent copper. At this location the right
portion (with plates) has a local average composition greater than
5.0 per cent copper. This means that a composition difference of
more than .8 per cent copper exists over a horizontal distance of
less than 2.5 cm.

Near the plates where v_x is expected to be 0 the composition should
be the same as the chill face composition (i.e., approximately 5.00 per
cent for the 4.56 per cent = C_0 alloy). That fact that the composition
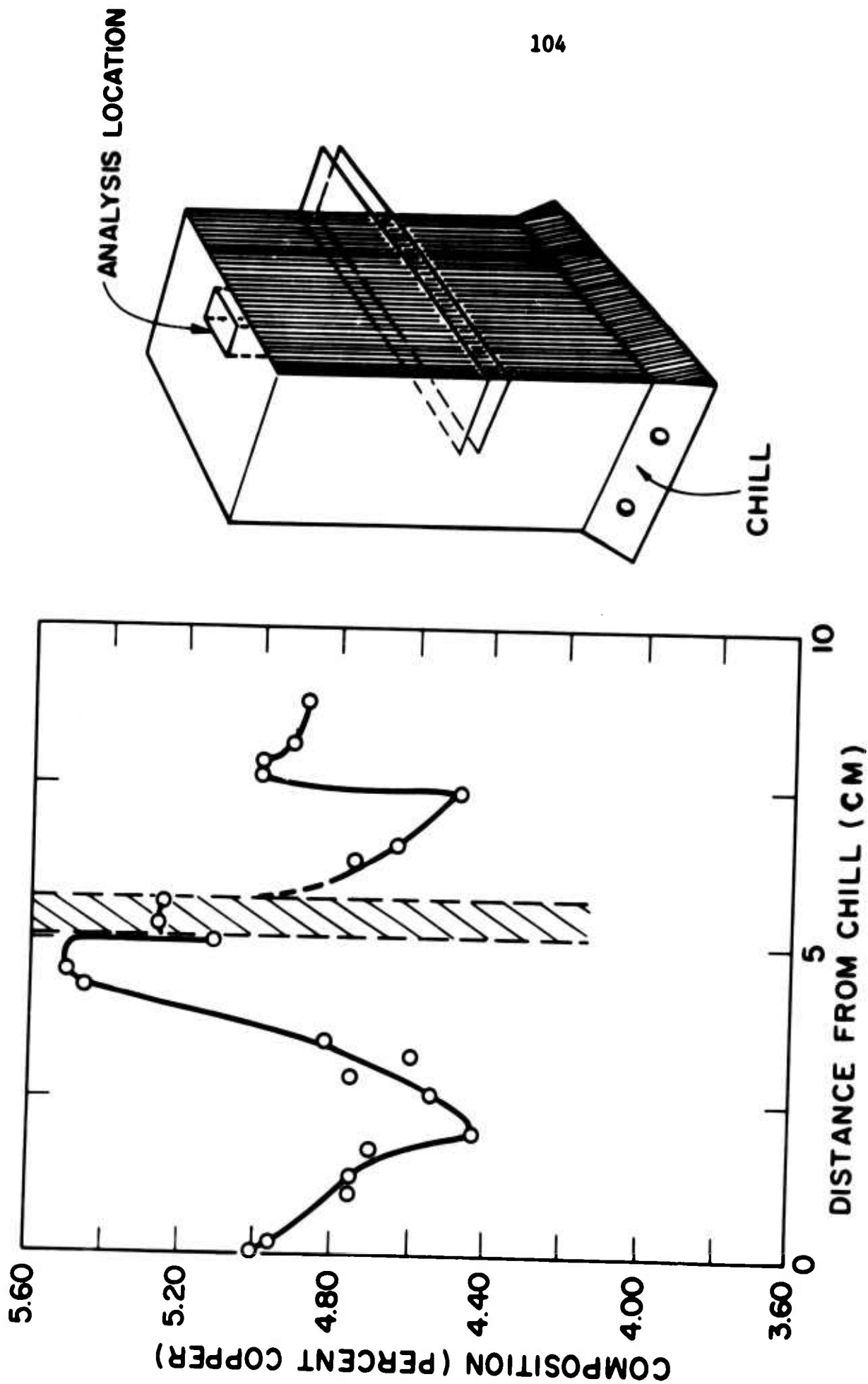
Figure 45: Solid composition versus distance from the chill in an ingot with horizontal plates (as sketched) extending half the width into casting. Composition determined on side with plates.

just under and between the plates is higher could be due to some "exudation" occurring as a result of solid contraction.

Just above the plate, solidification also is expected to occur with $v_x = 0$ and composition here is the same as at the chill face. Further above this plate, a minimum is observed which may be related to another set of plates (not shown) 15.25 cm from the chill.

The third example considered is the previous ingot (9/1 reduction) at one side of the heavy section (Figure 11). As discussed previously when theoretical calculations were made for this ingot, velocity v_x at a location y (for a given distance from the chill) was assumed constant except exactly at the riser-casting junction. In the actual case, however, this is not expected to be true. As feed metal enters the larger section the absolute value of v_x must be a maximum at the center and, just below the section reduction is expected to be greater than the flow velocity in unidirectional solidification, constant cross section; hence, final composition is here less than C_0, Figure 40.

To feed the heavy section out toward the edges, v_x is expected to approach zero for $x = L_R$ where L_R is distance from the chill to section reduction. Hence, composition at the top of the heavy section (away from the reduced section) should be that at a chill where v_x is also zero (5.15 per cent copper for a 4.68 per cent $= C_0$ alloy). This is seen in Figure 40.

2. Centerline Segregation.

While centerline segregation is considered as a separate problem, it can be treated as a limiting special case of non-unidirectional heat and fluid flow. As discussed in the theoretical section, Part III, the increased solute content at the centerline of an ingot can be related to the magnitude and component of the fluid flow velocity v_x. As an example, consider the simulated centerline ingot previously discussed, Figure 42. In Figure 46 the results of chemical analysis away from chill are presented at one location along a direction parallel to the heat flow direction. Composition remains relatively constant until the top is approached. At locations close to the chill, fluid flow to feed solidification is perpendicular to isotherms and v_x approaches a steady state value $\frac{\beta}{1 - \beta} \frac{\epsilon}{G}$. As the dendrite tips touch the top, fluid flow can no longer be perpendicular to isotherms and v_x approaches zero. As v_x approaches zero, local average composition increases. The maximum occurring when $v_x = 0$ and composition approaches the same as at a chill face. That this maximum was not reached in this ingot at the simulated centerline was presumably due to incomplete feeding along the very top of the ingot.

It can now be visualized how centerline segregation can occur in a large ingot where solidification fronts from the ingot walls meet at a central region. Before the dendrite tips touch, solidification is as above, when v_x is perpendicular to isotherms. Once the tips touch, however, flow is no longer perpendicular to isotherms but can even become parallel. When flow is parallel, $v_x = 0$ and local average
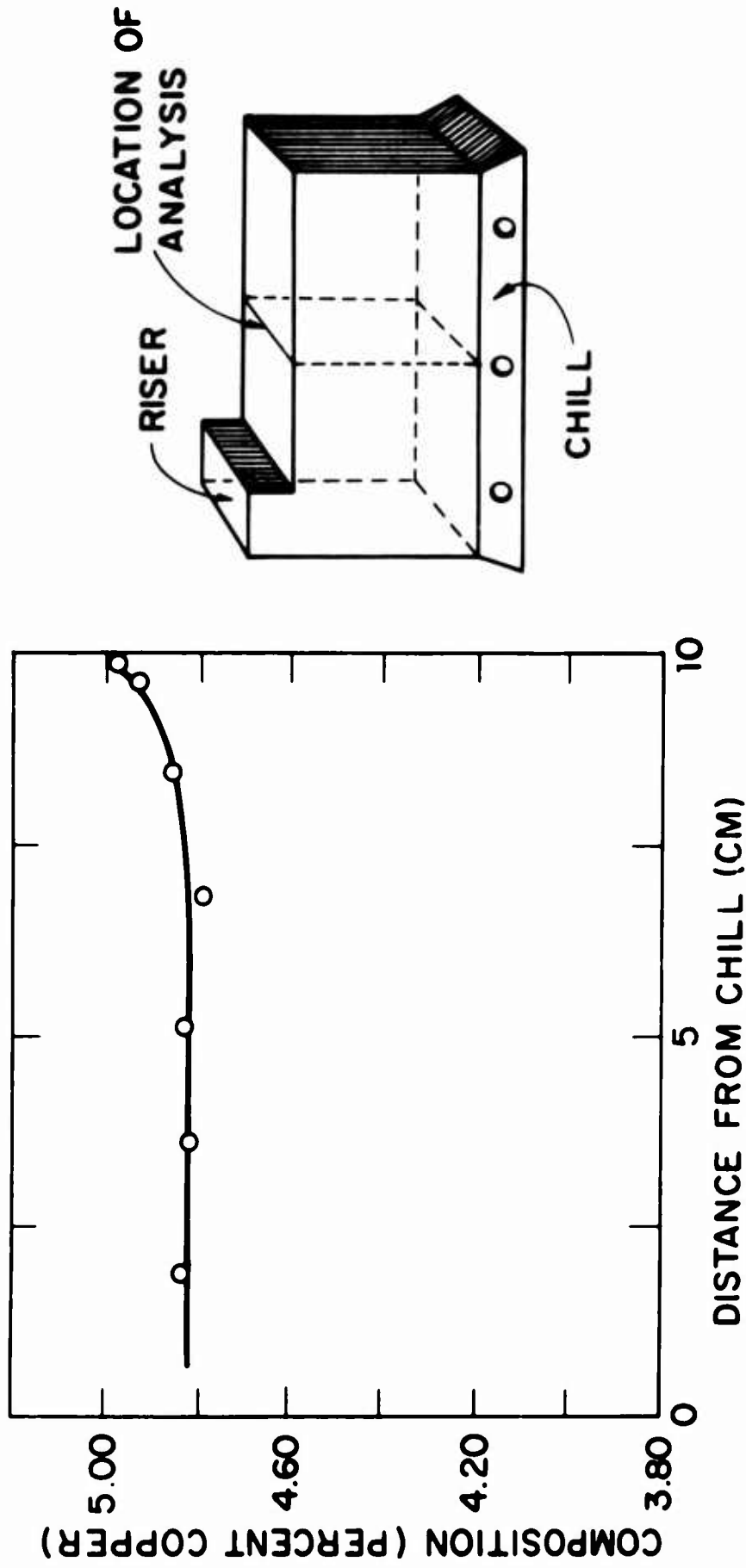
Figure 46: Solid composition versus distance from the chill in the simulated centerline ingot at the location shown.

composition will approach chill face composition (for perfect feeding). The extent that local average composition approaches chill face composition depends on:

1. How much solidification in the volume element occurred with $v_x = 0$.

2. How closely v_x approaches zero (which depends on details of fluid flow as discussed in the previous section).

As example of this, consider the ingot solidifying toward a common center from two flat chill walls, using the experimental set-up described in part I-B, Appendix E. Figure 47 presents the results of chemical analysis across this ingot at two locations[43]. Both show increases in comr. ition at the center even though casting width was only 3.75 cm an. total solidification time was 140 second. The qualitative similarity of the segregation curves in Figure 47 to those measured in large ingots is remarkable; see, for example, Reference 17.

Finally, consideration can again be given to both the reduced cross section ingot and the ingot with metal plates inserted. In these ingots, v_x is expected to approach zero at the following locations, as well as at the chill face:

1. In the reduced section ingot at the top of the heavy section (see Figure 40b).

2. In the ingot with inserted plates; on either side of the plates and inside the plates (see Figure 41).

Location between chills (CM)
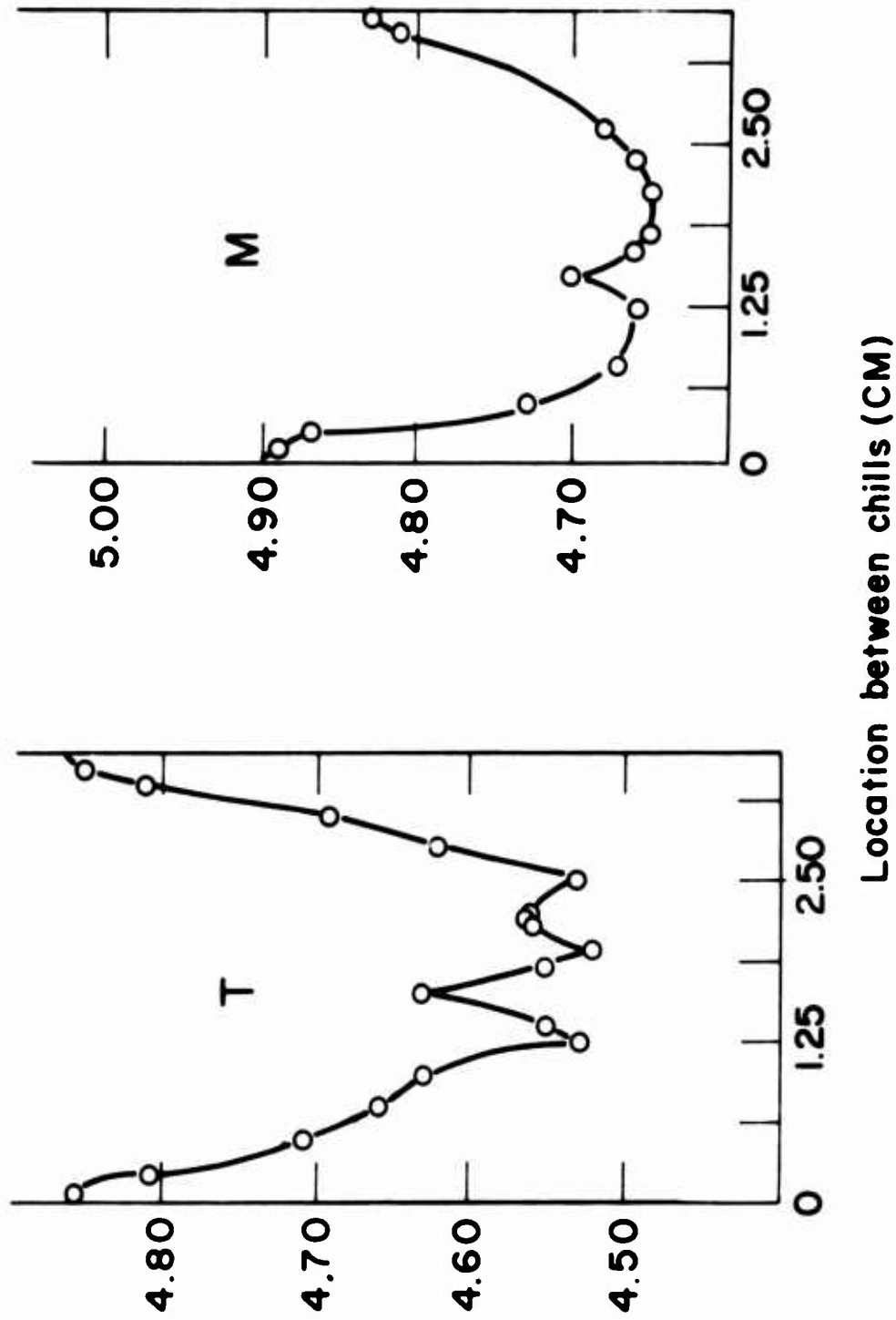
Figure 47: Solid composition versus distance between two chills in a bi-directionally
solidified casting at two locations.

(T) near top of casting.
(M) middle portion of casting.

Local average composition at these locations increases in a manner similar to the top of the simulated centerline ingot and the actual centerline of the experimental ingot.

IV. CONCLUSIONS

1. Flow of solute-rich liquid to feed solidification and thermal
   contractions, is the basic mechanism responsible for many
   apparently different types of segregation. Among these are:
   (a) inverse segregation

   (b) centerline segregation

   (c) banding

   (d) negative cone of segregation

   (e) localized solute rich regions

      (1) exudation

      (2) "hot tearing" type segregation

      (3) solute enrichment under risers and hot tops.

2. The final composition at any point x, y, z in a casting or ingot
   (and hence macrosegregation) can be calculated from knowledge of
   (a) phase diagram and other physical constants of the alloy,
   (b) thermal history at x, y, z during solidification, and (c)
   amount and direction of fluid flow at x, y, z to feed shrinkage
   of parts of the casting at lower temperatures.

3. Laboratory experiments on aluminum-4.5 per cent copper alloy
   qualitatively and quantitatively confirm analyses presented.
   These experiments comprise measurement of macrosegregation in
   small ingots of the following mold designs: (a) simple
   unidirectional, (b) unidirectional with restricted fluid flow,
   (c) unidirectional with variable heat extraction rate to

illustrate banding, (d) unidirectional with reduced cross
section, (e) edge-risered unidirectional to illustrate centerline
segregation, and (f) ingot with bi-directional heat flow to
illustrate centerline segregation.

V. SUGGESTIONS FOR FUTURE WORK

While much experimental work has been done in the area of unidirectional heat and fluid flow, further experimental work seems desirable on non-directional solidification. Specifically, work should be done on "hot tear" type segregation, segregation in sand castings, and under-riser segregation.

In conjunction with this work consideration should be given to the effect of porosity on macrosegregation results. While a theoretical and qualitative presentation is made, quantitative results should prove helpful.

A new area of investigation would be the effect of magnetic fields on macrosegregation. A sufficiently strong magnetic field should influence segregation by altering fluid flow during solidification.[44]

Another area needing study is that concerning the details of fluid flow in non-unidirectional solidification. Limiting cases have been considered herein, but treatment of intermediate areas (which more closely approximate real conditions) requires detailed fluid flow analysis.

A more applied area for future work would be application of the ideas presented herein to actual ingot solidification processes (static, continuous, consumable electrode). Such application would require numerical analysis and clearly would require use of high

speed digital computers. However, the application should be feasible, and certainly of great engineering usefulness.

VI. REFERENCES

1. <u>Pirotechnia</u> of Vannoccio Biringuccio, 1540. Translated by Smith, C. S., and Grudi, M. T., p. 259.

2. Phillips, A., and Brick, R. M., "Segregation in Single Crystals of Solid Solution Alloys", Trans. AIME, Vol. 133, 1937, p. 313.

3. Adams, D. E., "Segregation in Aluminum-Copper Alloys", Journal, Inst. of Met., Vol. 75, 1948, p. 809.

4. Sauerwald, F., Giesserei, Vol. 20, 1942, p. 25.

5. Masing, G., and Haase, C., Weissenschaftlicke Vetaffenlichungen, Siemers-Konz, Vol. 6, 1927, p. 211.

6. Scheil, E., Metallforschung, Vol. 2, 1947, p. 69.

7. Kirkaldy, J. S., and Youdelis, W. V., "Contribution to the Theory of Inverse Segregation", Trans. AIME, Vol. 212, 1958, p. 833.

8. Youdelis, W. V., and Colton, D. R., "Inverse Segregation in Aluminum-Zinc Ingots", Trans. AIME, Vol. 218, 1960, p. 628.

9. Vaughan, N. B., "Inverse Segregation: A Review", Journal Inst. of Metals, Vol. 61, 1937, p. 35.

10. Pell-Walpole, W. T., Metal Treatment and Drop Forging, Vol. 16, 1949, p. 103.

11. Vosskuhler, H., "Inverse Segregation in Ingots of Nonferrous Metals", Z. Metallkunde, Vol. 56, 1965, p. 719.

12. Basic Open Hearth Steelmaking, Physical Chemistry of Steelmaking Committee, Met. Soc. AIME, 3rd ed., Gerhard Derge ed., N.Y. 1964.

13. Bishop, H. F., Brandt, F. A., and Pellini, W. S., "Solidification Mechanism in Ingots", Trans. AIME, Vol. 194, 1952, p. 44.

14. Siegel, H., "Undercooling of Steel in Ingot Molds", Stahl und Eisen, Vol. 61, 1941, p. 991.

15. Report on the Heterogeneity of Steel Ingots, Iron and Steel Inst., London, Seventh Report, 1937, p. 12.

16. Marburg, E., "Solidification in Ingots: Its Influence on Ingot Soundness", Journal of Metals, Feb. 1953, p. 157.

17. Malinochka, J. N., Koval'chuk, G. Z., "Structure of a Spring Steel Ingot and the Liquation of Alloying Elements", Stahl und Eisen, Vol. 82, No. 6, 1963, p. 481.

18. Dennis, W. H., _Metallurgy of the Ferrous Metals_, Sir Isaac Pitman and Sons, Ltd., 1963, p. 203.

19. Garside, J. E., _Process and Physical Metallurgy_, Charles Griffin, and Co., Ltd., 2nd ed., 1957, p. 288.

20. Flemings, M. C., "Microsegregation in Castings and Ingots", Hoyt Memorial Lecture, Trans. AFS, Vol. 74, 1964, p. 353.

21. Takenaka, T., "Centrifugally Cast Steel Pipes for Civil Engineering and Construction Purposes", Foundry Trade Journal, Vol. 119, No. 2560, 1965, p. 863.

22. Northcott, L., and Dickin, V., "The Influence of Centrifugal Casting (Horizontal Axis) Upon the Structure and Properties of Metals", Journal Inst. of Metals, Vol. 70, 1944, p. 301.

23. Cumberland, J., "Centrifugal Casting Techniques", The British Foundryman, Vol. 56, 1963, p. 26.

24. Howson, H. O., Proc. IBF, Vol. 39, 1945, p. B110.

25. Wolf, F., "Inverse Ingot Segregation in Continuous Castings", Giesserei-Praxis, Vol. 18, 1964, p. 343.

26. Bierbaum, C. H., Technical Note, Journal Inst. of Metals, Vol. 37, 1927, p. 281.

27. Gayler, M. V. L., "The Study of the Relation Between Macro- and Microstructure in Some Non-Ferrous Alloys", Journal Inst. of Metals, Vol. 44, 1930, p. 97.

28. Genders, R., "The Mechanism of Inverse Segregation in Alloys", Journal Inst. of Metals, Vol. 37, 1927, p. 241.

29. Simon, A. C., and Jones, E. L., "The Role of Inverse Segregation and Redistribution of Solute Atoms in the Freezing of Hypoeutectic Lead-Antimony Alloys", J. Electrochemical Society, Vol. 101, 1955, p. 536.

30. Bishop, H. F., and Fritz, R. E., "Segregation in Small Steel Castings", Trans. AFS, Vol. 55, 1947, p. 412.

31. Bertoli, C., S.M. Thesis, Metallurgy Department, Massachusetts Institute of Technology, August 1966.

32. Rosenberg, R. A., Flemings, M. C., Taylor, H. F., "Hot Tearing in Non-Ferrous Binary Alloys", Trans. AFS, Vol. 68, 1960, p. 518.

33. Bishop, H. F., Ackerlind, C. G., Pellini, W. S., "Investigation of Metallurgical and Mechanical Effects in the Development of Hot Tearing", Trans. AFS, Vol. 65, 1957, p. 247.

34. Beckious, K., "Metallurgical Aspects on Hot Tearing in Cast Steel", International Foundry Congress, Stockholm, Vol. 8, 1957, p. 19.

35. Lees, D. C. G., "Hot Tearing Tendencies of Aluminum Casting Alloys", Journal Inst. of Metals, Vol. 72, 1946, p. 343.

36. Singer, A. R. E., Jennings, P. E., "Hot Shortness of Some Aluminum-Iron-Silicon Alloys of High Purity", Journal Inst. of Metals, Vol. 73, 1947, p. 273.

37. Brody, H. D., Flemings, M. C., "Solute Redistribution in Dendritic Solidification", Trans. Met. Soc. AIME, Vol. 236, 1966, p. 615.

38. Bower, T. F., Brody, H. D., Flemings, M. C., "Measurement of Solute Redistribution in Dendritic Solidification", Trans. Met. Soc. AIME, Vol. 236, 1966, p. 624.

39. Piwonka, T. S., Flemings, M. C., "Pore Formation in Solidification", to be published Trans. AIME.

40. Bower, T. F., Brody, H. D., Flemings, M. C., "Effect of Solidification Variables on the Structure of Aluminum-Base Ingots", Casting and Solidification Section, Massachusetts Institute of Technology, Final Report, Department of the Amry, Materiel Command, MUCOM, Contract No. DA-19-020-ORD-5706(A).

41. Brody, H. D., "Solute Redistribution in Dendritic Solidification", Sc.D. Thesis, Department of Metallurgy, Massachusetts Institute of Technology, 1966.

42. Ellwood, E. C., Silcock, J. M., "The Lattice Spacing of the Solid Solution of Copper in Aluminum", Journal Inst. of Metals, Vol. 74, 1948, p. 457.

43. Troup, R. L., "Centerline Segregation", S.B. Thesis, Department of Metallurgy, Massachusetts Institute of Technology, June 1966.

44. Flemings, M. C., Utech, H. P., Miksch, E. S., "Effect of Fluid Flow on Solidification Structure", Casting and Solidification Section, Massachusetts Institute of Technology, Final Report, Office of Naval Research, Contract NONR-3963(09).

45. Piwonka, T. S., "Risering Considerations for Aluminum-Copper Alloys", S.M. Thesis, Department of Metallurgy, Massachusetts Institute of Technology, September 1960.

46. Gebhardt, V. E., Becker, M. and Dorner, S., "Uber die Eigenschafter Metallischer Schmelzen (VII)", Aluminum, Vol. 31, 1955.

APPENDIX A

List of Symbols

a_L, a_E	intercepts of liquidus and eutectic isotherm movement equations
a_T	$a_L - a_E$
A, A', A_E, A_0	cross sectional areas at x, x', x_E, and chill face, respectively
$\bar{C}$	local average composition of liquid and solid (weight fraction, weight per cent solute)
C_α	average composition of the entire amount of primary α phase in the final solid ingot (weight fraction, weight per cent solute)
C_E	composition of eutectic (weight fraction, weight per cent solute)
C_L	liquid composition (weight fraction, weight per cent solute) within volume element
C_L^c	liquid composition (weight fraction, weight per cent solute) at x' when $x_E = 0$
C_L^v	liquid composition (weight fraction, weight per cent solute) when feeding stops
C_0	overall composition (weight fraction, weight per cent solute) in a binary alloy
$\bar{C}_S$	average solid composition (weight fraction, weight per cent solute) after solidification
C_S^*	solid composition (weight fraction, weight per cent solute) at the liquid-solid interface
ΔC	macrosegregation (weight fraction, weight per cent solute)
f_L	weight fraction liquid
f_S	weight fraction solid
g_E	volume fraction eutectic
g_L	volume fraction liquid

g_L^c	volume fraction liquid at x' when $x_E = 0$
g_L^v	volume fraction liquid when feeding stops completely
g_S	volume fraction solid
G	temperature gradient
k	equilibrium partition ratio
L	total solidification length from a chill or wall (i.e., unidirectional solidification L = total length of ingot, ingot solidification from two walls L = width/2 etc)
n_L, n_E	slope of liquidus and eutectic isotherm movement equation
n_q	$(n_L - n_E)/n_E$
p	dimensionless group of variables = $\dfrac{v_x G}{\epsilon} \dfrac{(1 - \beta)}{\beta}$
t_v	time when feeding stops completely
t_v°	time when dendrite tips reach L
T_E	non-equilibrium solidus
T_L	liquidus temperature
U_E	velocity of eutectic isotherm T_E
$\vec{v}$	local velocity of liquid relative to solid (resulting from solidification contraction), cm/sec
v_x	local velocity of liquid relative to solid in the x direction (perpendicular to isotherms) resulting from solidification contraction
x, y, z	coordinate axies for volume element under consideration
x', y', z'	general coordinate axies
x_c	location of the liquidus isotherm when the eutectic isotherm is at $x_E = 0$

x_L, x_E location of the liquidus and eutectic isotherms (distance from the chill)

x_v location of "volume element" when feeding stops

β_E sol tion shrinkage $(\rho_S - \rho_L)/\rho_S$

ρ_E solidi ion shrinkage of eutectic

ϵ rate c perature change, °C/sec

$\bar{\rho}$ local average density (liquid and solid), gm/cm^3

ρ_α density of α phase gm/cm^3

ρ_L liquid density gm/cm^3

ρ_S solid density gm/cm^3

ρ_{SE}, ρ_{LE} densities of solid and liquid eutectic respectively, gm/cm^3

APPENDIX B

Calculations of Solute Redistribution, Unidirectional Solidification Constant k, β

1. $x > x_c$

Assume first the distribution of liquid in the mushy zone is as sketched in Figure 5b. Solidification conditions are described by:

$$x_L = n_L t^b + a_L \tag{B1}$$

$$x_E = n_E t^b + a_E \tag{B2}$$

$$\frac{g_L' - g_E}{x' - x_E} = \frac{1 - g_E}{x_L - x_E} \tag{B3}$$

Differentiate (B3) with respect to time at constant x'

$$\frac{dg_L'}{dt} = -\left(\frac{1 - g_E}{x_L - x_E}\right)\left[\frac{dx_E}{dt} + \left(\frac{x' - x_E}{x_L - x_E}\right)\frac{d}{dt}(x_L - x_E)\right] \tag{B4}$$

Rewrite (B3) for $x' = x$, $g_L' = g_L$; differentiate with respect to time at constant g_L. Set equal to $-\epsilon/G$ for linear g_L and T versus x:

$$\left(\frac{\partial x}{\partial t}\right)_{g_L} = \left(\frac{g_L - g_E}{1 - g_E}\right)\left(\frac{\partial}{\partial t}\right)(x_L - x_E) - \frac{\partial x_E}{\partial t} = -\frac{\epsilon}{G} \tag{B5}$$

Now, for constant ρ_L, equation (22) is written:

$$g_L v_x = \frac{\beta}{1 - \beta}\left[\int_{x_E}^{x} \frac{dg_L'}{dt} \partial x' - g_E \frac{dx_E}{dt}\right] \tag{B6}$$

Substitute (B4) in (B6) and integrate:

$$g_L v_x = - \left(\frac{\beta}{1-\beta} \right) \left[(1-g_E)\left(\frac{x-x_E}{x_L-x_E}\right)\left[\frac{dx_E}{dt} + \frac{1}{2} \left(\frac{x-x_E}{x_L-x_E}\right)\frac{d}{dt} (x_L-x_E)\right] + g_E \frac{dx_E}{dt} \right]$$

$$\dotsb (B7)$$

Combine (B5) and (B7):

$$\frac{v_x G}{\varepsilon} = \frac{\beta}{1-\beta} \left(\frac{1}{g_L}\right) \frac{(1-g_E)\left(\frac{x-x_E}{x_L-x_E}\right)\left[\frac{dx_E}{dt} + \frac{1}{2} \left(\frac{x-x_E}{x_L-x_E}\right) \frac{d}{dt} (x_L-x_E)\right] + g_E \frac{dx_E}{dt}}{\left(\frac{g_L-g_E}{1-g_E} \right) \frac{\partial}{\partial t} (x_L-x_E) + \frac{\partial x_E}{\partial t}} \dotsb (B8)$$

Substitute in

$$\frac{x - x_E}{x_L - x_E} = \frac{g_L - g_E}{1 - g_E} \tag{B9}$$

$$\frac{dx_E}{dt} = \frac{\partial x_E}{\partial t} = bn_E t^{b-1} \tag{B10}$$

$$\frac{d}{dt} (x_L - x_E) = \frac{\partial}{\partial t} (x_L - x_E) = b (n_L - n_E)t^{b-1} \tag{B11}$$

$$n_q = \frac{n_L - n_E}{n_E} \tag{B12}$$

and (B8) becomes

$$\frac{v_x G}{\varepsilon} = \frac{1}{2} \left(\frac{\beta}{1 - \beta} \right) \left[\frac{g_L(g_L n_q + 2b) + n_q g_E^2}{g_L(g_L n_q + b)} \right] \tag{B13}$$

where $b = 1 - g_E - n_q g_E$

Solute redistribution, and from this, macrosegregation can now be determined analytically by substituting (B13) in equation (20) and integrating from $g_L = 1$ at $C_L = C_0$ to g_L, C_L. The analytic expression so obtained is cumbersome. For small g_E, however, (B13) reduces to:

$$\frac{v_x G}{\epsilon} = \frac{1}{2} \left(\frac{\beta}{1 - \beta} \right) \left[\frac{g_L n_q + 2}{g_L n_q + 1} \right] \tag{B14}$$

which is also the expression obtained by assuming the distribution of
liquid in the mushy zone as given in Figure 5c. Substitution of
typical values for unidirectionally solidified aluminum-4.5 per cent
copper shows that results obtained from (B14) are at most a few per
cent different from those obtained using (B13), and (B14) is therefore
used for subsequent analysis.

As example of the difference, consider the case of $k = .172$,
$\beta = .055$, $n_q = .52$. Calculated values of $\frac{v_x G}{\epsilon}$ obtained from the two
equations are given in Table B1:

TABLE B1

Values of $\frac{v_x G}{\epsilon}$ for Aluminum-4.5 Per Cent Copper

g_L	$\frac{v_x G}{\epsilon}$ (Eq.B14)	$\frac{v_x G}{\epsilon}$ (Eq.B13)	Per Cent Difference
1.0	–	–	–
.9	.0489	0.0480	– 1.6
.5	.0522	.0517	– 1.0
.1	.0567	.0578	+ 1.9
.0902 (eutectic)	.0569	.0582	+ 2.3

Now, substituting equation (B14) in equation (20), and integrating from the limits $g_L = 1$ at $c_L = C_0$ to g_L, C_L, the final solute redistribution expression is:

$$C_L = C_0 g_L^{-(1-k)} \left[\frac{g_L n_q a + 1}{n_q a + 1} \right]^{-\frac{(1-a)(1-k)}{a}} \tag{B15}$$

where $a = 1 - \frac{\beta}{2}$

2. $x < x_c$

For calculations of solute redistribution at locations close to the chill face a procedure similar to the foregoing is followed except that for $x < x_c$ and $g_L > g_L^c$, $g_L v_x$ (see equation B6 above) is calculated by integration of equation (22) from the limits 0 to x, not x_E to x. The resulting expression for $g_L = 0$ is:

$$\frac{v_x G}{\varepsilon} = \frac{x}{2} \left(\frac{\beta}{1 - \beta} \right) \frac{2(x - x_E) + g_L n_q (x - 2x_E)}{(x - x_E)^2 (g_L n_q + 1)} \tag{B16}$$

where

$$x_E = \frac{x + g_L a_E (n_q - 1) + a_L g_L}{g_L n_q + 1} \tag{B17}$$

Substitute (B17) in (B16)

$$\frac{v_x G}{\varepsilon} = \frac{x}{2} \left(\frac{\beta}{1 - \beta} \right) \frac{2P + (g_L Q - x) n_q}{g_L P^2} \tag{B18}$$

where

$$P = n_q x - a_E n_q + a_E - a_L \tag{B19}$$

$$Q = n_q x - 2a_E n_q + 2a_E - 2a_L \tag{B20}$$

Substitute (B16) in equation (20)

$$-\frac{1}{1-k}\frac{dC_L}{C_L} = \frac{dg_L}{N + Mg_L} \tag{B21}$$

where

$$N = \frac{\beta x(2P - xn_q)}{2P^2} \tag{B22}$$

$$M = \frac{x\beta Q n_q + 2(1 - \beta)P^2}{2P^2} \tag{B23}$$

Integrating between the limits $g_L = 1$ at $C_L = C_0$ and g_L, C_L

$$C_L = C_0 \left(\frac{N + Mg_L}{N + M}\right)^{-\frac{1-k}{M}} \tag{B24}$$

APPENDIX C

Calculation of Solute Redistribution in Final Transient Region During Unidirectional Solidification

From Figure (C-1)

$$(1 - x_v) = - \int_{t_v^\circ}^{t^v} v_x dt \tag{C1}$$

for $n_q = 0$, $x_L - x_E = $ constant

$$v_x = \frac{\beta}{1 - \beta} \frac{dx_E}{dt} \tag{C2}$$

$$g_L^v = \frac{x_v - x_E}{x_L - x_E} \tag{C3}$$

where $g_L^v = $ fraction liquid at x_v

Differentiating (C3) and rearranging

$$dx_E = dx_v - (x_L - x_E) \, dg_L^v \tag{C4}$$

Substituting in (C1)

$$1 - x_v = \int_{t_v^\circ}^{t_v} - \frac{\beta}{1 - \beta} [dx_v - (x_L - x_E) dg_L^v] \tag{C5}$$

at time t_v, $x_v = x_v$, $g_L^v = g_L^v$

at time t_v°, $x_v = L$, $g_L^v = 1$

Substituting these limits in (C5)

$$L - x_v = \frac{\beta}{1-\beta} \int_L^{x_v} dx_v - \frac{\beta}{1-\beta} \int_1^{g_L} (x_L - x_E) dg_L^v \qquad (C6)$$

Integrating between limits

$$1 - x_v = \frac{\beta}{1-\beta} [(x_v - L) - (x_L - x_E)(g_L^v - 1)] \qquad (C7)$$

Solving for g_L^v yields

$$g_L^v = 1 - \frac{(1 - x_v)}{(x_L - x_E)\beta} \qquad (C8)$$
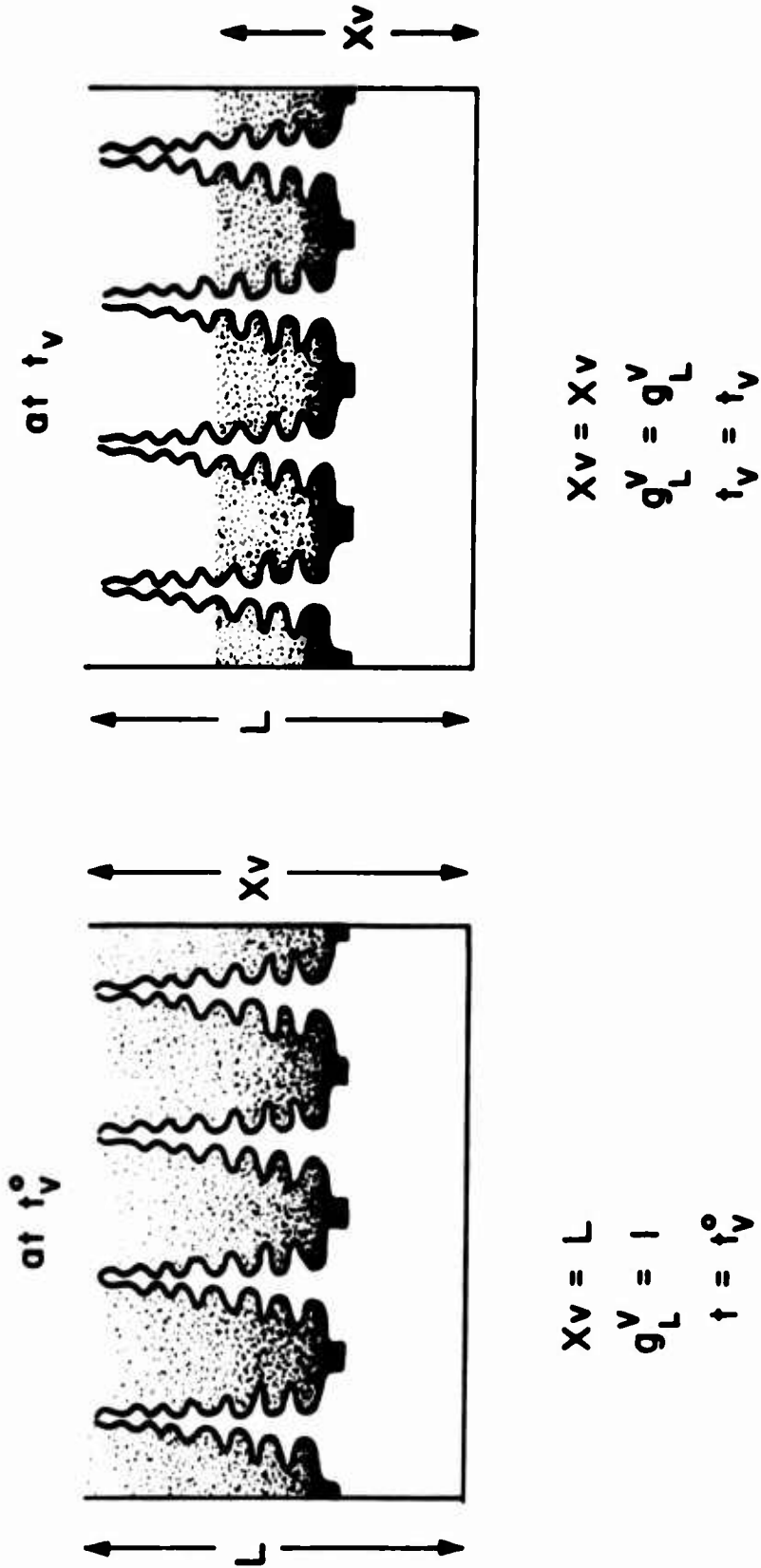
Figure C-1: Transient zone, end of solidification at ingot top: (a) time, t_v^o, when dendrite tips first reach top of ingot, (b) time, t_v, at a later stage of solidification (before completely solid).

APPENDIX D

Calculation of Solute Redistribution: Unidirectional Solidification; Constant k, β; Pyramid Shape Ingot

1. $x > x_c$

From equation (23) when $g_E = 0$

$$Ag_L v_x = - \frac{\beta}{1 - \beta} \int_{x_E}^{x} \frac{dg_L'}{dt} x'A' \qquad (D1)$$

where

$$A' = (1 - \frac{x'}{L}) A_0 \qquad (D2)$$

from (B4) with $n_q = 0$, $x_L = x_E$ = constant

$$\frac{dg_L'}{dt} = (\frac{1}{x_L - x_E}) [\frac{dx_E}{dt}] \qquad . \qquad (D3)$$

Substitution of (D2) and (D3) in (D1)

$$(1 - \frac{x}{L})g_L v_x = - \frac{\beta}{1 - \beta} \int_{x_E}^{x} \frac{1}{x_L - x_E} \frac{dx_E}{dt} (1 - \frac{x'}{L})\partial x' \qquad (D4)$$

integration yields

$$v_x = - \frac{\beta}{1 - \beta} (\frac{1}{L - x}) \frac{dx_E}{dt} [L \frac{(x - x_E)}{(x_L - x_E)} - \frac{x^2 - x_E^2}{2(x_L - x_E)} \qquad (D5)$$

from (B9) when $g_E = 0$

$$\frac{x - x_E}{x_L - x_E} = g_L \qquad (D6)$$

From (B17) when $n_q = 0$

$$x_E = x + a_T g_L \tag{D7}$$

where $a_T = a_L - a_E$ \hfill (D8)

From (B5)

$$\frac{\varepsilon}{G} = - \frac{dx_E}{dt} \tag{D9}$$

Substitution of (D7) and (D9) in (D5)

$$\frac{v_x G}{\varepsilon} = \frac{\beta}{1 - \beta} \left(\frac{1}{L - x} \right) \left(\frac{2L(x_L - x_E) + 2xa_T + a_T^2 g_L}{2(x_L - x_E)} \right)$$

2. $x < x_c$

Integration limits on (D1) change

$$Ag_L v_x = - \frac{\beta}{1 - \beta} \int_0^x \frac{dg_L'}{dt} \partial x' A' \tag{D10}$$

Substitution of (D2) and (D3), integration and substitution of (D9) yields

$$\frac{v_x G}{\varepsilon} = - \frac{\beta}{1 - \beta} \left(\frac{1}{L - x} \right) \left[\frac{x(2L - x)}{2g_L} \right] \tag{D11}$$

APPENDIX E

Experimental Casting Procedure

A. Introduction

    1. Unidirectional Heat Flow.

The typical experimental set up shown in Figure E-1 was used,
except for one series of centerline segregation experiments, for all
castings and ingots made as part of the current investigation. Since
unidirectional solidification is desired, essentially all heat must
be extracted from one surface of the ingot. This was accomplished by
doing all casting and solidification in an electrically heated
furnace.

After placing the entire assembly in the furnace with coolant pipes
extending outside, the unit was heated to 600-700°C. When the plaster
reached the desired temperature (usually 1-2 hours after the furnace
temperature) the mold was filled through a funnel extending from the
outside of the furnace into the cavity. The assembly, with liquid
was held for several minutes to allow convection to subside. The
coolant, either air or water (depending on the desired solidification
rate) was turned on and the ingot solidified. With the four sides
and top insulated, heat removal for solidification was through the
bottom surface, resulting in fully columnar structures.

Casting and ingot designs were varied, as discussed in Experimental
Results and Discussion section, to produce desired macrosegregation
effects. However, for casting solidified with unidirectional heat flow

the top was always open to the furnace atmosphere and temperature, the bottom surface rested on a chill through which the heat was extracted, and all other surfaces were insulated with plaster.

2. Centerline Segregation Experiment.

The centerline segregation experiment was designed to produce two unidirectionally solidifying fronts meeting at the ingot center, Figure E-2. Casting procedure was the same as in the straight uni-directional ingot with water or air used as coolant. (Piping is not shown in schematic drawing, however, continuous flow was supplied to both chills.)

B. Mold Preparation

In many ingots, thermocouples were used to obtain continuous records of solidification. In all cases these were chromel-alumel couples with output continuously monetered on a L & N Speedomatic W, Multipoint (12) recorder.

When it was necessary to locate many thermocouples accurately, the pattern for the ingot was first shaped from foamed polystyrene. The thermocouples (alumina sheathed, tips coated with boron nitride), were placed in the styrofoam pattern at the desired locations. The assembly was placed inside a stainless steel flask, the flask was then filled with liquid plaster which was allowed to set. The result was that the thermocouples remained accurately located since they were held in place by the plaster.

The mold was next fastened to the chill and placed in the furnace with the foamed polystyrene still in place. Upon subsequent heating the polystyrene vaporized and left a deposit-free cavity.

When castings were made without thermocouples, wood patterns were used rather than styrofoam. The greased wood pattern was placed inside a flask, liquid plaster poured around the pattern and allowed to set. After setting, the pattern was removed and the mold fastened to the chill. The assembly could then be placed in the furnace.

C. Metal Melting Procedure

All melts were prepared from aluminum-4.5 per cent master heats. These had been previously cast into 5 to 7 pound ingots from high purity aluminum (99.99 per cent) and 50-50 aluminum-copper OFHC master alloy. All melting was done in "Fiberfrax" coated graphite crucibles using a gas-fired furnace. After preheating the crucible for an hour or more, the charge was melted and superheated to a temperature of 690-720°C. After stirring the melt, a chlorine degas was carried on for 10 minutes. After stirring again for one minute a gas sample, under reduced pressure, was taken. When the sample was gas-free, the crucible was removed from the furnace, a chemical analysis specimen taken up into a 7 mm vycor tubing, and skimmed. Pouring temperature into the mold was about 680 to 700°C. After pouring, another chemical analysis specimen was taken from the remaining liquid metal.
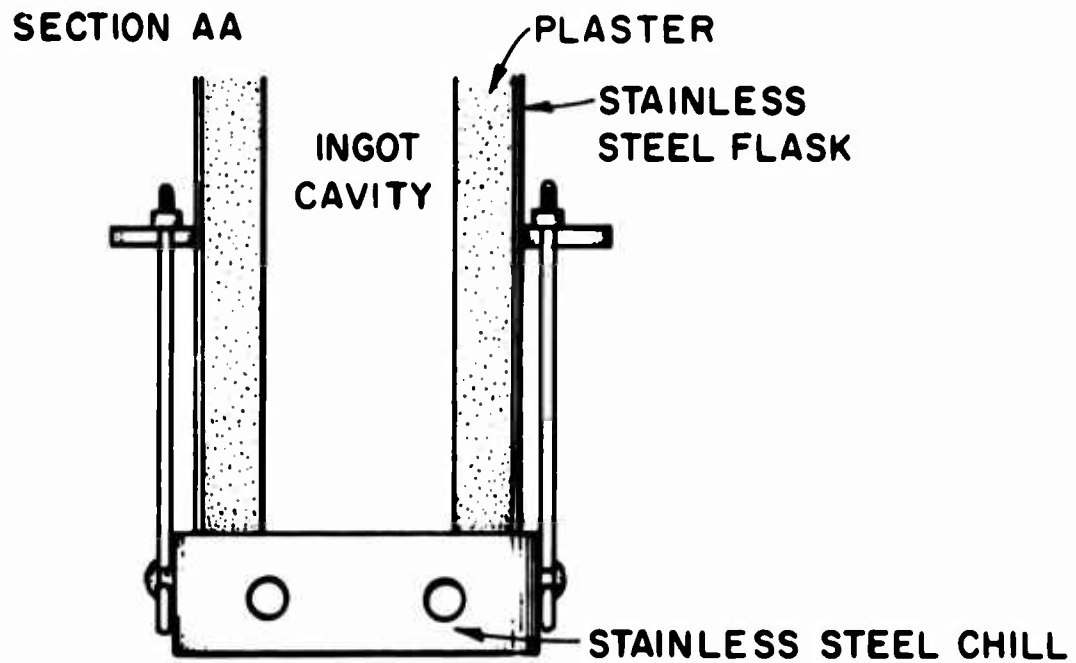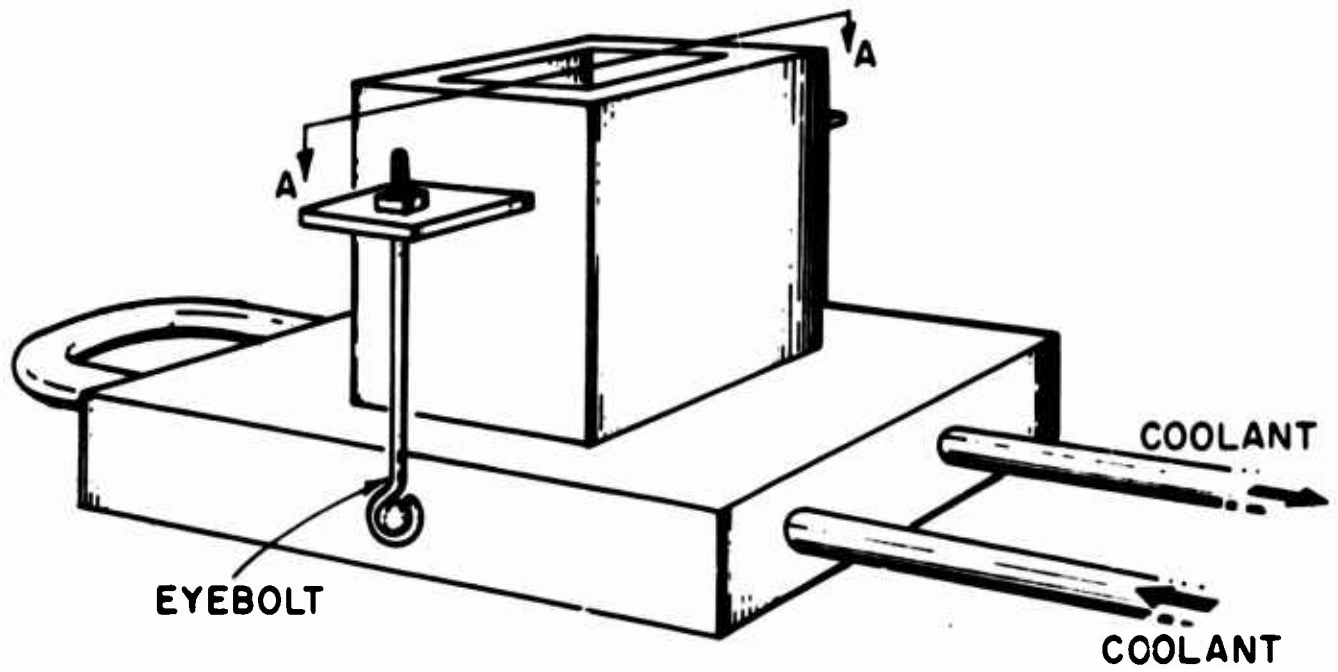
Figure E-1: (a) Schematic diagram of unidirectional solidification, mold-chill assembly.
(b) Cross section of assembly.

CHILLS

PLASTER

CHILL

FLASK
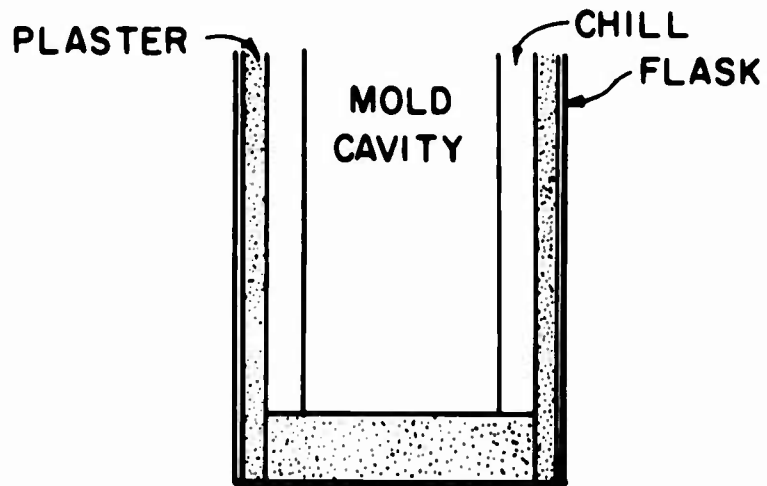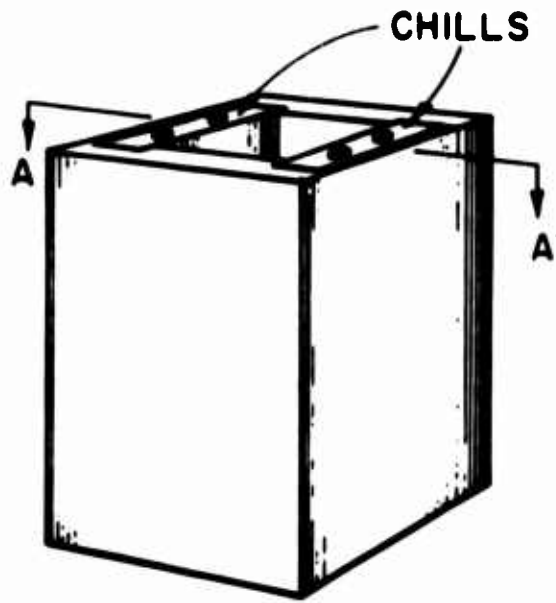
MOLD
CAVITY

Figure E-2: (a) Schematic diagram of centerline segregation, mold-chill assembly.
(b) Cross section of assembly.

APPENDIX F

Chemical Anlysis by Fluorescence

A. Introduction

When any material is bombarded with electrons of X-rays of high enough energy a characteristic line spectrum is emitted. This can be used as a basis for either qualitative or quantitative chemical analysis. For qualitative analysis the various elements in a sample are made to emit their "characteristic lines", these elements may then be identified by analyzing the emitted radiation and showing that the specific wavelengths characteristic of the element are present. By comparing the intensity of these lines with the intensities of lines from suitable standards, a method of quantitative analysis is available. For multicomponent systems, comparison with standards is complicated by interactions between elements. When dealing with binary systems however, it is a rapid, accurate method for obtaining reproducible chemical analysis.

In the present work a General Electric XRD-5, X-ray Spectrometer was used with a tungsten target tube. The primary white radiation from the tube was used to fluoresce aluminum-copper samples on an area 1.25 cm by 1.8 cm. This sample size insured that the analysis was representative and no microsegregation effects are recorded. That is, we are measuring local composition by integrating over many dendrites, which are typically $10-1000\mu$ center to center spacing.

The secondary radiation from the aluminum-copper alloy is then diffracted from a single crystal of known d spacing (lithium fluoride, d spacing 2.014).

The Bragg law predicts that for each angular setting of the crystal, radiation of only a single wavelength is reflected. The spectrometer was set at 45.08° which for the crystal and spacing used reflects the copper, K_α wavelength. The intensity of this "characteristic line" was measured and compared to a standard intensity curve.

B. Standards Preparation

Standards were prepared with the same apparatus used by Bower[40] in a study of solidification in thin plate castings. (Shown schematically in Figure F-1). By drawing a vacuum and placing the molds in the melt molten metal is forced between the two copper chills, spaced 1/8 inch apart, and allowed to solidify. Compositional variations were obtained by successively adding high copper master alloy to low alloy heats.

A 10 pound heat of aluminum-1 per cent copper was melted in a gas furnace using a graphite crucible. After degasing with chlorine, samples were sucked into the chill mold at 1500°F. Master alloy of 50 per cent copper-aluminum composition was added to increase alloy content of the melt to about 2.5 per cent copper. Again the melt was degassed and samples sucked into the chill mold. By progressively adding alloy, a series of standards were prepared. After cooling to room temperature the samples were sanded on coarse paper to remove any exuded layer. They were then sanded down to 300 grit emergy, a finish smooth enough

for use in fluorescent analysis. Table F-1 lists the compositions obtained.

TABLE F-1

Standard	Composition-% Copper
A	1.12
B	2.69
C	4.35
D	5.83
E	8.48

After sanding the cast surfaces on the edge, two pieces weighing about one gram each were removed from opposite sides and used for wet analysis. The average of these compositions was taken to be the composition of the plate.

C. Standard Curve Determination

Fluorescence of the five standards was carried out as previously described. The intensity from Standard E (maximum copper) was measured first with the power adjusted to give approximately 100,000 counts per second. This approaches the limits of the scaler used for counting. At greater than 100,000 counts/sec the unit can be flooded and inaccuracies result. After the intensity from Standard E was determined, Standards A through D were measured. Since the intensity of copper, K_α is being used for comparison, decreasing copper content means decreasing intensity. After all five samples are measured Standard E is normalized

to $I/I_o = 1$. The intensity of standards is A to D are divided by I_o (the intensity of Standard E) to give normalized intensities. (These values are plotted in Figure F-2).

D. Composition Determination

When the intensity from a series of unknowns is measured, Standard E is also measured. The intensity of the unknown divided by the intensity of Standard E (I_o) gives a fraction less than one (if the composition of the unknown is less than 8.48 per cent copper). This fraction can be directly translated to a per cent copper from Figure F-2.

Standard practice was to check one of the Standards A to D each time a series of unknowns was determined to be sure reproducibility of results was obtained. As a further check, periodically samples which had been analyzed by fluorescence were also checked by wet chemical methods. Agreement was found generally to be within $\pm$ 0.05 copper. Another method of insuring accuracy was the redetermination of standard curves. Three different times during the investigation the standard curves were redetermined. Each time, no significant difference was found between curves.
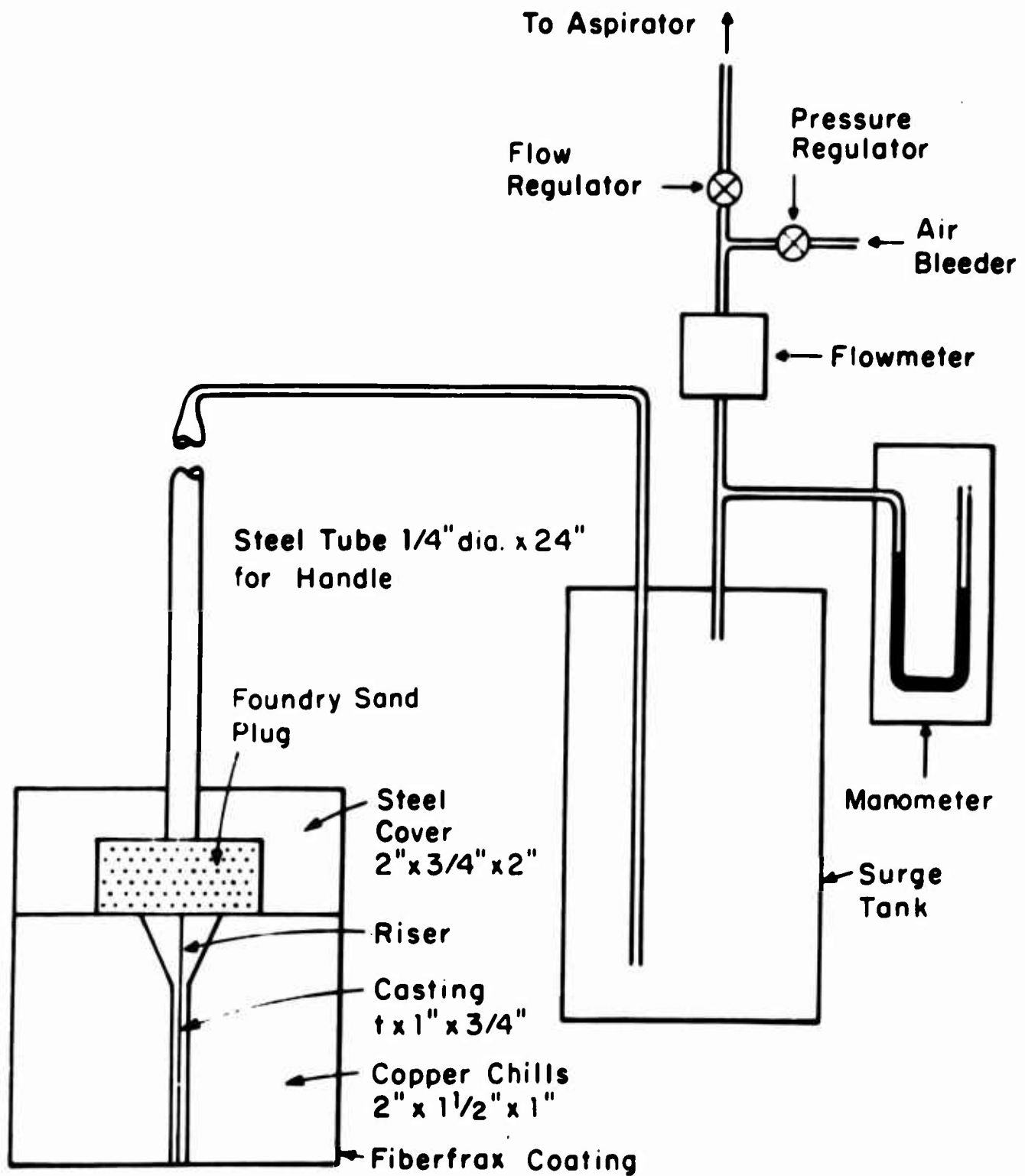
Figure F-1: Schematic diagram of apparatus used to prepare standard chemical analysis specimens.
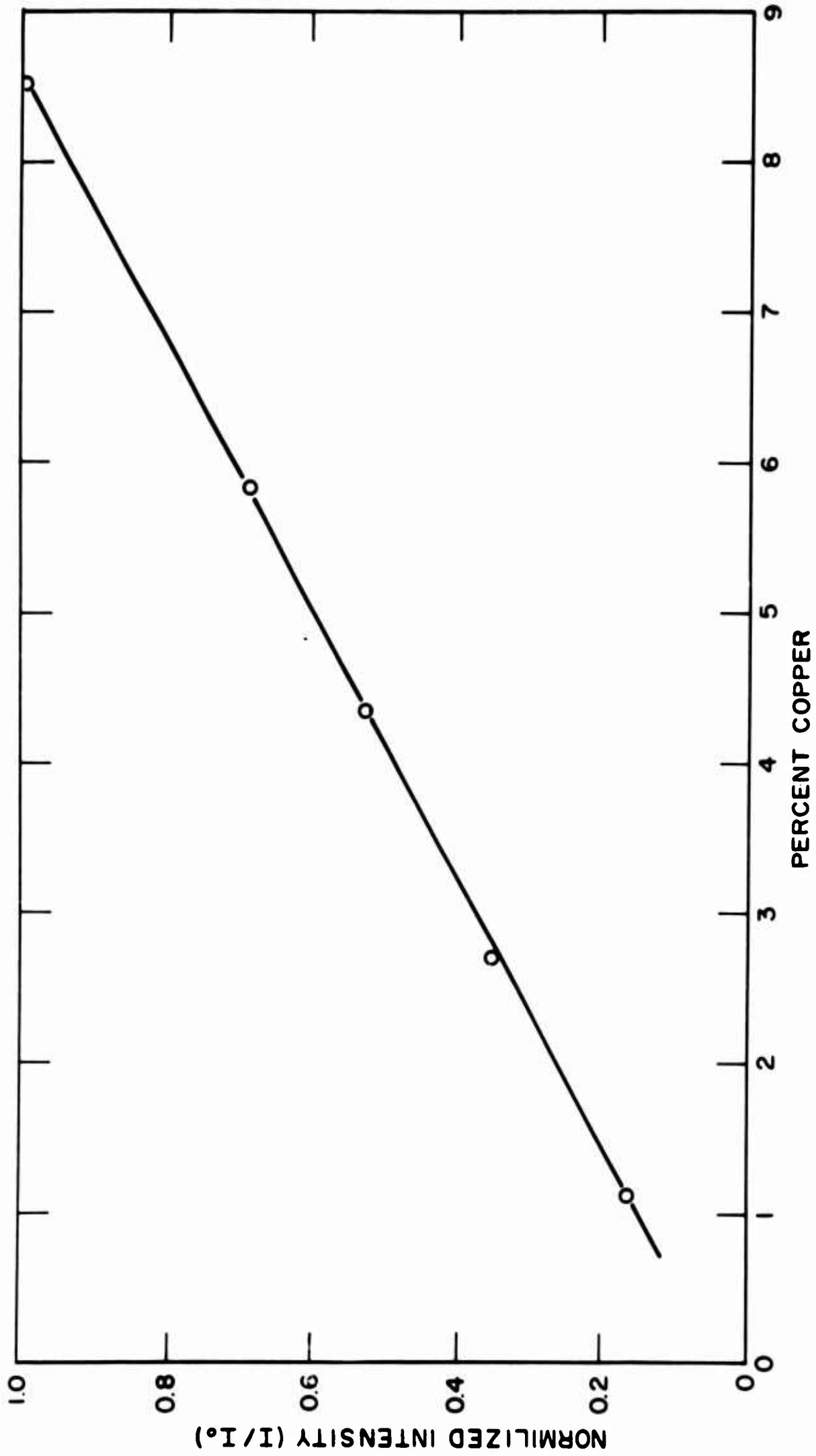
Figure F-2: Standard chemical analysis curve.

APPENDIX G

Outline for Composition Calculations

The following is an outline of the method used to calculate chemical composition at various locations in unidirectionally solidified ingots, using thermal data and relationships developed in the theoretical section. As example, the calculations are given for a point 7.9 cm from the chill, in the reduced section ingot described in the Experimental Results and Discussion section.

A. Thermal Data

Temperature versus time curves at the different thermocouple locations are made directly from the output recorded on the L & N Speedomatic W Recorder (Figure G-1).

B. Temperature Versus Fraction Liquid

A temperature versus fraction liquid curve is drawn assuming $g_E = 0$ and fraction liquid distribution in the mushy zone is linear (Figure G-2a). For comparison, a curve of actual fraction liquid in the mushy zone is shown, Figure G-2b (see Macrosegregation Versus Distance from Chill in Theoretical Section).

C. Calculation of v_x

By using the data from Figures G-1 and G-2a, Figure G-3 is constructed to be used for graphical integration to find v_x as follows:

(1) At a constant x, $\Delta g_L \Delta x$ is determined by adding up the number of squares from $g_L = 0$ to $g_L = 1$ between t_n and t_{n+1} and multiplying by the area of each square. Area to the left of the ingot reduction is weighted 9 times that to the right (ratio of area reduction). That is in equation form.

(2) Equation (23) is solved for the case of no eutectic:

$$A_2 g_L v_x = \frac{\beta}{1-\beta} A_1 \int_{x_E}^{x_c} \frac{\Delta g_L'}{t_{n+1} - t_n} dx' + \frac{\beta}{1-\beta} A_2 \int_{x_c}^{x} \frac{\Delta g_L'}{t_{n+1} - t_n} dx'$$

$$\ldots\ldots\ldots\ldots (G1)$$

Equation (G-1) is written for the reduced cross section ingot, for $x > x_c$ and for $x_E > 0$ where:

x_c = distance from chill to reduction in cross section

x = distance from chill to location where composition is being calculated

Δg_L = change in fraction liquid at x from t_n to t_{n+1}

A_1 = area of lower (large) section

A_2 = area of upper section

For the general case of constant cross section at locations in the ingot unaffected by the reduction, equation (G-1) becomes:

$$g_L v_x = \frac{\beta}{1-\beta} \left(\frac{\Delta g_L \Delta x}{t_{n+1} - t_n} \right) \qquad\qquad (G2)$$

D. v_x Versus g_L

Figure G-4 is obtained by taking v_x as being linear and averaged over the interval Δg_L. That is the determined value is plotted at:

$$g_L = \frac{(g_L)_n + (g_L)_{n+1}}{2} \qquad (G3)$$

where g_L = fraction liquid at x at time $t = \dfrac{t_n + t_{n+1}}{2}$

This is plotted as Figure G-4.

E. Calculation of G/ϵ

G/ϵ is calculated by first replotting the data of Figure G-3 as in Figure G-5 and then the reciprocal of these slopes are G/ϵ at a given x for various g_L. In Figure G-5 sample curves for two values of g_L are shown. In practice a whole family of curves is necessary to calculate G/ϵ as a function of g_L.

F. G/ϵ Versus g_L

Figure G-6 shows G/ϵ as a function of g_L. Using this and Figure 4, $\dfrac{v_x G}{\epsilon}$ as a function of g_L can be calculated.

G. Calculation of Local Average Composition

From the steady state solute redistribution expression $\dfrac{v_x G}{\epsilon}$ is found as a function of C_L. C_L being calculated from the values of g_L assuming steady state values. The final plot is $\dfrac{v_x G}{\epsilon}$ versus $\ln C_1$ which is necessary to solve the solute redistribution (equation 20). This is shown in Figure G-7.

Average composition is found as follows:

Solve by taking two cases of macrosegregation equation:

$$(1 - k) \frac{dg_L}{g_L} = - (1 - \beta)(1 + \frac{v_x G}{\epsilon}) \frac{dC_L}{C_L} \qquad (G4)$$

also take case where $v_x = 0$, at chill face where maximum segregation can be calculated

$$(1 - k) \frac{dg_L}{g_L^\circ} = - (1 - \beta) \frac{dC_L}{C_L} \qquad (G5)$$

Subtracting (1a) from (1)

$$(1 - k) \ln \frac{g_L}{g_L^\circ} = (1 - \beta) \int_{C_0}^{C_L} \frac{v_x G}{\epsilon} \frac{dC_L}{C_L} \qquad (G6)$$

.A plot of $\frac{v_x G}{\epsilon}$ versus $\ln C_L$ as in Figure G-7 allows graphical integration to solve the general macrosegregation equation. The area under the curve will give the term inside the integral of equation (3):

$$area = - \frac{(1 - k)}{(1 - \beta)} \ln \frac{g_L}{g_L^\circ} \qquad (G7a)$$

to find g_E

$$- \frac{area (1 - \beta)}{(1 - k)} = \ln \frac{g_E}{g_E^\circ} \qquad (G7b)$$

g_E (33% Copper in eutectic) $= C_E$

$C_\alpha \doteq 1.51 - 1.54$

$\bar{C}_S = C_\alpha + C_E$
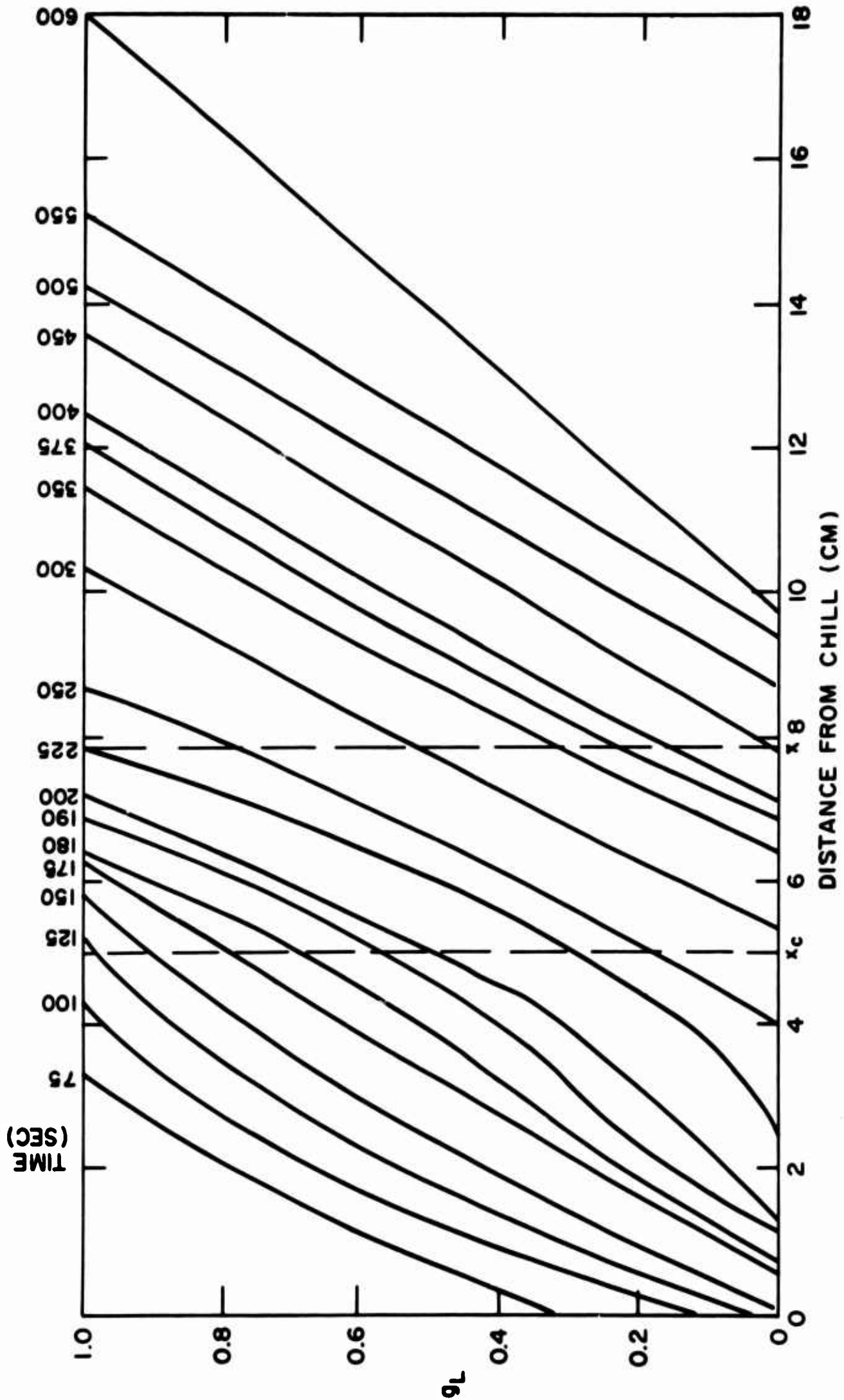
Figure G-3: Fraction liquid versus distance from the chill for the 9 to 1 reduced section ingot.
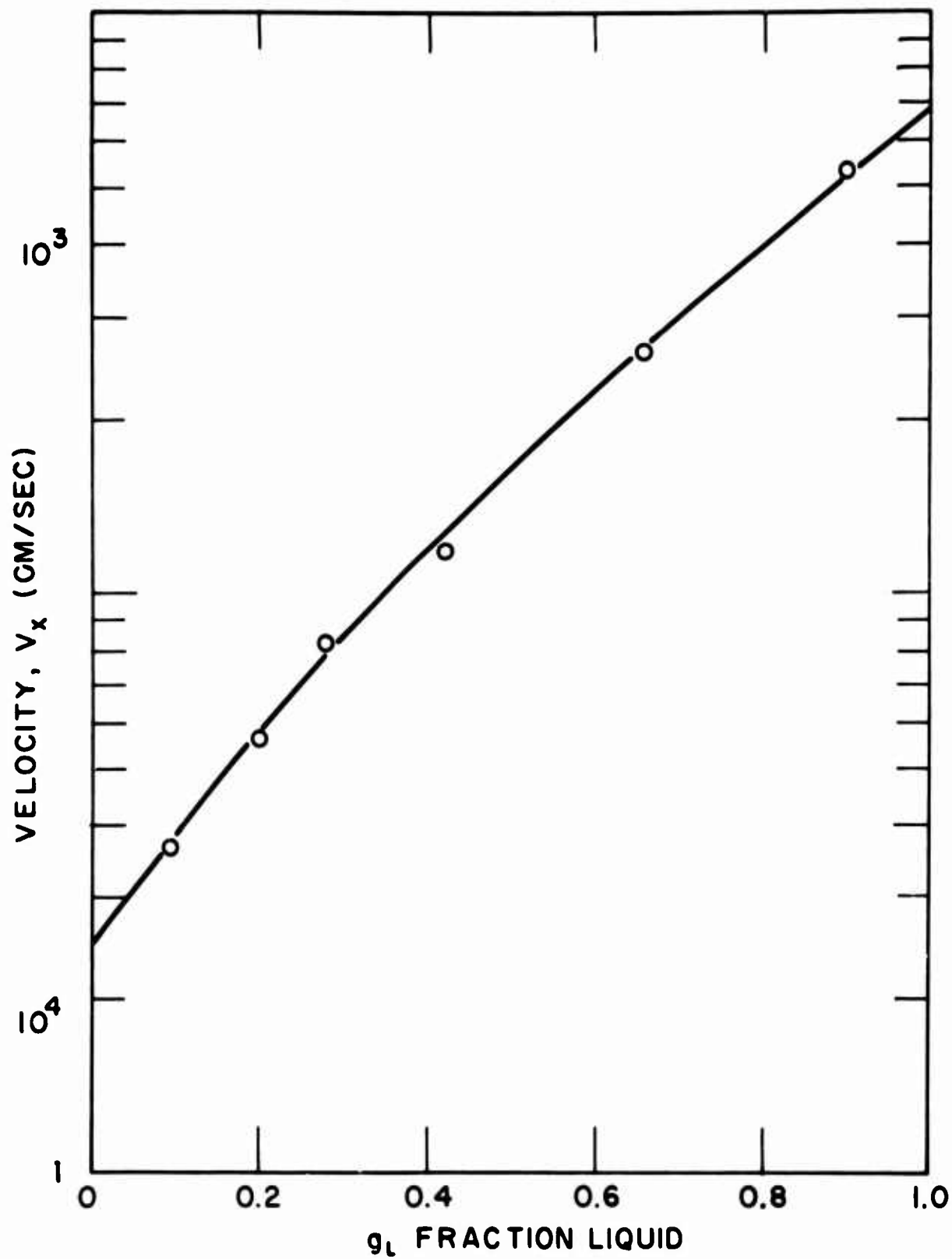
Figure G-4: Calculated v_x versus g_L for the 9 to 1 reduced
section ingot at $x = 7.9$ cm from the chill.
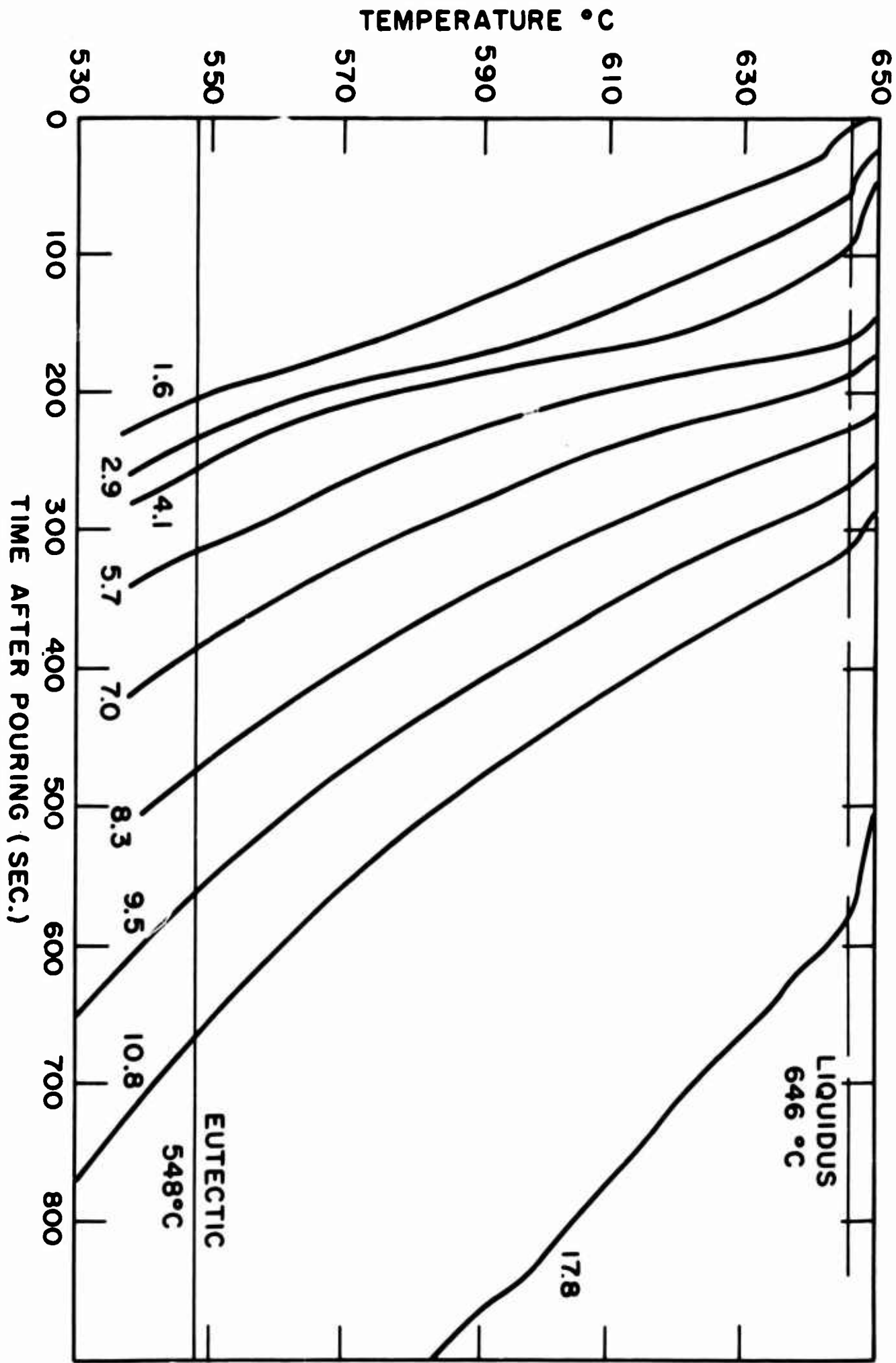
Figure G-1: Thermal data for 9 to 1 reduced section ingot (composition versus distance from chill presented in Figure 38). Numbers are location of thermocouple (cm from chill).
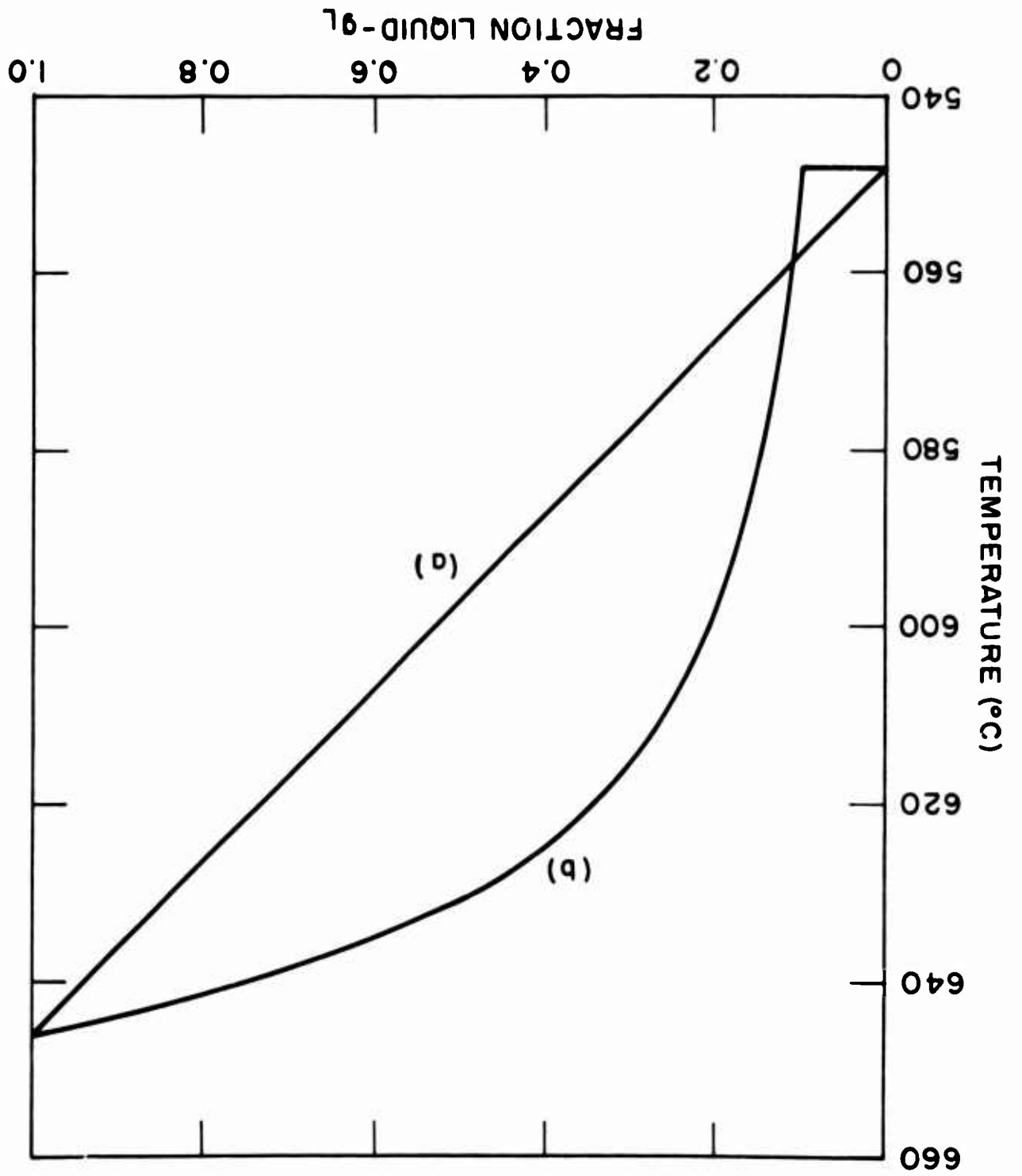
Figure G-2: Temperature versus fraction liquid for $C_0 = 4.68$ per cent copper alloy. (a) Assuming linear distribution in liquid-solid region. (b) Steady state solidification in the liquid-solid region.
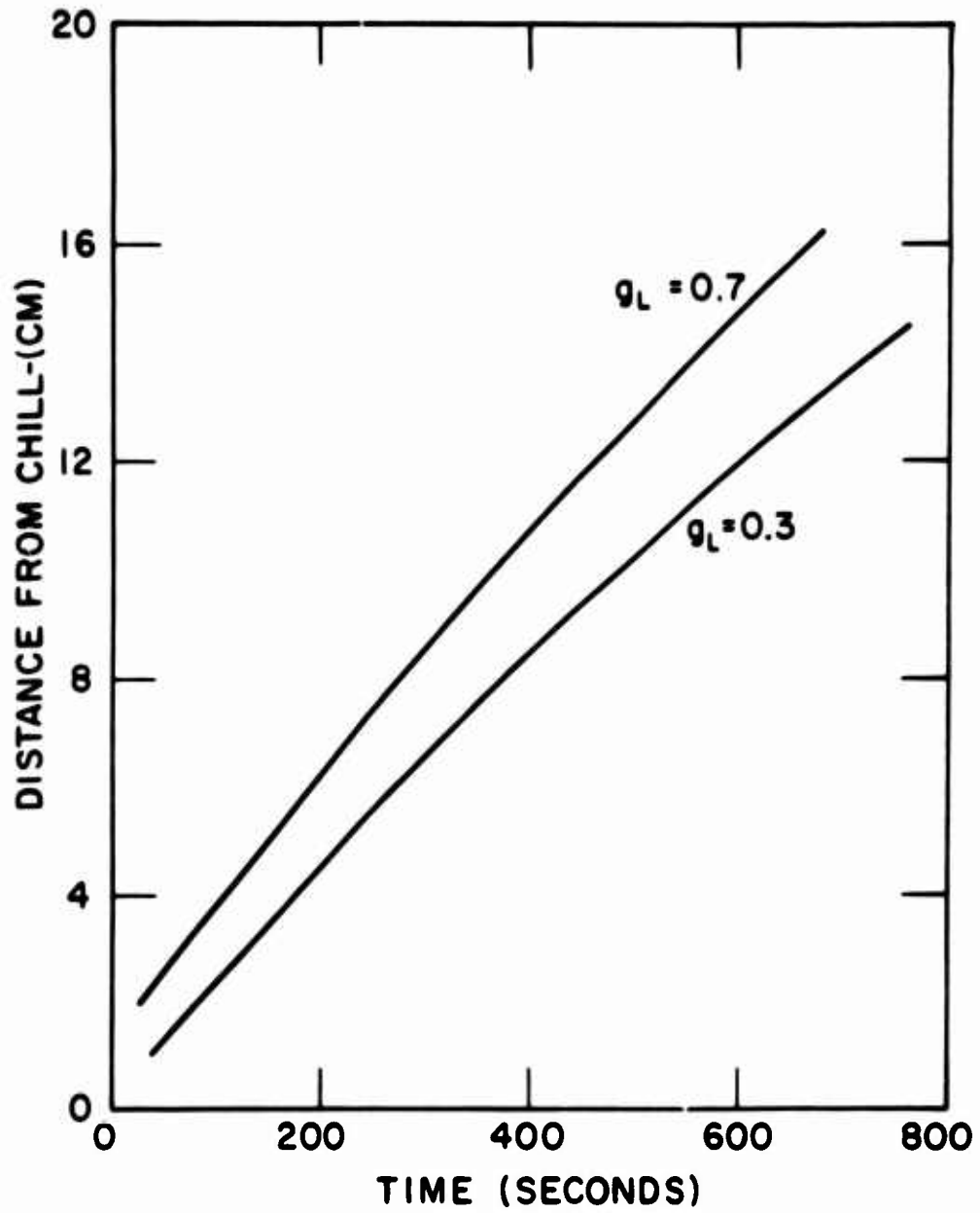
Figure G-5: Constant fraction liquid curves plotted as a function of time versus distance from the chill.
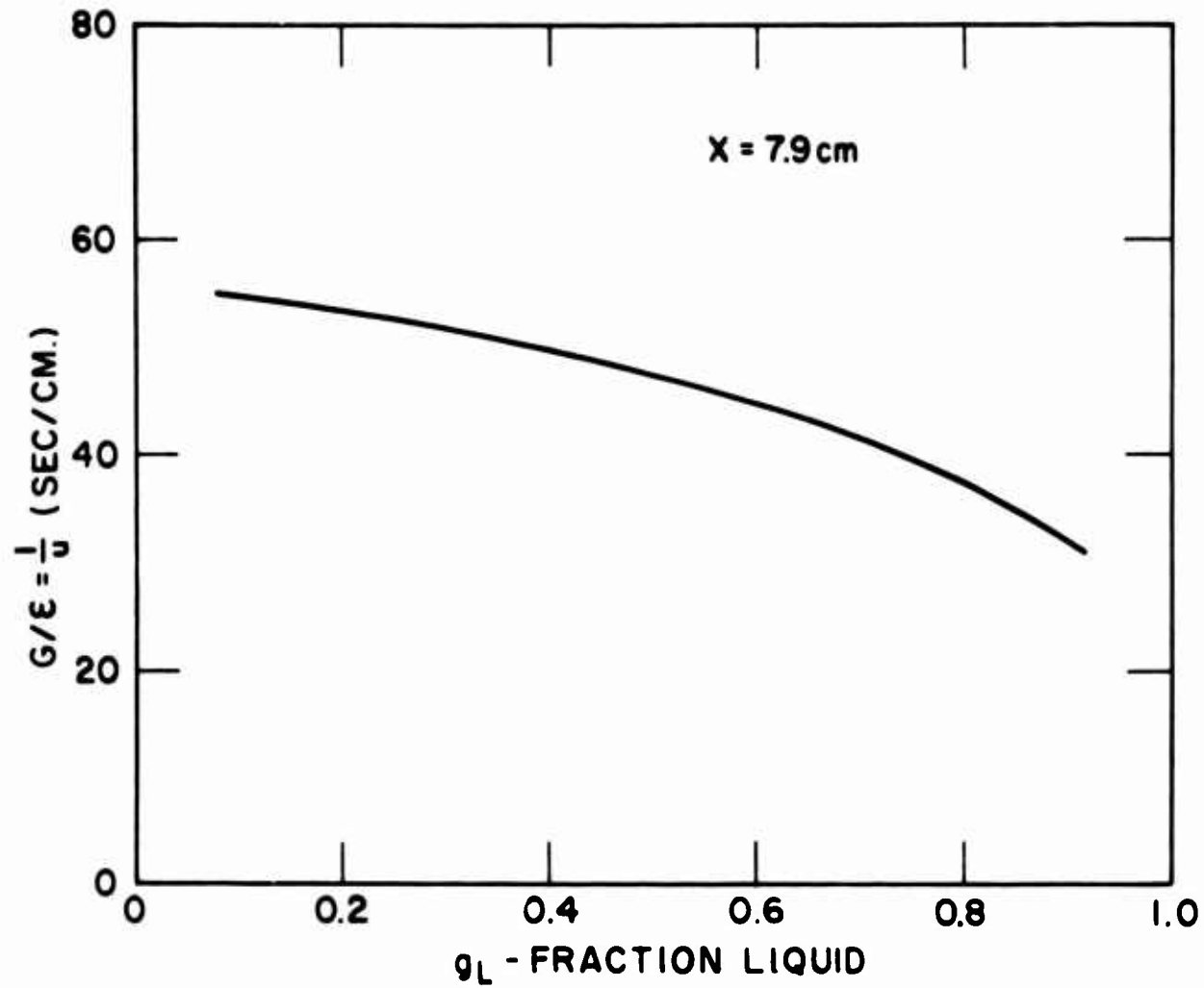
Figure G-6: G/ε versus fraction liquid (g_L) at 7.9 cm from chill
in the 9 to 1 reduced section ingot.
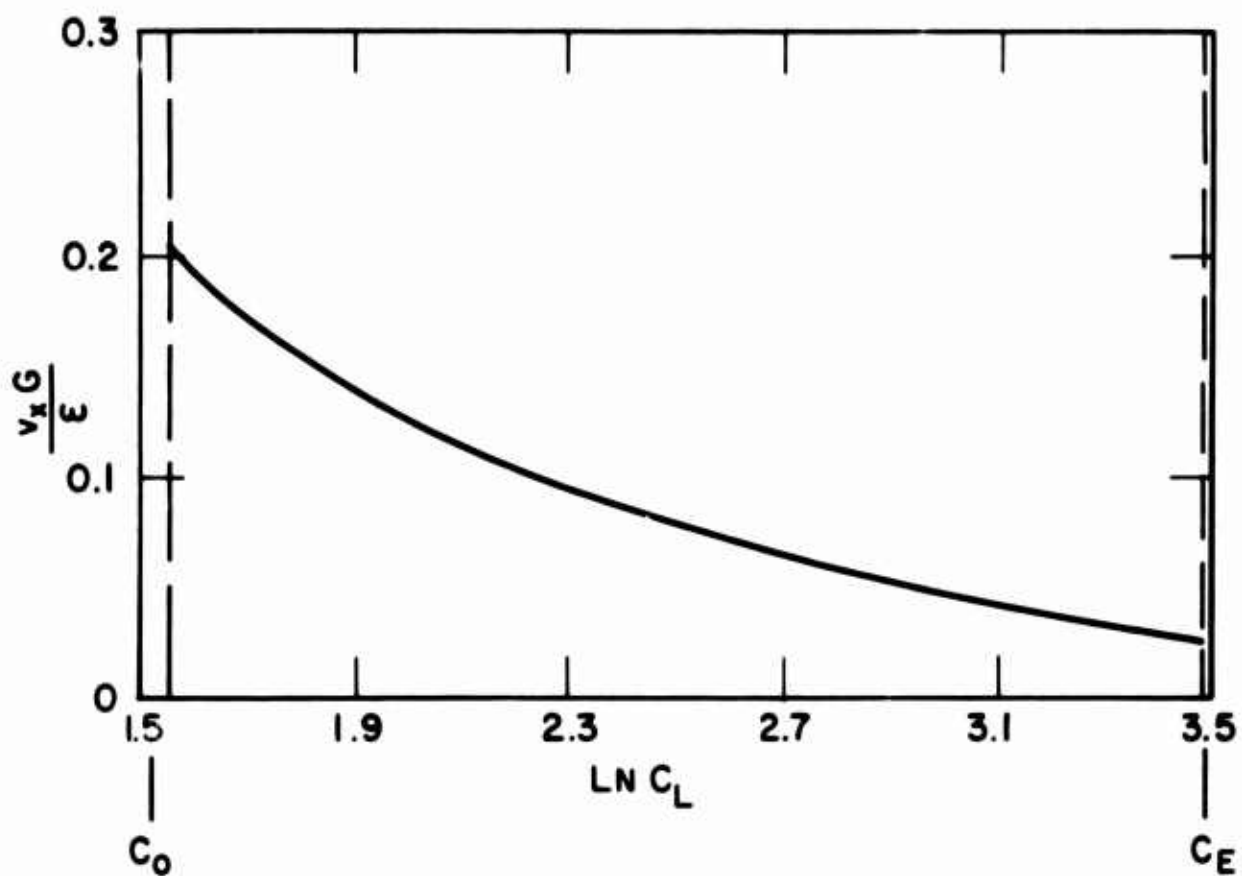
Figure G-7: Calculated data plotted in a form suitable for graphical integration using equations (G-4) - (G-7b).